Thesis for the Master's degree in chemistry

Marte Sofie Martinsen Holmsen

Synthesis, structure and dynamics of new metal *N*-heterocyclic carbene complexes

60 study points

DEPARTMENT OF CHEMISTRY

Faculty of mathematics and natural sciences

UNIVERSITY OF OSLO 05/2013

Preface

The work in this master thesis was performed at the Department of Chemistry, University of Oslo in the research group of Professor Mats Tilset. I would like to thank my supervisor Mats Tilset for introdicing me to the world of organometallic chemistry and for two great years in his research group. I would also like to thank the rest of my group, both present and past members. I feel we share a lot of good memories both in and outside of the lab after these years. A special thanks goes to Eirin for all the support and feedback while writing the thesis, I highly appreciate that. You have been a great office partner these years. I would like to thank Frode Rise and Dirk Petersen for all the help with the NMR instruments and for letting me book the instruments for several days so that I could record some nice spectra. I have had many great days in the NMR lab because of that. Thanks to Osamu Sekiguchi for recording all my MS spectra, and for always answering my questions regarding MS with a smile. Thanks to Sigurd Øien and Carl Henrik Gørbitz for performing X-ray analysis of my compounds and for solving the anion-mystery, great job! Thanks to David Balcells for all the help with the DFT calculations, it was a very nice experience.

Thanks to all 3rd and 2nd floor chemists for many funny lunches together. I think I never had a boring lunch during these years. And of course, thank you all for laughing at my puns, I highly appreciate that! Thanks to all of my fellow master students Michelle, Vladimiro and Victor. We started together and now we are soon finished, time flew fast and I think it has been two great years! Michelle, we have had so many good laughters during these years, and you have been awesome breakfast, lunch and dinner company during these last intensive weeks of writing the master thesis! Even though we were stressed with finishing the thesis, we had several good laughters these last weeks! I wish you the best luck with you thesis, big bamboo! Thanks to my family and friends for all the support and for understanding that I am sometimes a little bit busy. Especially thanks to my mother for all the support, it's nice that someone calls you to check that you're still alive. Last I would like to thank all my neighbours in the student housing for always being in a good mood. It's just a great feeling to come home and meet smiling neighbours in the hallway!

Blindern, mai 2013

Marte Sofie Martinsen Holmsen

Abstract

Metal complexes of *N*-heterocyclic carbenes are potential useful catalysts and are therefore of large interest. In this master thesis, it was attempted to synthesize several metal complexes bearing a new chelating *N*-heterocyclic carbene ligand. The synthesis of the planned Ru and Co complexes did not work out as planned, but two new Rh(III) *N*-heterocyclic carbene complexes were prepared successfully. The synthesis and characterization of the two new Rh(III) complexes is described in detail including NMR, IR, MS and single crystal X-ray analysis. The new complexes show dynamic behavior due to hindered rotation and this was investigated by variable temperature NMR. A DFT optimization of the structure of one of the new Rh(III) complexes was performed and showed good agreement with the experimental structure. The synthesis and characterization of a new Ag(I) *N*-heterocyclic carbene and a new imidazolium salt, which both are important precursors for preparing the above mentioned metal complexes of *N*-heterocyclic carbenes is described.

Abbreviations

acac	acetylacetonato
Ar	aryl
br	broad (NMR)
Bu	butyl
t-Bu	*t*-butyl
t-BuOK	potassium *t*-butoxide
cat.	catalyst
COD	1,5-cyclooctadiene
COSY	correlated spectroscopy (NMR)
Cp	cyclopentadienyl, η^5-C_5H_5
Cp^*	pentamethylcyclopentadienyl, η^5-C_5Me_5
Cy	cyclohexyl
δ	chemical shift in ppm (NMR)
d	day(s) or doublet (NMR)
DFT	density functional theory
DME	1,2-dimethoxyethane
DMSO	dimethylsulfoxide
EI	electron impact (MS)
equiv	equivalent(s)
ESI	electron spray ionization (MS)
Et	ethyl
h	hour(s)
HMBC	heteronuclear multiple-bond correlation (NMR)
HMQC	heteronuclear multiple-quantum correlation (NMR)
HRMS	high resolution mass spectrometry (MS)
HSQC	heteronuclear single-quantum correlation (NMR)
Hz	hertz

I	*iso* or *ipso*
IR	infrared
J	coupling constant (NMR)
L	ligand
M	metal
m	*meta*
m	multiplet (NMR)
Me	methyl
MeCN	acetonitrile
mesityl	2,4,6-trimethyl phenyl
MS	mass spectrometry
m/z	mass-to-charge ratio (MS)
η^n	hapticity, descriptor of
nbd	norbornadiene
NHC	*N*-heterocyclic carbene
NMR	nuclear magnetic resonance
NOE	nuclear overhauser effect
NOESY	nuclear overhauser effect spectroscopy (NMR)
o	*ortho*
ORTEP	Oak Ridge thermal ellipsoid plot
$^-$OTf	triflate, $CF_3SO_2O^-$
p	*para*
Ph	phenyl
ppm	parts per million
i-Pr	*iso*-propyl
rel	relative
s	singlet (NMR)
T	temperature
t	triplet (NMR)

THF	tetrahydrofurane
v	frequency (IR)
Å	ångstrøm

Table of Contents

The aim of the project

Synthesis and characterization of group 8 and 9 metal complexes of *N*-heterocyclic carbenes

Lately, a great amount of work on a ligand system with a chelating imino-functionalized *N*-heterocyclic carbene has been performed in the Tilset-group (see **Figure 1**).[1-11] This ligand system has been the topic of several master and PhD theses.[9-11] Metal complexes bearing this chelating ligand system are potential useful catalysts and are therefore of large interest. Among the interesting applications found for these systems is *cis*-selective cyclopropanation by using a Rh(I) complex.[8]

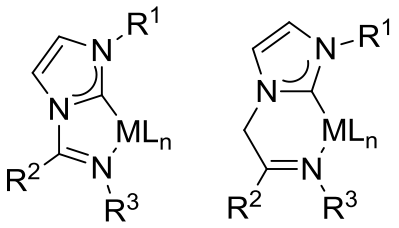

Figure 1: Types of metal complexes of imino-functionalized *N*-heterocyclic carbene complexes reported by the Tilset-group (L = different ligands, R = alkyl or aryl groups).[1]

In these types of metal complexes, it is expected that the $C_{carbene}$ is strongly bound to the metal, while the imine part is more weakly bonded.[4] This hemilabile ligand may then decoordinate from the metal and thus open up a coordination site at the metal where catalysis might take place after binding of a suitable substrate at the vacant site, or one of the other ligands may be dissociated to create an open coordination site.[4]

The aim of this project was to develop new metal complexes of the type described above, then characterize them and perform catalytic testing utilizing these complexes. The target metals of choice were Ru, Co and Rh which all play important roles in different catalytic processes such as catalytic hydrogenation, carbonylation, alkene metathesis, ethylene dimerization, CH-functionalization etc.[12] Unfortunately there was not enough time to perform the planned catalytic testing of the new complexes within the time limitations of this master thesis.

Chapter 1

Introduction

1.1 Carbenes

Carbenes play an important role in organic and organometallic chemistry and great efforts have been made in order to understand their structure, reactivity and stability.[13-14] Carbenes are neutral divalent species containing a carbon atom with only six valence electrons.[15-17] Carbenes can be classified as either triplet carbenes or singlet carbenes.[15] A singlet carbene has one lone-pair in a nonbonding sp^2 orbital and an empty p orbital while the triplet carbene has two unpaired electrons, one in an sp^2 orbital and one in a p orbital, and hence exhibit radical character (see **Figure 2**).[15]

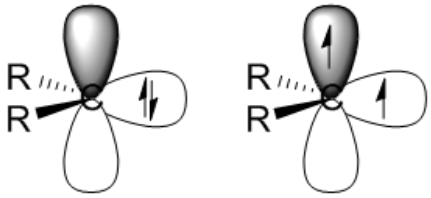

Figure 2: A singlet carbene (left) and a triplet carbene (right).[15]

This master thesis will mainly focus on *N*-heterocyclic carbenes and their properties and applications in organometallic chemistry which will be discussed in more detail in section **1.2**.

1.2 *N*-Heterocyclic carbenes

N-Heterocyclic carbenes, often abbreviated NHC's, are cyclic carbenes containing at least one α-amino substituent.[18] *N*-Heterocyclic carbenes are used as ligands in metal complexes and in organocatalysis.[18-22] The structure of some of the most common classes of *N*-heterocyclic carbenes are shown in **Figure 3**.[18]

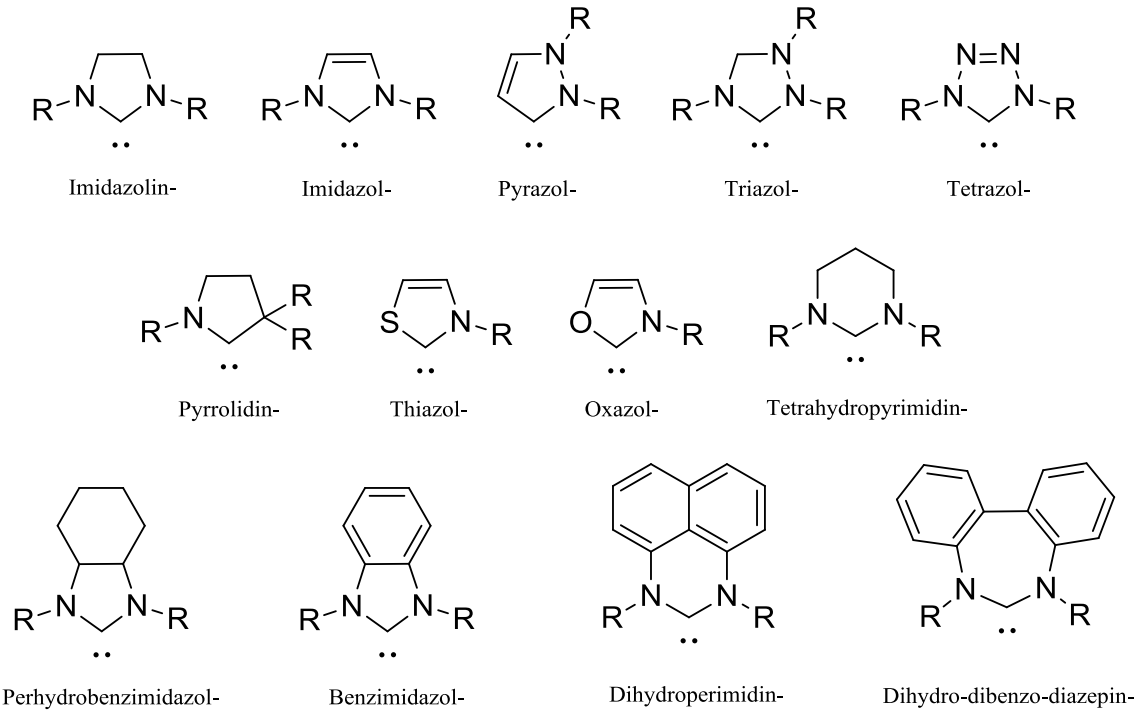

Figure 3: Some of the commonly encountered *N*-heterocyclic carbene subclasses.[18] In order to obtain the general name of each subclass, the suffix "-ylidene" should be added.

Structural features such as bond angles and bond lengths together with *ab initio* calculations of the electronic structure indicate that *N*-heterocyclic carbenes are singlet carbenes.[14, 23-24] The *N*-heterocyclic carbenes are more stable than the traditional carbenes.[16-17, 19] This is due to both steric and electronic stabilization. The α-amino substituent(s) acts as a π-donor substituent towards the empty *p*-orbital of the singlet carbene, thus stabilizing the carbene (see **Figure 4)**. [14, 24] This is consistent with X-ray diffraction studies, showing that the N-$C_{carbene}$ bond is shorter than an usual N-C single bond.[14] It has been shown by *ab initio* calculations that the triplet state of the imidazolylidene *N*-heterocyclic carbene, which cannot be stabilized by the lone-pairs from the α-amino substituents, is 84.5 kcal/mol higher in energy than the corresponding singlet state carbene.[14, 16, 19, 24]

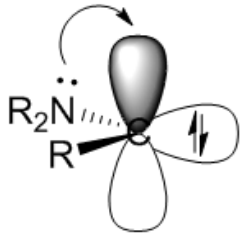

Figure 4: Stabilization of the carbene by donation of the lone-pair on of the α-substituents into the empty *p* orbital of the carbene.[14]

The α-nitrogens also stabilize the carbene moiety by an inductive effect, by pulling some of the electron density of the $C_{carbene}$ lonepair away.[19, 25] *N*-heterocyclic carbenes often have large substituents on one or two of the α-nitrogens in order to sterically shield the carbene moiety.[14, 16-17, 19, 26]

In 1991 the interest in *N*-heterocyclic carbenes accelerated when Arduengo and co-workers reported the isolation of the first stable *N*-heterocyclic carbene. The carbene was synthesized by deprotonation of the corresponding imidazolium salt as shown in **Figure 5**.[25] The carbene bears two large adamantyl substituents on the two α-nitrogens which contribute to the stability of the carbene by shielding the carbene moiety. The carbene was stable in the absence of oxygen and moisture.[25]

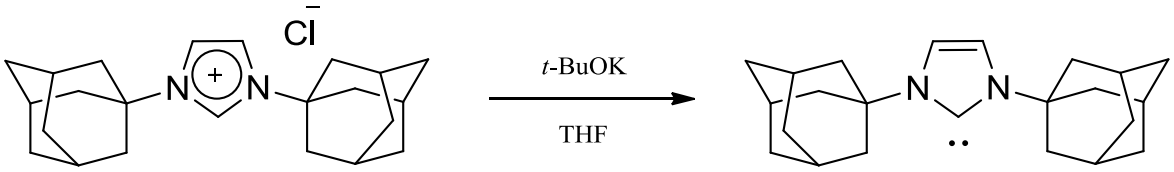

Figure 5: Synthesis of Arduengo's carbene.[25]

Some of the most frequently encountered *N*-heterocyclic carbenes and their abbreviations are listed in **Figure 6**.[22]

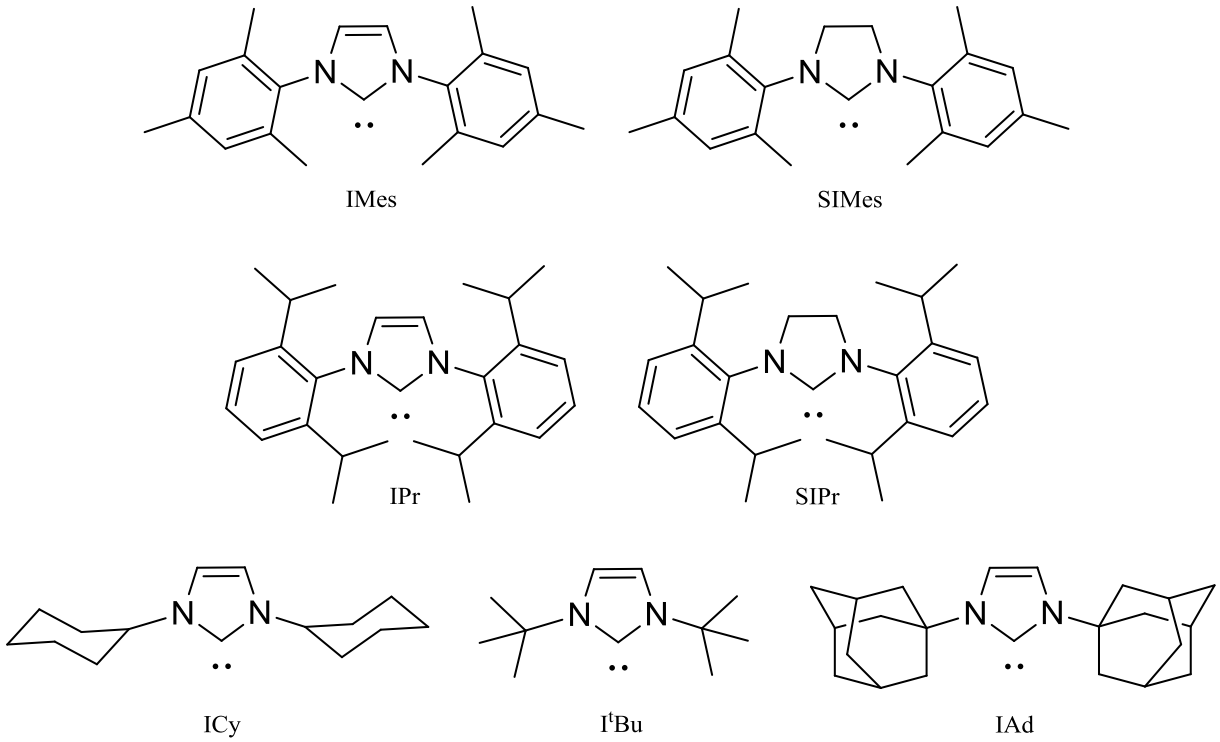

Figure 6: Some of the most common *N*-heterocyclic carbenes and their abbreviations whom are in frequent use.[22]

1.2.1 *N*-Heterocyclic carbenes as ligands in metal complexes

The two first metal complexes of *N*-heterocyclic carbenes were reported by Wanzlick and Öfele already in 1968, a long time before Arduengo's report on the existence of a stable free *N*-heterocyclic carbene.[25, 27-28]

When bound to metals, *N*-heterocyclic carbenes are relatively unreactive and can be considered as spectator ligands.[29] The *N*-heterocyclic carbenes are primarily bound through σ-donation of the carbene lone-pair to the metal with little π-acceptor character.[17, 19, 21] The amount of π-back donation from the metal is dependent upon the particular metal and carbene in question.[21]

In this thesis, it is chosen to represent the *N*-heterocyclic carbene metal complexes as shown in structure **a** in **Figure 7**. This is to emphasize that there is no proton on the $C_{carbene}$. Both representations **a** and **b** are found in the literature.[18, 20-21]

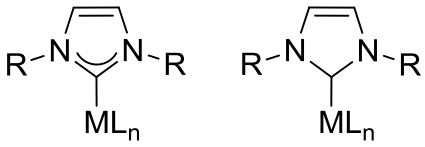

a **b**

Figure 7: Two different ways to represent metal complexes of *N*-heterocyclic carbenes. Both are widely used in the literature.[18, 20-21]

N-Heterocyclic carbenes can be regarded as similar to the well known phosphines. Both are neutral two electron donors and can be tuned both sterically and electronically.[19, 26, 29] However, there are some advantages of *N*-heterocyclic carbenes over phosphines.[29] When using the *N*-heterocyclic carbenes, it is possible to vary the steric and electronic properties independently. An increased size of the substituents on the α-amino substituents have shown to have little effect on the electronic properties of the carbene since the substituents are not directly attached to the $C_{carbene}$.[29] In the phosphines the substituents will have to sit directly on the donor atom, phosphorous, and a change in the substituents will then change both the steric properties and the electronic properties of the phosphine ligand.[29]

If there is a need to change the electronic properties of the *N*-heterocyclic carbenes, a change in the nature of the heterocycle is possible (see **Figure 3**). For example, the imidazole ring has a higher electron donor power than benzimidazole, and imidazoline is a better electron donor than imidazole.[17, 29]

There is also a difference in how the substituent groups in the *N*-heterocyclic carbenes and the phosphines will sterically effect the metal center.[17, 19, 29] In the phosphine ligands, the substituents are pointing away from the metal center while in the *N*-heterocyclic carbenes the substituents are pointing towards the metal center giving the *N*-heterocyclic carbene ligands a larger impact on the metal center. This is illustrated in **Figure 8**.[17, 19, 29]

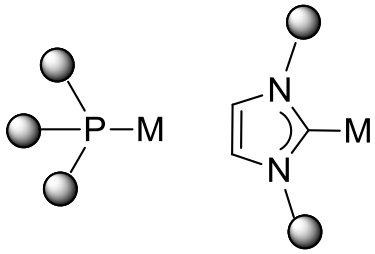

Figure 8: Illustration of the difference in steric effects caused by *N*-heterocyclic carbenes and phosphines.[29]

1.2.2 Preparation of metal complexes of *N*-Heterocyclic carbenes

There are several different methods available for the preparation of metal complexes of *N*-heterocyclic carbenes. The three most common routes are listed below.[17, 20, 25, 30]

i. Preparation of the free carbene followed by reaction with a suitable metal precursor.
ii. By reaction of the desired azolium salt with a suitable basic transition metal complex.
iii. By a carbene transfer from the corresponding Ag(I) carbene.

Traditionally the first method has been the most employed.[17, 20, 30] A strong base, such as *t*-BuOK or BuLi, is needed in order to deprotonate the azolium salt.[17, 20, 25, 30] However, it is not always possible to generate the free carbene in this way.[20-21] There may be functionalities present that are not stable towards such basic conditions. Another option where such strong bases are not required is to react the desired azolium salt with a suitable basic transition metal salt, however, this introduces a limitation in which metal precursors can be used and it is not always possible to find a suitable precursor for this method.[20, 30]

In 1998 Lin and Wang reported that *N*-heterocyclic carbene complexes of Ag(I) were versatile carbene transfer reagents for preparation of *N*-heterocyclic carbene complexes of other metals.[31] The Ag(I) *N*-heterocyclic carbene complexes were prepared by reacting the desired azolium salt with a mild silver base such as Ag_2O.[31] This new method opened up for preparation of several new metal complexes of *N*-heterocyclic carbenes and in the following years several new metal complexes of *N*-heterocyclic carbenes were reported.[20-21] Carbene transfer reactions from Ag(I) *N*-heterocyclic carbenes to other metals have been reported for several different transition metals such as Ru(II), Ru(III), Ru(IV), Rh(I), Rh(III), Ir(I), Ir(III), Ni(II), Pd(II), Pt(II), Cu(I), Cu(II) and Au(I).[20, 30]

Some examples of preparation of metal complexes of *N*-heterocyclic carbenes are given in **Figure 9**.

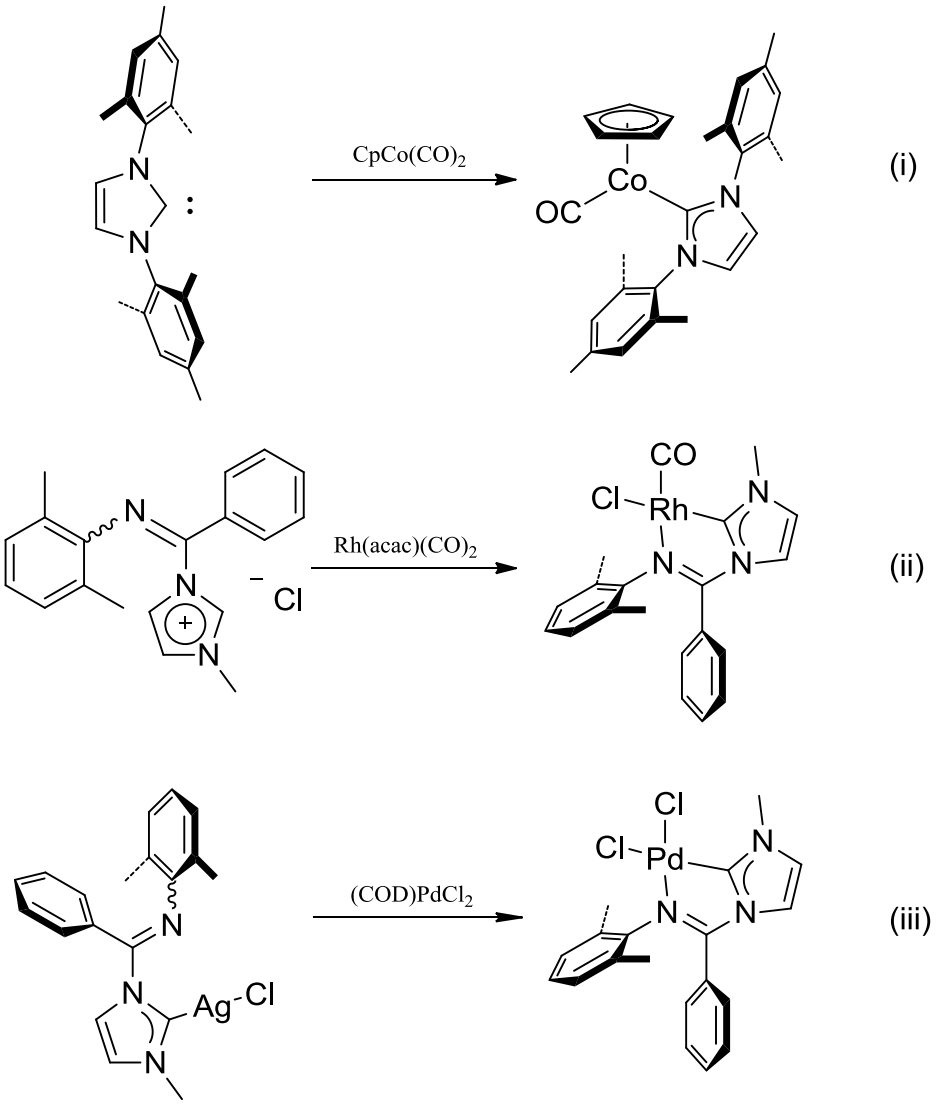

Figure 9: Preparation of metal complexes of *N*-heterocyclic carbenes. (i): Preparation of the free carbene followed by reaction with a suitable metal precursor.[32] (ii): By reacting a suitable imidazolium salt with a basic transition metal complex.[8] (iii): By carbene transfer from the Ag(I) *N*-heterocyclic carbene.[1]

1.2.3 Donor-functionalized *N*-heterocyclic carbenes

Donor-functionalized *N*-heterocyclic carbenes are *N*-heterocyclic carbenes containing at least one anionic or neutral $2e^-$ donor atom (e.g. such as C, N, O, S or P) which can act as a polydentate ligand upon coordination to a metal centre.[33-34] Some examples of donor-functionalized *N*-heterocyclic carbenes are given in **Figure 10**.[33] The donor functionalized *N*-heterocyclic carbenes often form chelates on the metal centre and the donor atom can in some cases be hemilabile meaning that during catalysis it may decoordinate and thus create an open coordination site where catalysis may take place.[33]

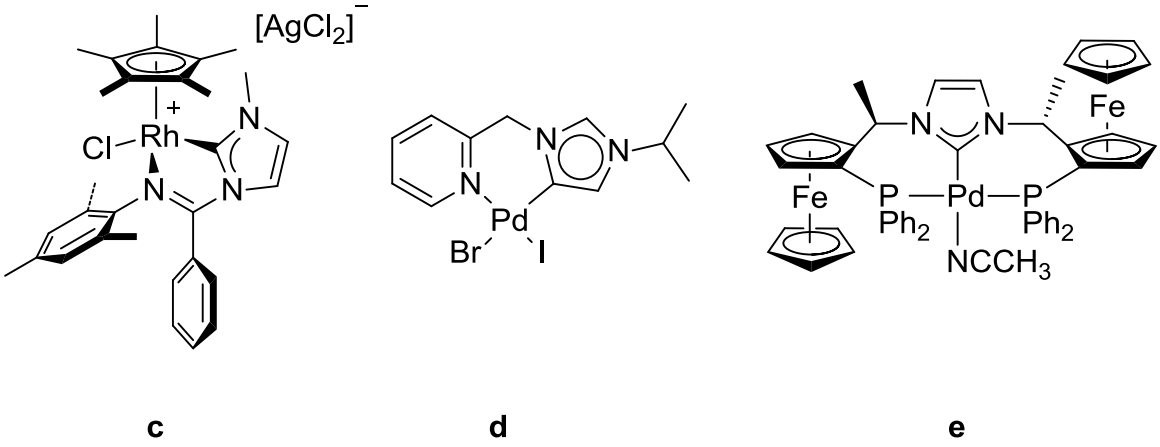

Figure 10: Some types of donor functionalized *N*-heterocyclic carbenes. **a**: Imine-functionalized. **b**: Pyridine-functionalized.[33] **c**: Phosphine-functionalized.[33]

1.2.4 Imino-functionalized *N*-heterocyclic carbenes

Imino-fuctionalized *N*-heterocyclic carbenes are *N*-heterocyclic carbenes with an imino-functionality incorporated into the molecule.[33] One example was shown in compound **c** in **Figure 10** above. This type of imino-functionalized *N*-heterocyclic carbenes has been studied extensively in the Tilset-group and they are also the main focus of this master thesis. [1-11] A selection of the previously reported metal complexes of imino-functionalized *N*-heterocyclic carbenes prepared in the Tilset-group is listed in **Figure 11**.[1, 4-5, 8] Rh(I) complex **f** was prepared by reaction of the imidazolium salt with the basic transition metal complex $Rh(acac)(CO)_2$.[8] Pd(II) complexes **g-i** were prepared by a carbene transfer reaction from the corresponding Ag(I) carbene.[1, 4-5]

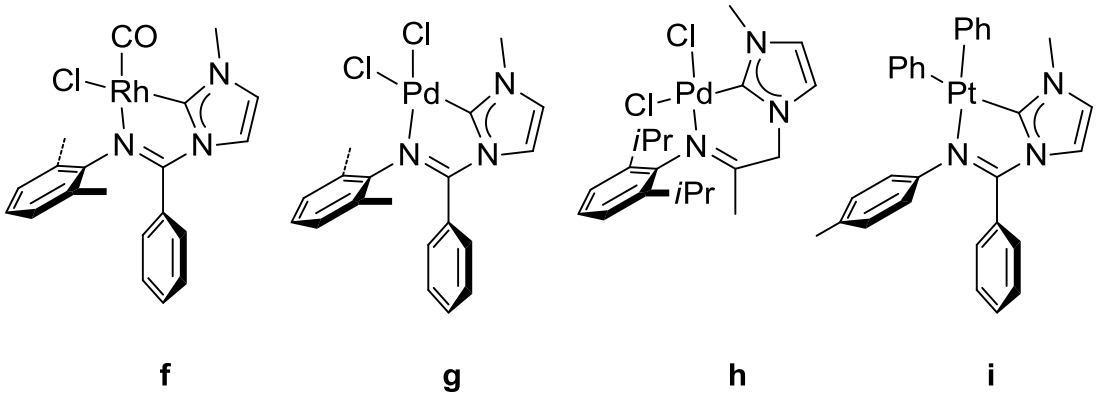

Figure 11: A selection of the previously reported imino-functionalized *N*-heterocyclic carbene metal complexes reported by the Tilset-group.[1, 4-5, 8]

1.2.5 Rearrangement of imino-functionalized *N*-heterocyclic carbenes

It has been reported by Bildstein and co-workers that imidazolium salts with an *N*-iminoyl and an *N'*-alkyl group such as those listed in **Figure 11** undergo rearrangements if prepared as the free carbene.[35] Upon deprotonating the imidazolium salt, the initially formed *N*-heterocyclic carbene rearranges spontaneously by a migration of the *N*-iminoyl group from the nitrogen to the former $C_{carbene}$ yielding a 2-iminoylimidazole (see **Scheme 1**).[35] The rearranged ligand system is now a [N,N]-chelating ligand system and no longer a [C,N]-chelating ligand system and will bind to metals via the two nitrogens (see **Scheme 1**).[35]

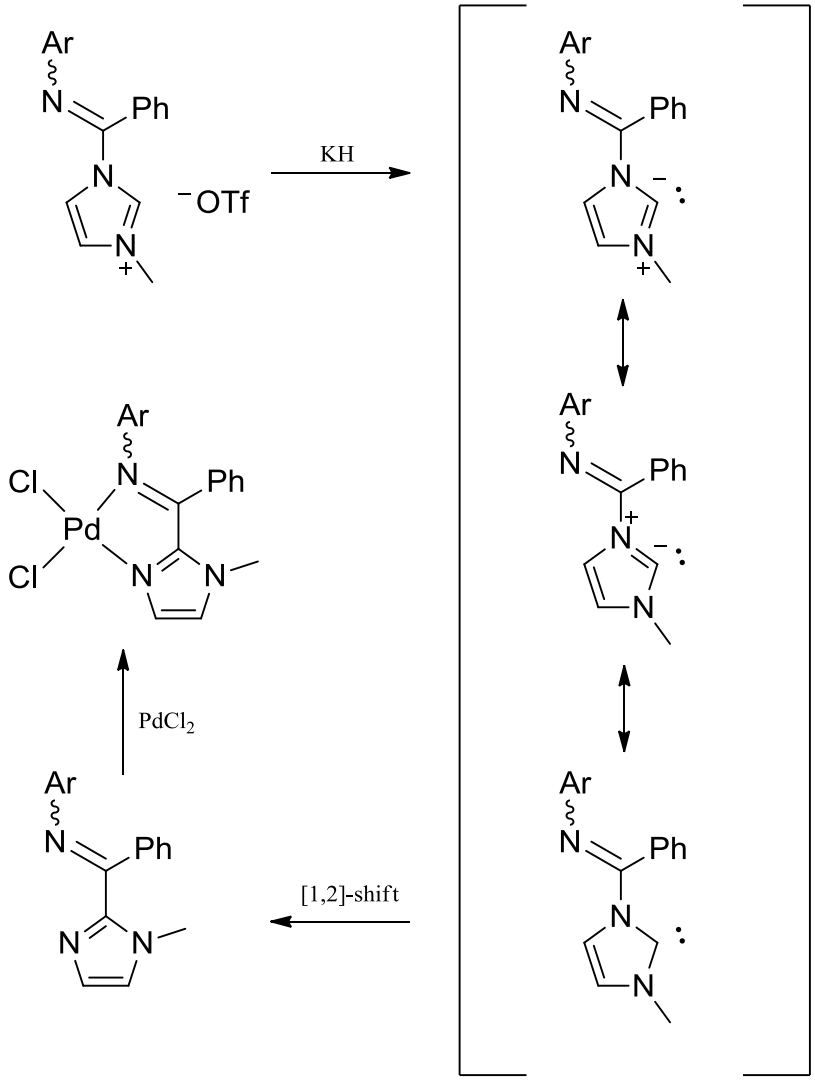

Scheme 1: Rearrangement of an imino-functionalized *N*-heterocyclic carbene.[35]

The ligand system used in this master thesis falls within the category which will undergo rearrangement upon preparing the free carbene.[35] Due to this rearrangement, preparation of the free carbene of the ligand system was not attempted. Other routes than the free carbene

route to the metal complexes of *N*-heterocyclic carbenes had to be chosen, such as the carbene transfer from Ag(I) *N*-heterocyclic carbenes.

1.2.6 Catalytic applications of metal complexes of *N*-heterocyclic carbenes

Probably the most well-known application of *N*-heterocyclic carbenes is their use in alkene metathesis.[36] By replacing one of the PCy_3 (Cy=cyclohexyl) ligands in the traditional Grubbs' 1st generation catalyst with an imidazolylidene *N*-heterocyclic carbene, an improved catalyst was obtained.[36]

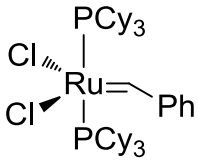

1st generation
Grubbs' catalyst

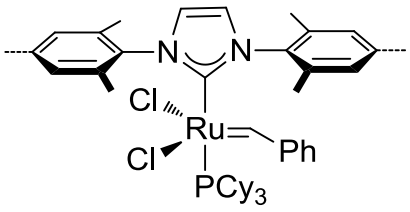

2nd generation
Grubbs' catalyst

The IMes in the 2nd generation Grubbs' catalyst is a better donor than the PCy_3 in the 1st generation which enhances the catalyst performance.[37] IMes is also more sterically demanding than PCy_3 leading to less bimolecular carbene decomposition of the catalyst.[37] The 2nd generation Grubbs' catalysts are also more thermally stable than the traditional 1st generation Grubbs' catalysts.[37]

Another well known application of the metal complexes of *N*-heterocyclic carbenes are their use in cross-coupling reactions.[38] Cross-coupling represents an extremely versatile tool in organic synthesis because C-C bond formation is a key step in a wide range of preparative organic processes.[38] *N*-heterocyclic carbenes have found highly successful applications as supporting ligands in cross-coupling reactions, for example in the Suzuki-Miyaura reaction.[19, 38] Their strong donor ability makes the oxidative addition of the aryl halide more facile, and the bulky substituents facilitate the reductive elimination. One example is given in **Scheme 2**.[38] The Pd *N*-heterocyclic carbene complex is prepared *in situ* from $Pd(dba)_3$, the imidazolium salt of the IPr *N*-heterocyclic carbene and a base, giving the cross-coupled product in good yields.[38]

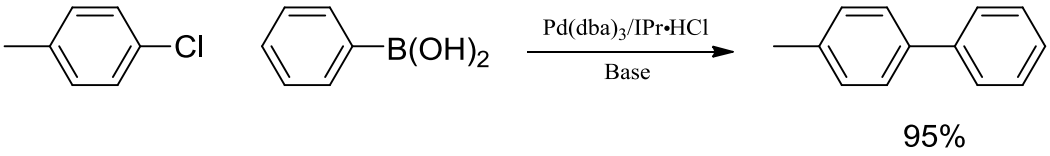

Scheme 2: The Suzuki-Miyaura cross coupling reaction of an aryl halide with an aryl boronic acid.[38]

Rh(I) complexes bearing a chelating *N*-heterocyclic carbene have shown to be excellent catalysts for achieving *cis*-selective catalytic cyclopropanations.[6-9, 11] Extensive work on *cis*-selective Rh(I) *N*-heterocyclic carbene complexes have been performed in the Tilset-group.[6-9, 11] **Scheme 3** shows a highly *cis*-selective cyclopropanation reaction with diethyl diazoacetate using an imino-functionalized Rh(I) *N*-heterocyclic carbene complex as catalyst.[6]

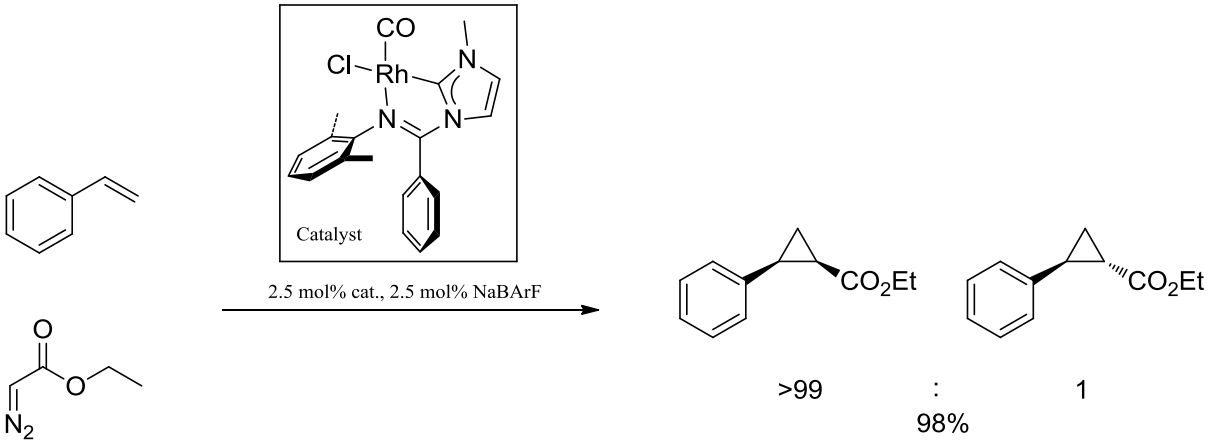

Scheme 3: *Cis*-selective cyclopropanation reported by the Tilset-group.[6]

1.3 Chiral metal complexes

The traditional way of preparing chiral metal complexes is by utilizing chiral ligands.[39] A less investigated category of chiral metal complexes are those in which the stereogenic center is located at the metal.[39] There are some disadvantages connected to having the chirality information at the metal.[39] A major challenge is the racemization of an enantiopure metal complex over time.[39-41] Configurational lability caused by labile ligands may lead to racemization and therefore during catalysis, racemization may occur when opening up a coordination site.[39] For some catalytic applications, there are examples where the metal complexes with the chirality information at the metal centre turned out to be more effective than the traditional chiral metal complexes.[39] One example being a Mo-based complex with a stereogenic metal centre which has been reported to catalyze enantioselective alkene metathesis.[40]

The two Rh(III) *N*-heterocyclic carbene complexes **8** and **9** prepared in this master thesis also contain stereogenic centers at the metal rendering them chiral. **Figure 12** shows the two enantiomers of the Rh(III) *N*-heterocyclic carbene **8**. However, no enantioselective synthesis or separation of the enantiomers was investigated. **8** and **9** will only be shown as one of their enantiomers throughout the thesis. The enantiomer chosen is the one found in the structure based on the X-ray analysis.

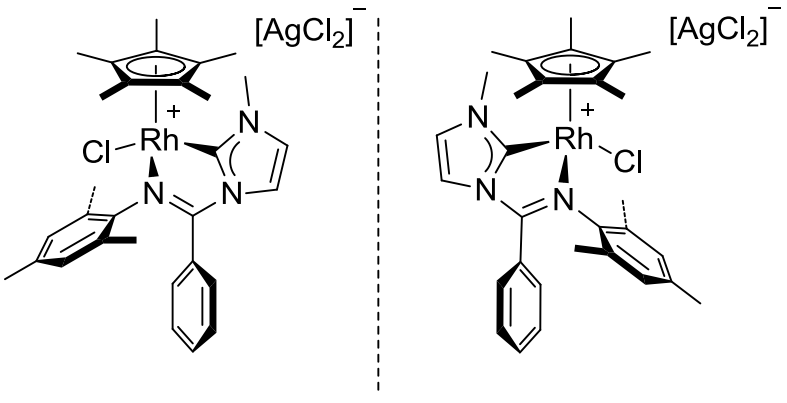

8

Figure 12: The chiral Rh(III) *N*-heterocyclic carbene **8**, where the stereogenic centre is located at Rh.

1.4 The CO ligand and its bonding to the metal

The neutral $2e^-$ donor CO ligand is frequently used in organometallic chemistry.[12] The bonding of CO to metals occurs by two types of interactions, as seen from **Figure 13**. The CO donates an electron pair into the empty *d* orbital on the metal (**j**) and the metal backdonates electrons from its filled *d* orbital into the antibonding π^* orbital in CO (**k**). The backdonation of electrons into the π^* of CO will weaken the C≡O bond which can be seen by a lowering of the ν_{CO} in the infrared spectrum.[12] Thus, the ν_{CO} gives valuable information about the electron density at the metal centre in which the CO is attached: a more electron rich metal center will have a stronger backdonation into the π^*, lowering the $\nu_{co,}$ and thus binding the CO more tightly. A higher ν_{CO} indicates that the CO is less tightly bond to the metal as is seen in **Figure 14** where $CpCo(CO)I_2$ exhibits a larger ν_{CO} than $CpCo(CO)_2$ indicating that the CO is less tightly bond in $CpCo(CO)I_2$.[12, 42] It has been shown that substitution of the CO in $CpCo(CO)I_2$ occurs readily with both triphenylphosphine and pyridine indicating the quite weak bonding of the CO in this complex.[43]

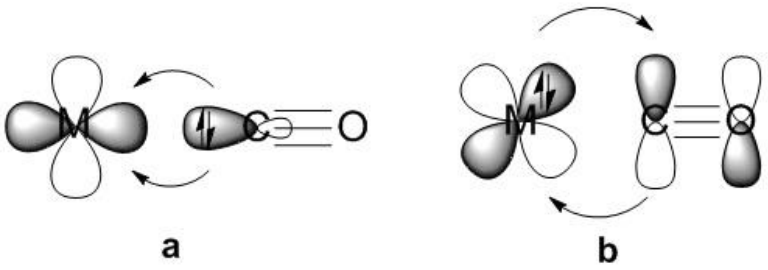

Figure 13: The two component bonding in the CO-ligand.[12] **j**: Donation of a lone-pair on CO into an empty *d*-orbital at the metal. **k**: Backdonation of electrons from a filled *d* orbital on the metal into the antibonding π^* orbital on the metal.[12]

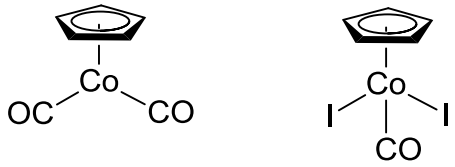

ν_{CO}: 2028, 1967 cm^{-1} ν_{CO}: 2077 cm^{-1}

Figure 14: ν_{CO} of $CpCo(CO)_2$ and $CpCo(CO)I_2$.[42]

1.5 Lineshape analysis and the Eyring equation

The Eyring equation gives the relationship between the rate constant and the absolute temperature.[15] If one have the rate constants and their corresponding temperatures, it is possible to perform an Eyring plot (see **Figure 15**) to obtain the enthalpy of activation ($\Delta H^{\#}$) and the entropy of activation ($\Delta S^{\#}$). Dynamic behavior of molecules can frequently be observed by broadened signals in the NMR spectra. The broadening is temperature dependent because the rates of the dynamic process depend on the temperature. Acquiring ^{1}H-NMR spectra at different temperatures followed by lineshape analysis with a program such as gNMR gives access to the rate constants at the different temperature for the dynamic process.[44] The linear form of the Eyring equation is given in **Equation 1**.

$$\ln\left(\frac{k}{T}\right) = \frac{-\Delta H^{\#}}{R} \cdot \frac{1}{T} + \ln\left(\frac{k_B}{h}\right) + \frac{\Delta S^{\#}}{R}$$

Equation 1: The linear form of the Eyring equation.[15]

A plot of ln(k/T) versus 1/T yields a straight line with slope $-\Delta H^{\#}/R$ and intercept $\ln(k_B/h) + \Delta S^{\#}/R$, where R is the gas constant, k_B is Boltzmann's constant and h is Planck's constant, and thus it is possible to determine the enthalpy and entropy of activation.[15]

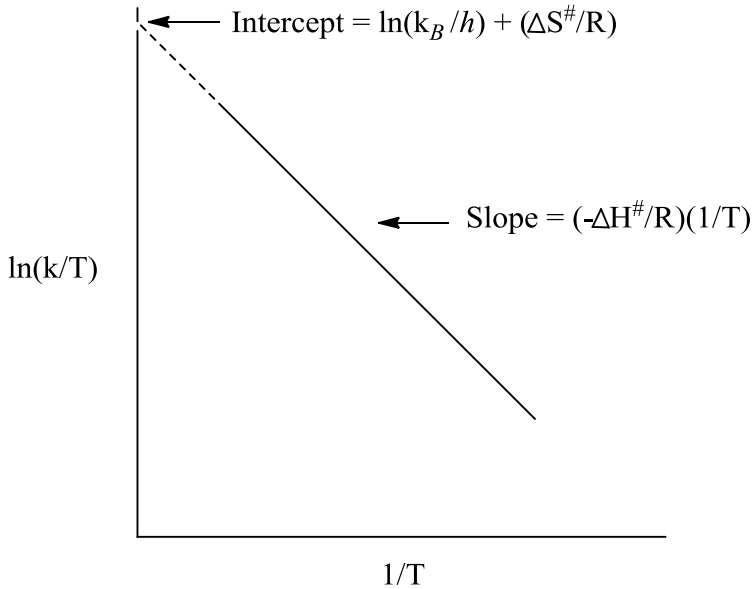

Figure 15: Illustation of an Eyring plot.[15]

Chapter 2

Synthesis of a new imidazolium salt and Ag(I) *N*-heterocyclic carbene complex

2.1 The scope of the chapter

N-heterocyclic carbene complexes of Ag(I) are versatile precursors for preparing *N*-heterocyclic carbene complexes of other metals. Ag(I) *N*-heterocyclic carbenes can be prepared from their corresponding imidazolium salts.[20-21] In this chapter, the synthesis of imidazolium salt **3a** and Ag(I) carbene **4a** will be described as well as the synthesis of the previously reported imidazolium salt **3b** and Ag(I) carbene **4b**.[1] Imidazolium salts **3a** and **3b** and Ag(I) carbenes **4a** and **4b** are shown in **Figure 16**.

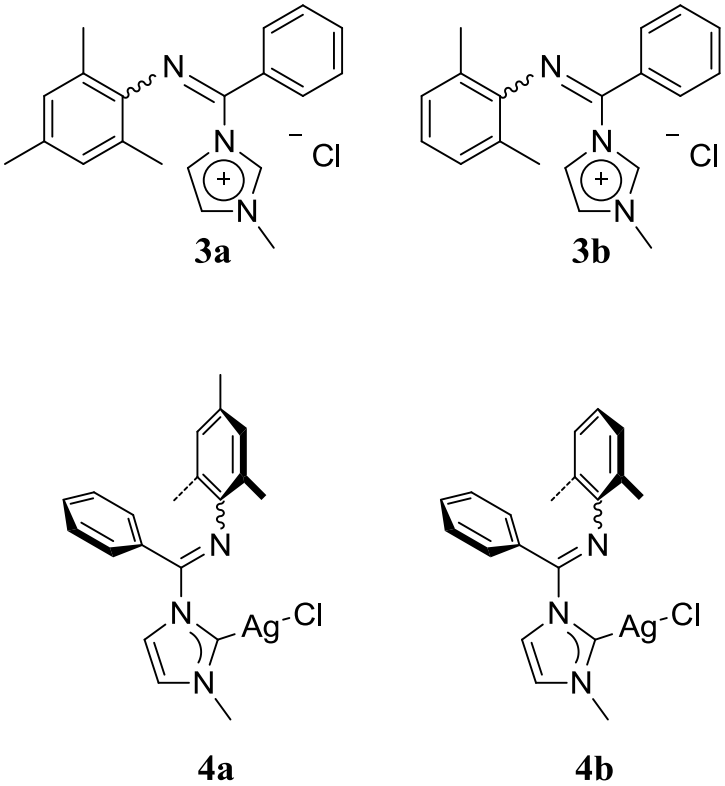

Figure 16: Imidazolium salts **3a** and **3b** and Ag(I) carbenes **4a** and **4b**.[1]

2.2 Results and discussion

2.2.1 Synthesis of imidazolium salts 3a and 3b

Imidazolium salt **3b** has been prepared previously by the Tilset-group according to **Scheme 4**.[1] The new imidazolium salt **3a** was thus synthesized by the same strategy with only a few minor modifications in the work-up procedure.

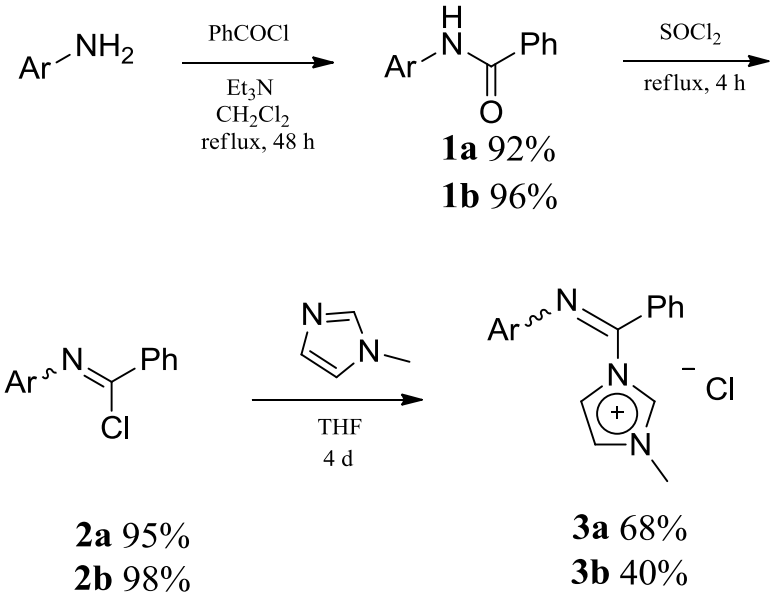

a: Ar = 2,4,6-trimethylphenyl
b: Ar = 2,6-dimethylphenyl

Scheme 4: Synthesis of imidazolium salt **3a** and **3b**.[1]

The imidazolium salts were synthesized by a three step procedure. First amides **1a** and **1b** were prepared in good yields from their corresponding anilines and acid chlorides in the presence of a base.[45-46] In the subsequent step the iminochlorides **2a** and **2b** were prepared in good yields by treating their corresponding amides with $SOCl_2$.[46-47] In the last step the imidazolium salts **3a** and **3b** were synthesized in moderate to good yields by substitution of the chloride in **2a** and **2b** with 1-methylimidazole.

2.2.2 Characterization of amide 1a and 1b, iminochloride 2a and 2b and imidazolium salt 3b

^{1}H-NMR, MS and IR data corresponded with the reported data for **1a**, **1b**, **2a, 2b** and **3b**.[1, 46-47] For both the amides **1a** and **1b** the characteristic broad resonance of the N**H** was observed in the ^{1}H-NMR spectra, and in the ^{1}H-NMR spectra of the iminochlorides **2a** and **2b** this peak had disappeared indicating a full conversion of the amide to the iminochloride. In the ^{1}H-NMR spectrum of imidazolium salt **4b** the characteristic NC**H**N proton was seen downfield at 10.38 ppm. For both iminochlorides **2a** and **2b** and imidazolium salt **3b** only one set of peaks was observed indicating the presence of only one isomer. It was not further investigated if it was the *E* or *Z* isomer which was observed.

2.2.3 Characterization of imidazolium salt 3a

The new imidazolium salt **3a** was characterized by NMR, IR and MS. **3a** decomposes in $CDCl_3$ solution over time, which made the NMR characterization challenging due to the appearance of an extra set of peaks from the decomposed species with time. In the ^{1}H-NMR spectrum of **3a** the characteristic resonance of the NC**H**N proton was observed downfield at 10.39 ppm. Only one set of peaks was observed initially indicating the presence of only one isomer of **3a.** It was not further investigated if it was the *E* or *Z* isomer which was observed. Upon investigating **3a** by MS, the molecular ion minus one chloride was seen. High resolution mass spectrometry (HRMS) confirmed that the elemental composition of this peak was correct.

2.2.4 Decomposition of imidazolium salt 3a and 3b in solution

Both imidazolium salts decomposes in $CDCl_3$ solution over time, the decomposition of **3a** is shown in **Figure 17.** It is seen that new peaks appear and the peaks belonging to imidazolium salt **3a** decrease in intensity. Already 15 minutes after preparing the NMR sample decomposition is observed. What the imidazolium salts **3a** and **4b** decompose to was not extensively investigated. However, it was observed that the peak at ca 3.7 ppm grew upon adding 1-methylimidazole which may indicate that the 1-methylimidazole is dissociating. However, this did not cause any problems for utilizing **3a** and **3b** in the subsequent reactions discussed later in this chapter.

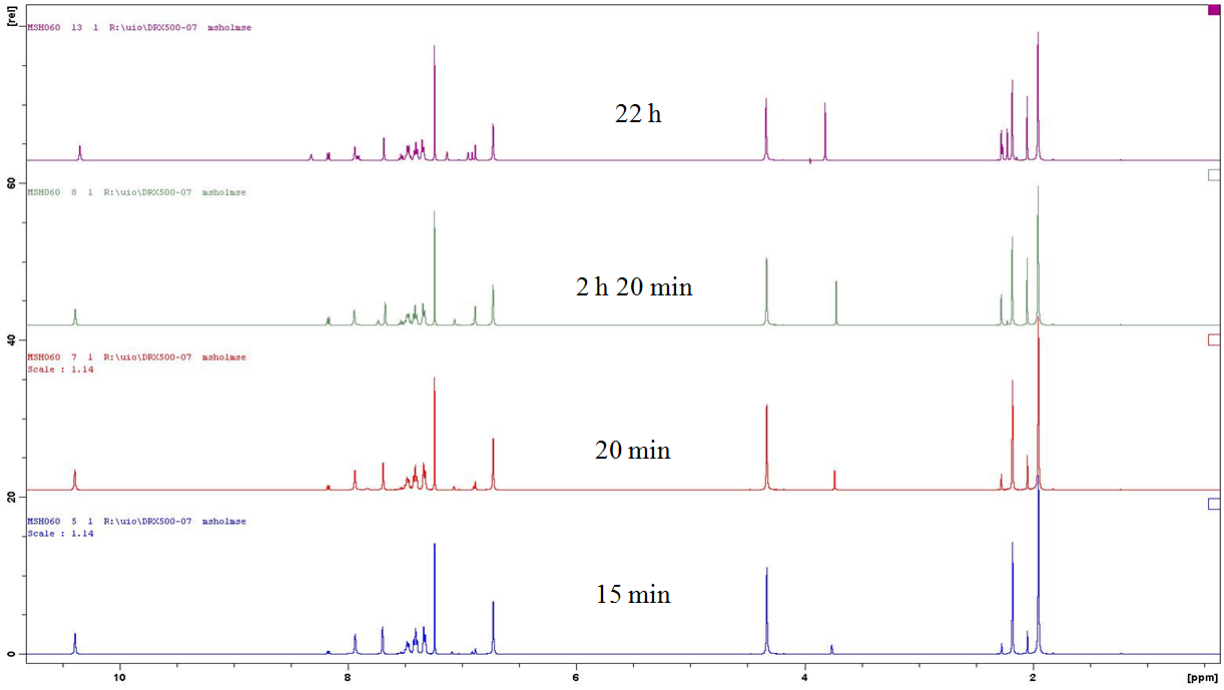

Figure 17: Decomposition of **3a** observed by ^{1}H-NMR (500 MHz, $CDCl_3$). Dry $CDCl_3$ was used. A larger version of the spectra can be found in the Appendix.

2.2.5 Synthesis of Ag(I) carbene complexes 4a and 4b

Ag(I) carbene **4a** and **4b** were synthesized in good yields according to **Scheme 5**: Ag(I) *N*-heterocyclic carbenes of the imidazolylidene type are often synthesized by deprotonating their corresponding imidazolium salts with a mild silver base, such as Ag_2O.[20] Ag(I) carbene **4b** has already been prepared in our group by this method.[1] It was therefore chosen to synthesize Ag(I) carbene **4a** by the same method. 3 Å molecular sieves were used in order to remove the water formed during the reaction. Ag(I) carbenes **4a** and **4b** are stable if stored under inert atmosphere in the absence of light.

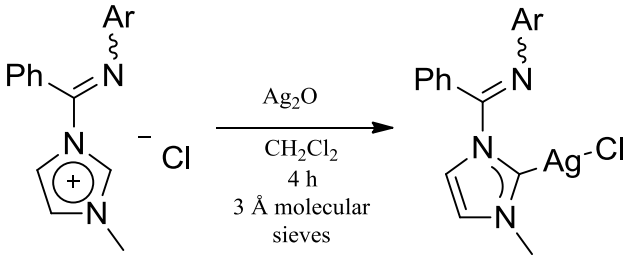

3a-b

4a 84%
4b 80%

a: Ar = 2,4,6-trimethylphenyl
b: Ar = 2,6-dimethylphenyl

Scheme 5: Synthesis of Ag(I) carbenes **4a** and **4b**.[1]

2.2.6 Characterization of Ag(I) carbene complex 4b

^{1}H-NMR, MS and IR data corresponded with the reported data on Ag(I) carbene **4b**.[1] In the ^{1}H-NMR of **4a** it was observed that the NC**H**N proton of imidazolium salt **3b** was absent, which indicated full conversion of **3b** to **4b**. Only one set of peaks was observed, indicating the presence of only one isomer of **4b**. It was not investigated further if it was the *E* or *Z* isomer, however, in the previously reported structure of **4a**, the *E*-isomer was observed.[1]

2.2.7 Characterization of Ag(I) carbene complex 4a

The new Ag(I) carbene **4a** was characterized by NMR, MS, IR and single crystal X-ray analysis.

2.2.7.1 NMR, IR and MS

In the ^{1}H-NMR spectrum of **4a** it was observed that the the NC**H**N proton of imidazolium salt **3a** was absent, which indicated a full conversion of **3a** to **4a**. As for compound **4b** only one set of peaks was observed indicating that only one isomer is present. It was not investigated further if it was the *E* or *Z* isomer, however, in the structure based on the X-ray analysis, the *E*-isomer was observed. This indicates that the *E*-isomer is favored in the solid state.

At first it was not possible to observe the $C_{carbene}$ of compound **4a** by ^{13}C-NMR. However, it was seen indirectly by a heteronuclear HMBC correlation at 184.21 ppm from the methyl protons sitting on the nitrogen in the imidazolylidene moiety. Later, a ^{13}C-NMR spectrum was recorded on an AV600 spectrometer equipped with a cryoprobe to enhance the signal to noise ratio.[48] Upon recording a ^{13}C-NMR experiment with a relaxation delay of 10 s and 7 k scans, it was possible to detect a broad peak at the same chemical shift as the HMBC correlation

seen earlier (see **Figure 18**). Silver has two naturally occurring isotopes ^{107}Ag (52%) and ^{109}Ag (48%).[21] Both of these are NMR active and both have a nuclear spin of ½.[21] Given this information, one would expect to observe two doublets in the ^{13}C-NMR spectrum due to the different couplings with the two different isotopes.[21] However, coupling between $C_{carbene}$ and Ag is observed in only a few complexes, but the majority show no coupling pattern.[21] A significant number of Ag(I) *N*-heterocyclic carbene complexes have also been reported without any observable $C_{carbene}$ resonances.[21] It has been proposed that a fluxional behavior in which there is an equilibrium between the monomeric AgX(NHC) and the dimeric $[Ag(NHC)_2]^+$ $[AgX_2]^-$ within the NMR time scale leads to broadening and eventually disappearance of the $C_{carbene}$ peaks.[21, 31] This fluxional behavior is shown in **Scheme 6**. As the rate of exchange increases, the $C_{carbene}$ resonances will first become broader and then eventually coalesce into a sharp singlet.[21, 31] Due to the broadness of the signals of the $C_{carbene}$ in the ^{13}C-NMR spectrum it was not possible to measure the exact coupling constants $^1J(^{107}Ag\text{-}^{13}C)$ and $^1J(^{109}Ag\text{-}^{13}C)$. However, an average of them was found to be ca 250 Hz by measuring the distance in Hz between the two broad peaks seen in **Figure 18**. This is in good agreement with previously reported coupling constants between Ag and $C_{carbene}$. $^1J(^{107}Ag\text{-}^{13}C)$ and $^1J(^{109}Ag\text{-}^{13}C)$ usually range from 180-234 Hz and 204-270 Hz, respectively.[21] The couplings are proportional to the magnetogyric ratios of -1.089×10^7 rad s^{-1} T^{-1} and -1.252×10^7 rad $s^{-1}T^{-1}$ for ^{107}Ag and ^{109}Ag respectively.[49]

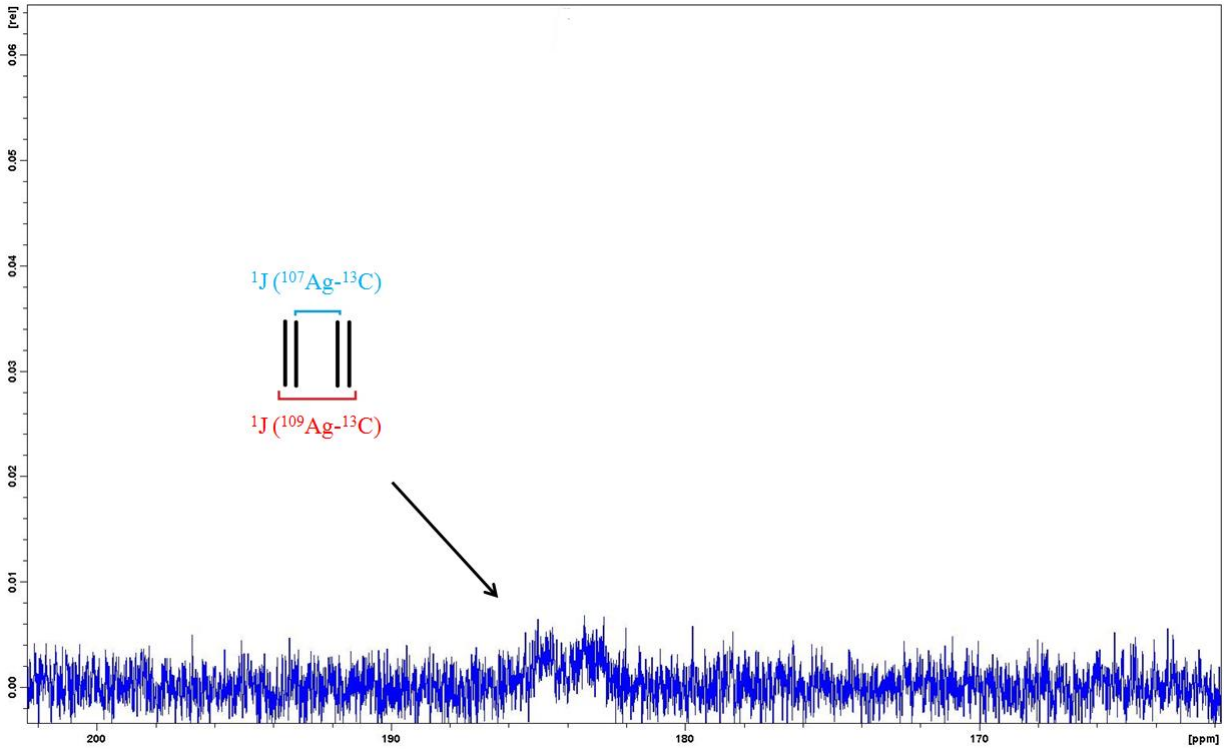

Figure 18: ^{13}C-NMR (150 MHz, $CDCl_3$) of **4a**. $C_{carbene}$ is seen as a broad signal that may resemble two doublets.

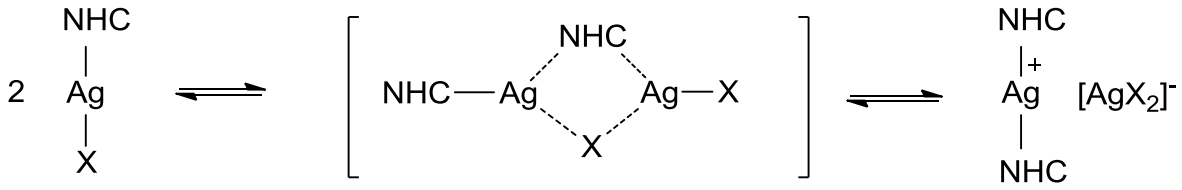

Scheme 6: Proposed fluxional behavior in solution, a suggested explanation of broadening of the $C_{carbene}$ shifts in the ^{13}C-NMR of Ag(I) *N*-heterocyclic carbenes.[21, 31] (X= Cl, Br, I).

Upon investigating **4a** by mass spectrometry the peak of $[Ag(NHC)_2]^+$ is observed. It has been reported that Ag(I) carbenes of the Carbene-Ag-Cl-type forms biscarbenes $[(NHC)_2\text{-}Ag]^+$ in the gas phase.[21] This is also consistent with what is seen for Ag(I) carbene **4b** and other similar complexes previously reported by our group.[1-2] High resolution mass spectrometry (HRMS) confirmed that the elemental composition of this peak was correct.

Compound **4a** was investigated by infrared spectroscopy (IR). $\nu_{C=N}$ of **4a** was found to be 1663 cm^{-1}, which is within the range of a free imine, indicating that there is no significant coordination of the imine nitrogen to the metal in this case.[50] This is in agreement with the structure based on the X-ray analysis of **4a** and other similar Ag(I) carbenes reported by the

Tilset-group.[1-3, 5] However, it should be kept in mind that the IR data gives information about **4a** in solution, while the X-ray analysis gives information about **4a** in the solid state.

2.2.7.2 Crystallographic structure determination of Ag(I) carbene complex 4a

Ag(I) carbene **4a** was investigated by single crystal X-ray analysis. The structure of **4a** is shown in **Figure 19**. Selected bond lengths and bond angles are listed in **Table 1** and **Table 2**.

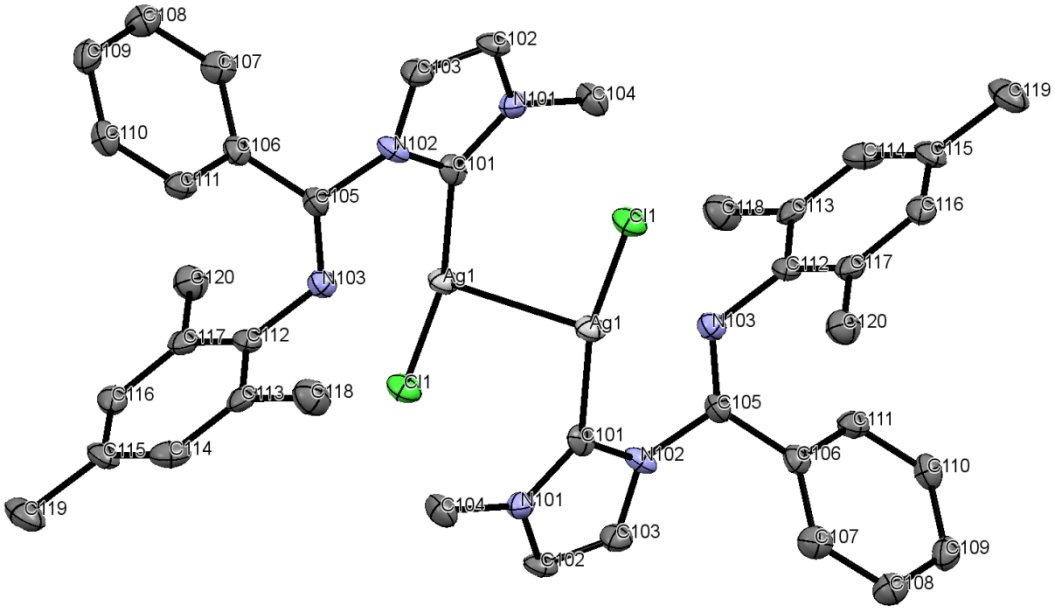

Figure 19: ORTEP-drawing of complex **4a**. Hydrogens and CH_2Cl_2 are omitted for clarity. Ellipsoids at 50% probability.

Table 1: Selected bond lengths from structure based on the X-ray analysis of **4a**.

Bond	Bond length [Å]
Ag(1)-C(101)	2.075(8)
Ag(1)-C(l1)	2.343(2)
Ag(1)-Ag(1)	3.073(2)
N(101)-C(101)	1.345(10)
N(102)-C(101)	1.349(11)
N(103)-C(105)	1.264(10)

Table 2: Selected bond angles from structure based on the X-ray analysis of **4a**.

Angle	Degrees [°]
C(101)-Ag(1)-Cl(1)	165.9(2)
C(101)-Ag(1)-Ag(1)	76.1(2)
Cl(1)-Ag(1)-Ag(1)	117.85(6)
N(101)-C(101)-N(102)	103.9(7)
N(101)-C(101)-Ag(1)	132.4(6)
N(102)-C(101)-Ag(1)	123.6(6)

The Ag(I) carbene **4a** is seen as a dimer in the structure based on the X-ray analysis. The two units are associated through an Ag-Ag interaction, as is seen by the Ag-Ag distance of 3.0073(2) Å which is considerably shorter that the sum of the van der Waals radii of 3.44 Å.[51] A similar, although slightly longer, Ag-Ag interaction of 3.0577(10) Å was reported for the previously reported Ag(I) carbene **4b**.[1] This interaction leads to a slight bending away from linearity of the $C_{carbene}$-Ag-Cl angle to 165.9(2)°. The Ag-$C_{carbene}$ distance is 2.075(8) Å which is in agreement with what was seen for the already published **4b**. The bonds between the $C_{carbene}$ and the α-nitrogens show a significant double bond character indicating the donation of the lone-pair on the nitrogens into the empty *p*-orbital on the carbene to stabilize the carbene, as was discussed in the introduction section. A normal C-N single bond is usually within the range of 1.46-1.48 Å,[15] while in complex **4a** they are 1.345(10) Å and 1.349(11) Å which is considerably shorter. The imine C=N bond is short, 1.264(19) Å, indicating that there is no significant coordination of the imine nitrogen to the metal, this is also consistent with what was observed by IR as discussed in the last paragraph.

2.3 Conclusion

The new Ag(I) *N*-heterocylic carbene **4a** and imidazolium salt **3a** were successfully prepared in good yields. Compound **3a** and **4a** were thoroughly characterized, including NMR, IR and MS. A crystallographic structure determination of **4a** was also performed and was in good agreement with the other spectroscopic data. The rarely observed coupling of $C_{carbene}$ with ^{107}Ag and ^{109}Ag was detected in the ^{13}C-NMR spectrum of **4a**. The previously reported imidazolium salt **3b** and Ag(I) *N*-heterocyclic carbene **4b** were also prepared.

Chapter 3:

Synthesis, characterization and properties of new Rh(III) *N*-heterocyclic carbene complexes

3.1 The scope of the chapter

In this chapter, Rh(III) complexes **8** and **9** (**Figure 20**) have been prepared and thoroughly characterized. It is hoped that these complexes after further studies may be useful catalysts, for example in catalytic hydrogenation, hydroformylation, ethylene dimerization or C-H functionalization by virtue of them having a potentially labile coordination site.[12] As is seen from **Figure 20** complexes **8** and **9** bear a chelating imino-functionalized *N*-heterocyclic carbene in which the imine may decoordinate to create an open coordination site were catalysis can occur after binding of a substrate. Another option for creating an open coordination site may be to remove a chloride by using a silver salt such as AgOTf.[12]

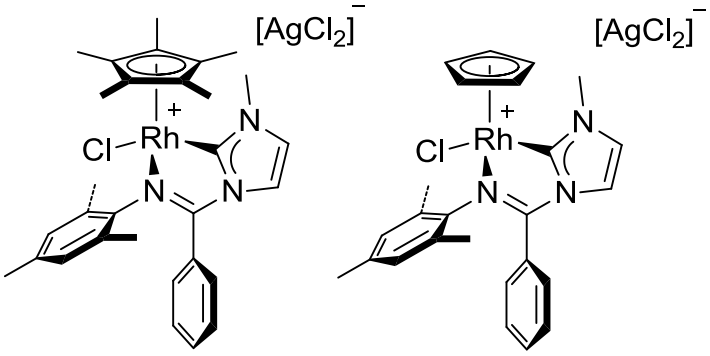

8 **9**

Figure 20: The two new Rh(III) complexes **8** and **9**.

3.2 Results and discussion

As precursors for complexes **8** and **9** the two chloride bridged Rh(III) dimers **5** and **6** shown in **Figure 21** were chosen. An attempt to make a Rh(I) complex from Rh(I) dimer **7**, was also performed, however, this turned out to be less successful.

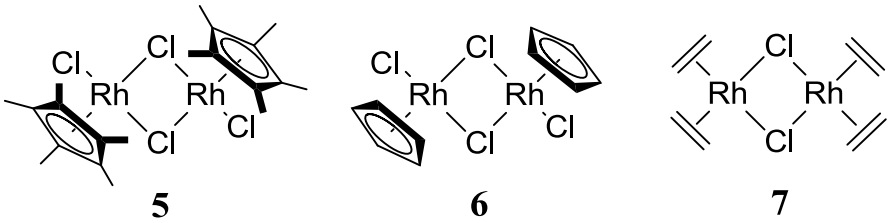

Figure 21: Rh dimers **5** [52], **6** [53] and **7** [54].

Two electron donor ligands are known to cleave dimers such as **5-7** to form monomeric products.[20-21] The strategy was to attempt to coordinate the desired *N*-heterocyclic carbene ligand to Rh by cleavage of these dimers. A successful attempt on preparating a *N*-heterocyclic carbene from complex **5** has been reported previously.[55]

As discussed in the Introduction, Ag(I) *N*-heterocyclic carbenes are versatile precursors for making metal complexes of *N*-heterocyclic carbenes, especially when it is not possible to generate the free carbene, as is the case with the ligand system used in this work.[20-21] Therefore, it was chosen to go via the Ag(I) carbene to make the desired Rh complexes. The Ag(I) carbene of choice is shown in **Figure 22**. The synthesis and characterization of Ag(I) carbene **4a** was discussed in the previous chapter.

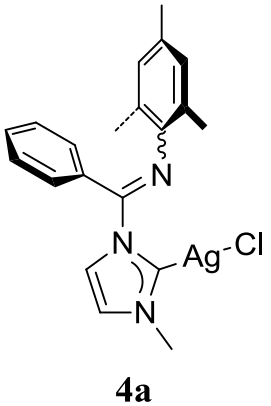

4a

Figure 22: Ag(I) carbene **4a**.

3.2.1 Synthesis and characterization of Rh(III) and Rh(I) dimers 5, 6 and 7

Three different chloride bridged Rh(III) and Rh(I) dimers were prepared by previously reported procedures.[52-54] Rh dimers **5-7** were synthesized according to **Scheme 7** giving **5** in a good yield and **6** and **7** in poor yields. Compounds **5-7** are stable in air. Compound **7** is thermally unstable and could only be handled at room temperature for short periods of time.[54]

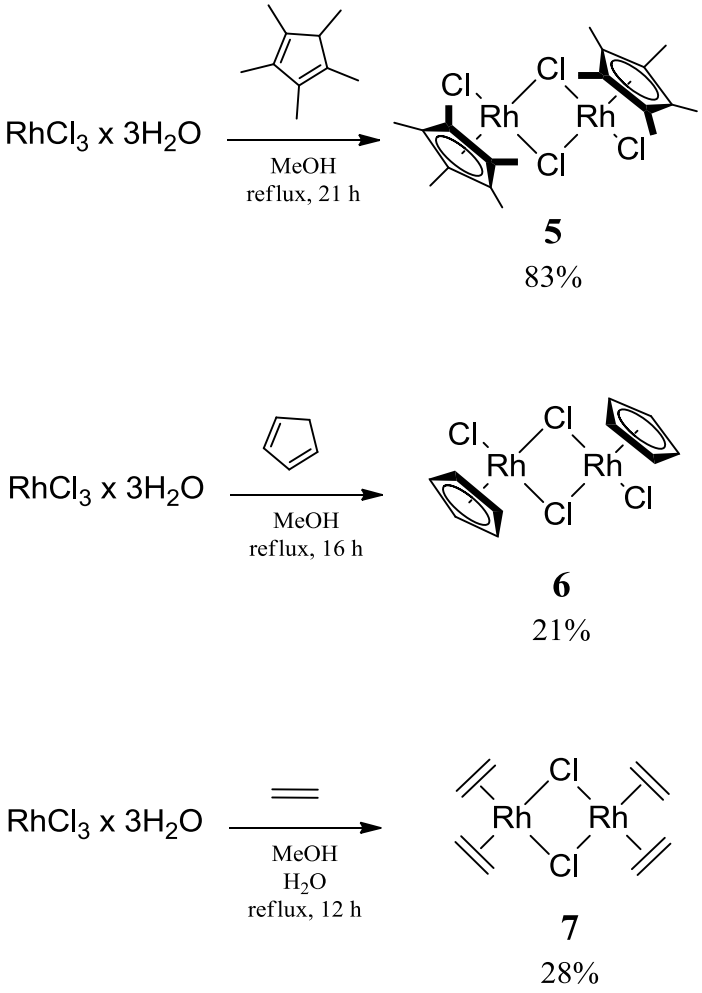

Scheme 7: Synthesis of Rh-complex **5 - 7**.[52-54]

The synthesis of compound **6** should, according to literature, yield around 60%.[53] The yield for compound **7** is reported on the low side due to work-up problems. Since these are previously reported reactions, too much effort was not put into optimizing the yields.[54]

^{1}H-NMR data corresponded with the reported data for compound **5** and **7**.[52-54] Compound **5** shows the characteristic singlet for the methyls on the Cp* at 1.60 ppm and compound **7** shows the characteristic broad peak at 2.84 ppm for the two ethylenes due to hindered rotation

around the Rh-ethylene bond. Compound **6** is not very soluble in any common organic solvents, and is therefore hard to characterize.[53] However, if **6** is suspended in DMSO-d_6 a homogenous mixture eventually forms and it is possible to obtain a NMR spectrum of something that is probably [$CpRhCl_2$(DMSO-d_6)]. A singlet at 6.02 ppm which probably stems from the Cp is observed in the ^{1}H-NMR spectrum. Compound **7** was only characterized by ^{1}H-NMR due to its thermal instability.

3.2.2 Synthesis of Rh(III) complex 8

The Rh(III) *N*-heterocyclic carbene complex **8** was synthesized in good yields by a carbene transfer reaction from the Ag(I) carbene **4a** to Rh as shown in **Scheme 8**. N_{imine} forms a chelate by displacing one of the chlorides and thus creates a cationic Rh(III) complex. Complex **8** is a Rh(III) d^6 18 electron complex and is stable towards air over long periods of time.

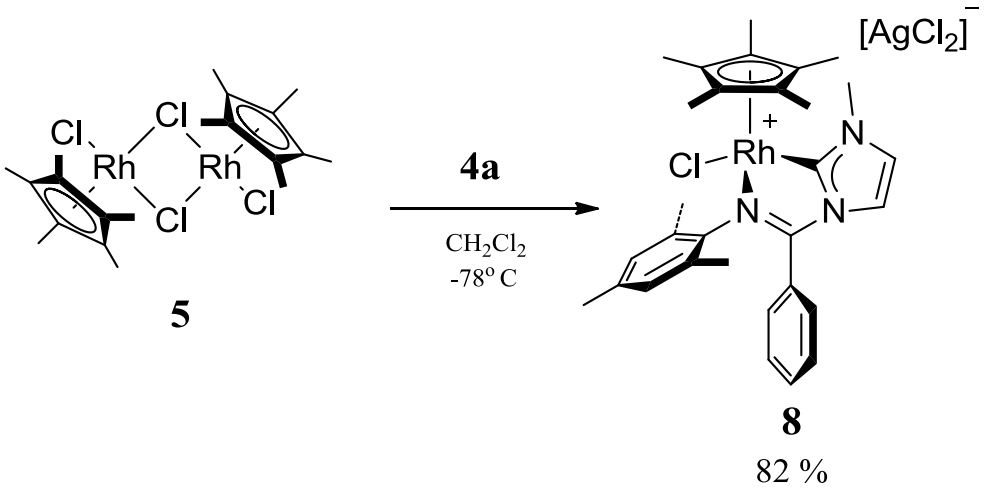

Scheme 8: Synthesis of the new Rh(III) complexes **8** and **9**.

3.2.3 Characterization of Rh(III) complex 8

Rh(III) complex **8** was characterized by NMR, MS, IR and single crystal X-ray analysis. A variable temperature NMR investigation also proved valuable for the characterization, since not all the peaks were clear at room temperature.

3.2.3.1 NMR, IR and MS

In the ^{1}H-NMR spectrum of **8** the characteristic resonance of the Cp* is seen at 1.49 ppm. The two methyls and the two *meta* protons on the mesityl appears to be chemically inequivalent, they give two different peaks in the ^{1}H-NMR indicating that there is some hindered rotation present in the complex. The four protons in *ortho* and *meta* position on the phenyl substituent give rise to four broad peaks indicating some dynamic behavior in the complex, this will be

discussed further in detail later in the text. The $C_{carbene}$ was observed at 184.46 ppm in the ^{13}C-NMR spectrum and a splitting with the NMR active spin ½ ^{103}Rh was observed, $^{1}J(^{103}Rh\text{-}^{13}C)$ = 51 Hz. A splitting of the ^{13}C-NMR signal of Cp* was also observed.

Upon investigation by mass spectrometry (MS), the parent peak of the cationic part of complex **8** was observed. High resolution mass spectrometry (HRMS) confirmed that the elemental composition of this peak was correct.

The IR stretch of the imine can give an indication on whether or not the N_{imine} is coordinated to the metal. If the N_{imine} is coordinated to the metal the C=N bond will be weakened and the $\nu_{C=N}$ will be lowered. $\nu_{C=N}$ for a free imine is usually between 1690-1640 cm^{-1}.[50] The IR stretches of the imine in imidazolium salt **3a**, Ag(I) complex **4a** and Rh(III) complex **8** are listed in **Table 3**.

Table 3: $\nu_{C=N}$ for imidazolium salt **3a**, Ag(I) complex **4a** and Rh(III) complex **8**.

	3a	**4a**	**8**
$\nu_{C=N}$	1674 cm^{-1}	1663 cm^{-1}	1615 cm^{-1}

As seen from **Table 3** the $\nu_{C=N}$ of Rh(III) complex **8** is significantly lower than those for the imidazolium salt **3a** and Ag(I) carbene **4a** indicating a coordination of the N_{imine} to Rh in complex **8.** This was later confirmed by single crystal X-ray analysis which will be discussed later. The IR stretch of the imine in the imidazolium salt **3a** and the Ag(I) complex **4a** are within the range for a free imine.

3.2.3.2 Crystallographic structure determination of complex 8

Crystals of **8** were grown by diffusion crystallization. A nearly saturated solution of **8** in CH_2Cl_2 was layered with Et_2O to form the crystals. At first, very small crystals were formed, but after several days the crystals grew larger. An X-ray analysis of **8** was performed by Professor Carl Henrik Gørbitz and Sigurd Øien. The structure of the cationic part of complex **8** based on the X-ray analysis is given in **Figure 23**. The structure is in agreement with the other spectroscopic data for **8** discussed earlier. The three legged piano stool-geometry is evident. As expected from the IR-measurements discussed earlier, chelation of the N_{imine} is observed, forming a five membered metallocycle. Both the phenyl and the mesityl substituents are rotated out of plane compared to the heterocyclic ring due to steric hindrance. This is consistent with what was seen in the ^{1}H-NMR spectrum of **8** where both the mesityl and the phenyl substituent were hindered from rotating freely. This hindered rotation was investigated by variable temperature NMR which will be discussed later.

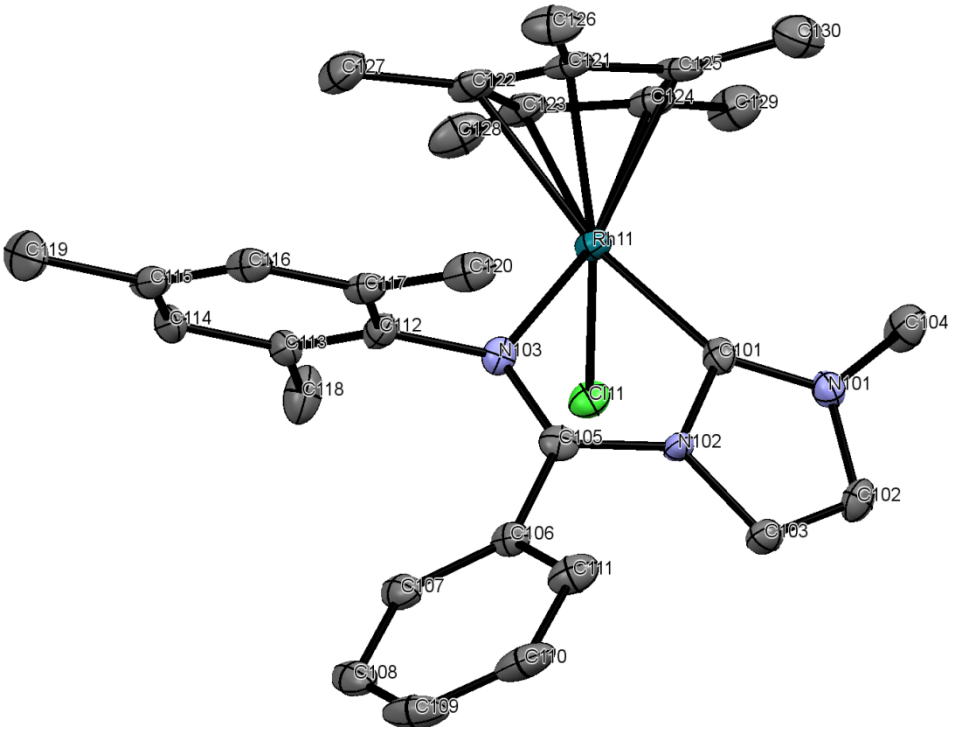

Figure 23: ORTEP-drawing of Rh(III) complex **8**. Hydrogens, the anions and CH_2Cl_2 are omitted for clarity. Ellipsoids at 50% probability.

The counteranion for complex **8** turned out not to be Cl^- as expected. For each cation it appears that there are a 1/4 $[AgCl_2]^-$ unit and a 1/8 $[Ag_6Cl_{12}]^{6-}$ unit.

This is also supported by the data obtained by MS. In MS, with detection of negative ions, a fragment corresponding to n$[AgCl_2]^{n-}$ was observed. It is not possible to determine if this fragment is $[AgCl_2]^-$, $[Ag_2Cl_4]^{2-}$ or any other values of n without looking at the isotopic pattern since the information obtained from MS is the mass/charge (*m/z*) value, which will be the same for all of these fragments.[50] By looking at the isotopic pattern and the spacing of the peaks seen by MS, an isotopic pattern similar to the one expected for $[AgCl_2]^-$ was observed together with a spacing of the peaks in the isotopic pattern by two units indicating that $[AgCl_2]^-$ is likely to be the true identity of the peak.[56] HRMS confirms that the peak seen actually corresponds to $[AgCl_2]^-$.

$[Ag_nX_{2n}]^{n-}$ anions sometimes forms when utilizing Ag(I) carbenes as carbene transfer reagents. Danopoulos and co-workes reported a mixture of Cl^- and $[AgCl_2]^-$ anions when transferring a *N*-heterocyclic carbene from its corresponding Ag(I) carbene to Pd(II).[57] Wittlesey and co-workers observed $[AgBr_2]^-$ as the anion upon preparing an Ir(I) *N*-heterocyclic carbene.[58]

Complex **8** has a triclinic unit cell unit with space group $P\bar{1}$. The unit cell of **8** consists of 4 cations, 1 $[AgCl_2]^-$ unit and 1/2 $[Ag_6Cl_{12}]^{6-}$ unit (see **Figure 24**).

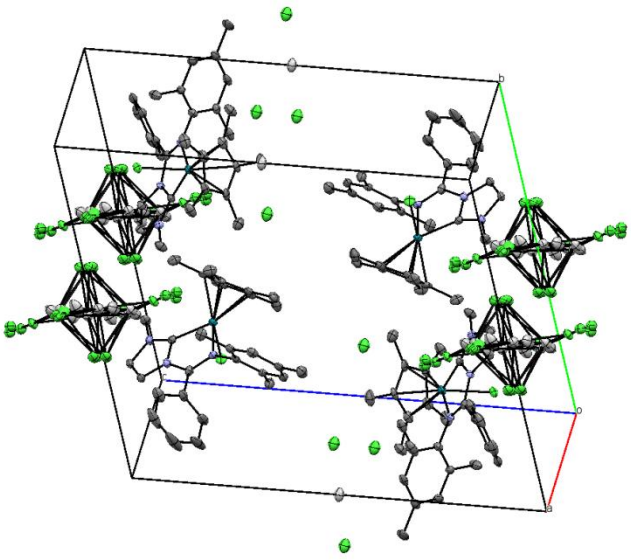

Figure 24: ORTEP-drawing of the unit cell of Rh(III) complex **8**. Hydrogens and CH_2Cl_2 are omitted for clarity. Ellipsoids at 50% probability.

A close-up view of the $[Ag_6Cl_{12}]^{6-}$ cluster is shown in **Figure 25.** The $[Ag_6Cl_{12}]^{6-}$ cluster consists of two different $[Ag_3Cl_6]^{3-}$ units which are rotated 90^o with respect to each other. Each of them are disordered through a centre of inversion which has the effect that in some places in the structure, up to four different atomic positions end up superimposing each other. Such a structure has to the best of our knowledge not been reported before. Selected bond lengths and bond angles for complex **8** are given in **Table 4** and **Table 5**.

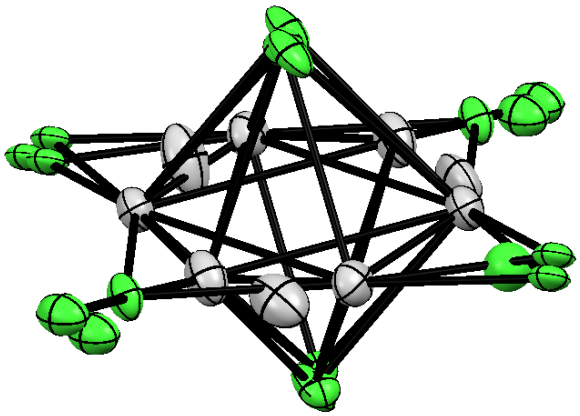

Figure 25: ORTEP-drawing of the $[Ag_6Cl_{12}]^{6-}$ cluster in Rh(III) complex **8**. Ellipsoids at 50% probability.

Table 4: Selected bond lengths from the structure based on the X-ray analysis of Rh(III) complex **8**.

Bond	Bond length [Å]	Bond	Bond length [Å]
Rh(11)-C(101)	2.014(4)	C(105)-N(103)	1.289(5)
Rh(11)-N(103)	2.137(3)	C(101)-N(101)	1.328(5)
Rh(11)-Cl(11)	2.4058(11)	C(101)-N(102)	1.375(5)
Rh(11)-C(121)	2.166(4)	C(121)-C(122)	1.453(7)
Rh(11)-C(122)	2.241(4)	C(122)-C(123)	1.400(6)
Rh(11)-C(123)	2.229(4)	C(123)-C(124)	1.450(6)
Rh(11)-C(124)	2.163(4)	C(124)-C(125)	1.423(6)
Rh(11)-C(125)	2.183(4)	C(125)-C(121)	1.434(6)
Rh(11)-Cp(avg.)	2.196		

Table 5: Selected bond angles from the structure based on the X-ray analysis of Rh(III) complex **8**.

Angle	Bond angle [°]
C(101)-Rh(11)-N(103)	76.01(15)
C(101)-Rh(11)-Cl(11)	79.07(12)
N(103)-Rh(11)-Cl(11)	91.21(10)
N(101)-C(101)-N(102)	104.9(4)
N(101)-C(101)-Rh(11)	136.6(3)
N(102)-C(101)-Rh(11)	115.5(3)

Based upon the information gained by MS and crystallographic structure determination it will be assumed that with each cation, there is one $[AgCl_2]^-$ fragment associated. Therefore, the molecular formula $[Cp^*RhCl(NHC)]^+[AgCl_2]^-$ was used to determine the yield of the reaction.

3.2.4 Synthesis of Rh(III) complex 9

The Rh(III) *N*-heterocyclic carbene complex **9** was synthesized in good yields by a carbene transfer reaction from the Ag(I) carbene **4a** to Rh as shown in **Scheme 9**. The N_{imine} forms a chelate by displacing one of the chlorides and thus creates a cationic Rh(III) complex. Complex **9** is a Rh(III) d^6 18 electron complex and is stable towards air over longer periods of time.

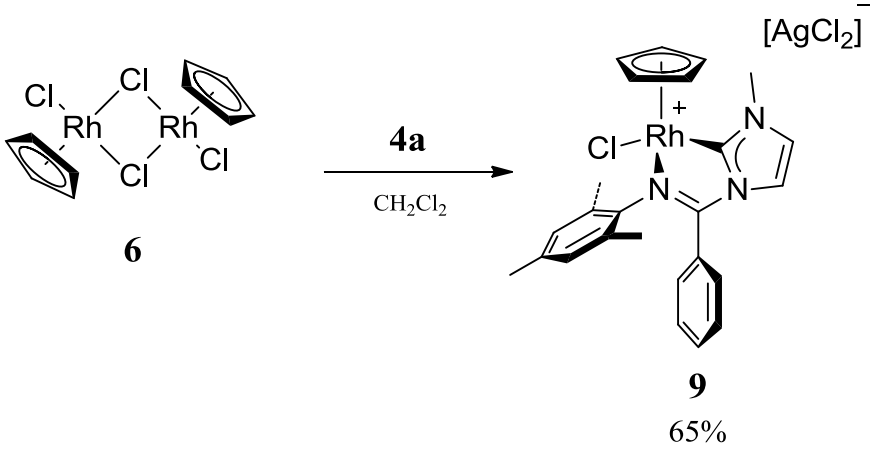

Scheme 9: Synthesis of Rh(III) complex **9**.

3.2.5 Characterization of Rh(III) complex 9

Rh(III) complex **8** was characterized by NMR, MS, IR and single crystal X-ray analysis. A variable temperature NMR investigation also proved valuable for the characterization, since not all the peaks were clear or visible at room temperature

3.2.5.1 NMR, IR and MS

In the ^{1}H-NMR spectrum of **9** the characteristic resonance of the Cp is seen at 5.68 ppm. The two methyls and the two *meta* protons on the mesityl appear to be chemically inequivalent and give two different peaks in the ^{1}H-NMR indicating that there is some hindered rotation present in the complex, as was also observed for complex **8**. The two protons in *meta* position on the phenyl substituent give rise to a broad peak. At room temperature the peaks of the two protons in *ortho* position could not be observed due to their broadness at this temperature. The dynamic features of the ^{1}H-NMR spectrum will be discussed in more detail later in the text. The $C_{carbene}$ was observed at 181.75 ppm in the ^{13}C-NMR spectrum and a splitting with the NMR active spin ½ ^{103}Rh was observed, $^{1}J(^{103}\text{Rh}\text{-}^{13}\text{C})$ = 46.8 Hz. A splitting of the ^{13}C-NMR signal of the Cp was also observed.

Upon investigation by MS, the peak of the cationic part of the complex **9** was seen. HRMS confirmed that the elemental composition of this peak was correct. A lowering of $\nu_{C=N}$ compared to the $\nu_{C=N}$ of Ag(I) carbene **4a** indicates a coordination of the N_{imine} to Rh. This was later supported by X-ray analysis.

3.2.5.2 Crystallographic structure determination of complex 9

Crystals of complex **9** were grown by the vapor diffusion-diffusion technique.[59] A small capped vial with a small opening on the top containing a nearly saturated solution of **9** in CH_2Cl_2 was placed into a larger vial containing Et_2O. The crystals were formed within 24 hours.

An X-ray analysis of **9** was performed by Professor Carl Henrik Gørbitz and Sigurd Øien. The structure of complex **9** based on the X-ray analysis is shown in **Figure 26**. The structure is in agreement with the other spectroscopic data on **9** discussed earlier. As complex **8**, **9** also show the three legged piano stool-geometry. Chelation of the N_{imine} is observed, consistent with the IR data of complex **9** discussed earlier. The phenyl and the mesityl are rotated out of plane compared to the heterocyclic ring due to steric hindrance. This is consistent with what was seen in the ^{1}H-NMR spectrum of **9** where both the mesityl and the phenyl substituent were hindered from rotating freely. This hindered rotation was investigated by variable temperature NMR which will be discussed later.

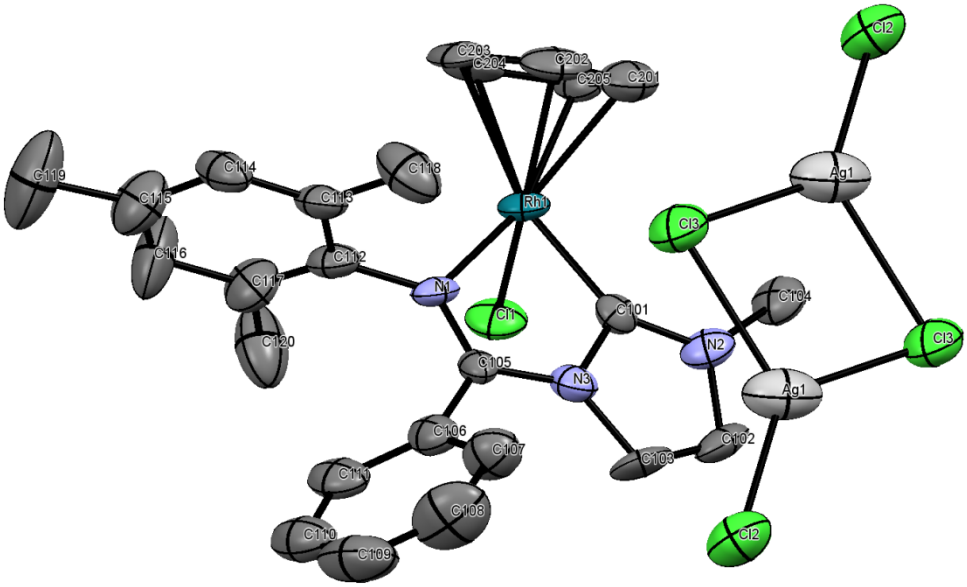

Figure 26: ORTEP-drawing of Rh(III) complex **9**. Hydrogens and disordered CH_2Cl_2 are omitted for clarity. Ellipsiods at 50% probability.

The crystal structure of **9** was recorded at 193 K, while the crystal structure of **8** was recorded at 105 K. At higher temperature, there will be more thermal vibrations, which lead to larger and more elongated ellipsoids. This is seen in the ORTEP-drawing of structure **9** (see **Figure 26**).

As for compound **8**, the anion is not the expected Cl^- in complex **9**. For **9**, a silver-chloride cluster is also observed. In complex **9** one $[Ag_2Cl_4]^{2-}$ unit is shared between two cations. The unit cell of compound **9** is given in **Figure 27**. The unit cell is triclinic with space group $P\overline{1}$ and consists of two cations sharing one $[Ag_2Cl_4]^{2-}$ unit. This is also supported by the data obtained by MS. In MS, with detection of negative ions, a fragment corresponding to $[AgCl_2]^-$ was observed.

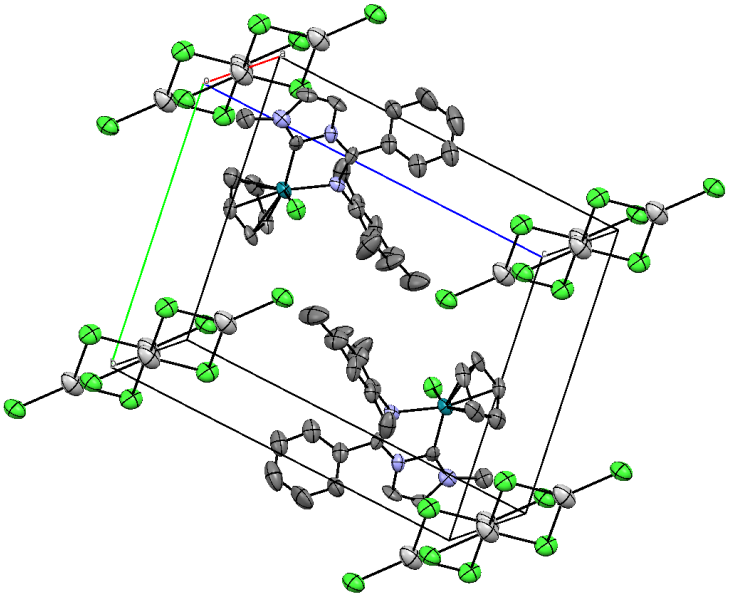

Figure 27: ORTEP-drawing of the unit cell of Rh(III) complex **9**. Hydrogens and CH_2Cl_2 are omitted for clarity. Ellipsoids are shown at 50% probability.

Based upon the information gained by MS and crystal structure determination it will be assumed that with each cation, there is one $[AgCl_2]^-$ fragment associated. Therefore, the molecular formula $[CpRhCl(NHC)]^+[AgCl_2]^-$ was used to determine the yield of the reaction.

Selected bond lengths and bond angles for Rh(III) complex **9** are given in and **Table 6** and **Table 7**.

Table 6: Selected bond lengths from the structure based on the X-ray analysis of Rh(III) complex **9**.

Bond	**Bond length [Å]**	**Bond**	**Bond length [Å]**
Rh(1)-C(101)	1.989(11)	C(105)-N(1)	1.273(13)
Rh(1)-N(1)	2.097(9)	C(101)-N(2)	1.335(14)
Rh(1)-Cl(1)	2.380(3)	C(101)-N(3)	1.375(13)
Rh(1)-C(201)	2.160(13)	C(201)-C(202)	1.391(19)
Rh(1)-C(202)	2.160(12)	C(202)-C(203)	1.462(19)
Rh(1)-C(203)	2.214(11)	C(203)-C(204)	1.389(16)
Rh(1)-C(204)	2.211(11)	C(204)-C(205)	1.410(17)
Rh(1)-C(205)	2.165(11)	C(205)-C(201)	1.411(17)
Rh(1)-Cp(avg.)	2.182		

Table 7: Selected bond angles from the structure based on the X-ray analysis of Rh(III) complex **9**.

Angle	Degrees [^{o}]
C(101)-Rh(1)-N(1)	76.2(4)
C(101)-Rh(1)-Cl(1)	83.5(3)
N(1)-Rh(1)-Cl(1)	92.9(2)
N(2)-C(101)-N(3)	106.9(9)
N(2)-C(101)-Rh(1)	137.3(8)
N(3)-C(101)-Rh(1)	114.8(8)

3.2.6 Comparison of the spectroscopic properties and structures of Rh(III) complexes 8 and 9

At room temperature, the ^{1}H-NMR spectra of both compound **8** and **9** indicate that there is hindered rotation within the complexes. The ^{1}H-NMR spectra of compound **8** and **9** with a close-up view of the aromatic region are given in **Figure 28**. For both complexes the mesityl group is prevented from rotating freely around the $N_{imine.}$-mesityl bond, which is shown in the NMR spectra given in **Figure 28** by that the two *meta* protons on the mesityl substituent turn out to be chemically inequivalent, that is; they give rise to two different chemical shifts. Dynamic behavior within the NMR timescale is observed for the phenyl substituent in both complexes. The phenyl substituent is prevented from rotating freely around the C_{imine}-Ph bond resulting in four broad peaks for the *ortho* and *meta* protons on the phenyl substituent in complex **8**, in **9** a broad peak of the two *meta* protons and the absence of the peak of the two *ortho* protons on the phenyl substituent is observed. This dynamic behavior was investigated further by variable temperature NMR which will be discussed later in the text.

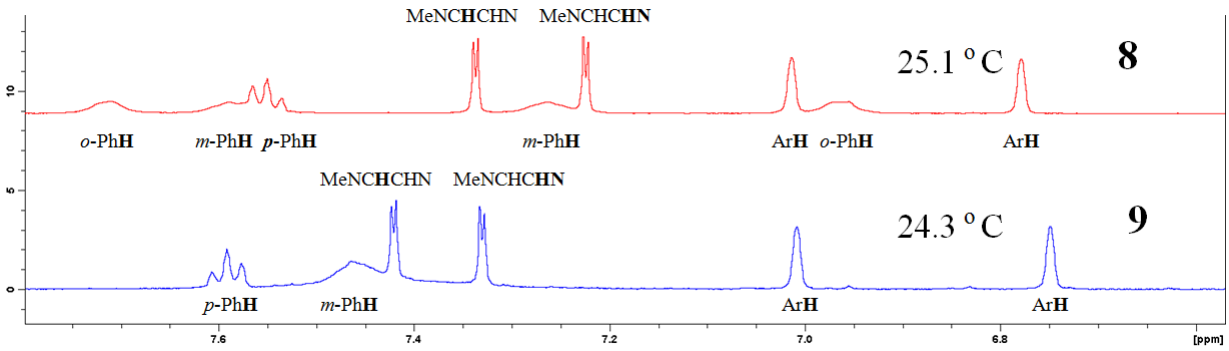

Figure 28: ^{1}H-NMR spectra of compound **8 (**top) and compound **9** (bottom) at ambient temperature.

For all the bonds connected to Rh, the bonds in complex **8** are slightly longer than those in complex **9**. For example, the Rh-$C_{carbene}$ bond in complex **8** is 2.014(4) Å where in complex **9** it is 1.989(11) Å. The N_{imine} is bond more tightly in complex **9** than in complex **8**. The reasons for this might be due to the steric effects of the Cp^*. The Cp^* is significantly larger than the Cp.[12] The average bond length of the bonds between the carbons in the Cp^* and Rh in complex **8** are longer than the average length of the bonds between the carbons in the Cp and Rh in complex **9**. For both complexes **8** and **9** the bonds between the $C_{carbene}$ and the α-nitrogens show a significant double bond character. A normal C-N single bond is usually within the range of 1.46-1.48 Å, while in complexes **8** and **9** they range from 1.33-1.38 which is considerably shorter.[15] This indicates a donation of the lone-pair on the nitrogens into the empty *p*-orbital on the carbene to stabilize the carbene, as was discussed in the introduction section.[14]

The lengths of the bonds between the metal and the N_{imine} and the lengths of the C=N bonds of **4a**, **8** and **9** are listed in **Table 8**. For the two compounds where the N_{imine} is coordinated to the metal, the C=N bond is increased. For complex **4a**, which has been discussed in the previous chapter, no significant coordination of the N_{imine} is seen in the structure based on X-ray analysis, and the C=N bond is shorter. These bond lengths based on the X-ray analysis are also consistent with the $\nu_{c=N}$ of the imines as discussed earlier. The uncoordinated imine in complex **4a**, shows a higher $\nu_{C=N}$ and thus a shorter C=N bond than the coordinated imines in complex **8** and **9**.

Table 8: Bond lengths for the metal-N_{imine} bonds and the C=N bonds in complexes **4a**, **8** and **9**.

	4a	**8**	**9**
N_{imine}-M bond length	-	2.137(3) Å	2.097 (9) Å
C=N bond length	1.264(10) Å	1.289(5) Å	1.273(13) Å
$\nu_{C=N}$	1663 cm^{-1}	1615 cm^{-1}	1616 cm^{-1}

For both complexes **8** and **9** the bite angle of the N_{imine}-Rh-$C_{carbene}$ chelate is close to 76°. In comparison, previously reported square planar complexes bearing this type of chelating *N*-heterocyclic carbene published by our group show N_{imine}-Rh-$C_{carbene}$ bite angles in the range 78-79°. [6] For complex **8** the $C_{carbene}$-Rh-Cl angle is slightly smaller than for complex **9**, this is probably due to the Cp^* being more sterically demanding compared to Cp. The same is seen for the N_{imine}-Rh-Cl angle.

One can not say if the preferred conformation in solution is the same as the solid state structure. However, it is possible to do some experiments to support the structure based on the X-ray analysis. By performing a NOESY NMR experiment, showing which protons are close in space, a few things that support the X-ray structure were observed.[48]

1. The methyl sitting on the nitrogen in the imidazolylidene is pointing towards the Cp.
2. One of the *ortho* methyls on the mesityl is pointing towards the Cp.

The above mentioned NOE correlations were observed for complex **9**. The NOE correlations are shown in **Figure 29**, the correlations of interest are circled. Since the NOESY spectrum was measured on a solution of complex **9**, it supports that the solid state structure might also be the preferred conformation in solution. The same correlations were observed for complex **8**, however, for **8** a NOE correlation between both the *ortho* methyls was observed.

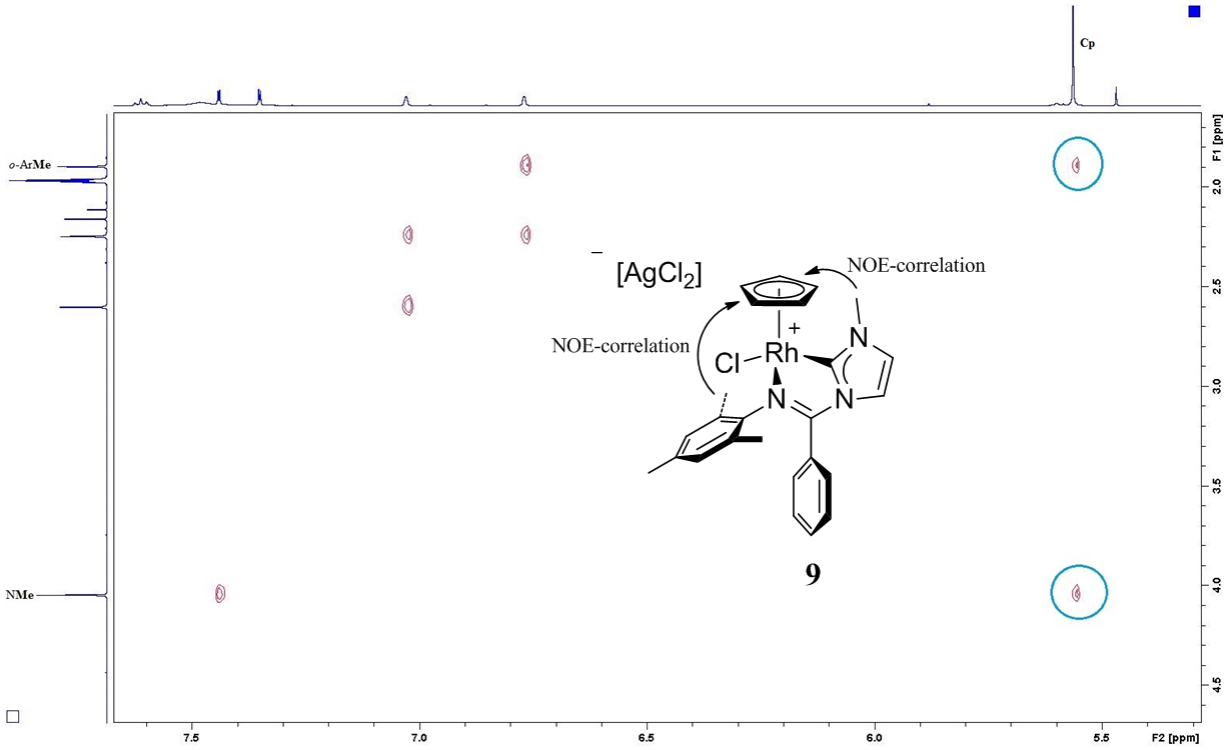

Figure 29: NOESY (600 MHz, MeCN-d_3, mixing time = 1.20 s) of **9**. The NOE correlations discussed in the text are circled.

3.2.7 Chirality of complexes 8 and 9

The two Rh(III) complexes prepared, **8** and **9**, have a stereogenic centre at Rh and are thus chiral. The separation of the two enantiomers or an enantioselective synthesis of them was not investigated. It was chosen to represent the complexes as the same enantiomers as was seen in the crystal structures. However, it should be kept in mind that the synthesis route chosen to prepare these complexes gives a racemic mixture.

3.2.8 Variable temperature NMR of complexes 8 and 9

Due to the mentioned indications of fluxional behavior of **8** and **9** the ^{1}H-NMR spectra of complex **8** and **9** were recorded at different temperatures. For complex **8**, ^{1}H-NMR spectra were recorded at temperatures ranging from 1.1 ^{o}C to 77.4 ^{o}C and for complex **9** at temperatures ranging from -39.3 ^{o}C to 66.2 ^{o}C. Deuterated acetonitrile, which has a liquid range from -45 ^{o}C to 82 ^{o}C was used. In all the NMR spectra discussed in this section, it is chosen to show only the spectra of the aromatic region, as this is where the peaks of interest are located, the complete spectra can be found in Appendix. The assignments of the peaks were shown in **Figure 28**.

3.2.8.1 Variable temperature NMR of complex 8

As mentioned previously the mesityl substituent in complex **8** is prevented from rotating freely. Upon raising the temperature on complex **8** no significant broadening of the resonances of the mesityl is observed, indicating a large barrier to rotation for this substituent. The hindered rotation is also consistent with what is seen in the crystal structure of **8** (see **Figure 23**). If the mesityl substituent wants to rotate, there will be a steric clash with both the Cp* and the phenyl.

The phenyl group, however, rotates more freely than the mesityl. The spectrum of **8** shows a slow rotation at 25 ^{o}C as is seen from **Figure 30**. Four broad signals are seen for the protons in *ortho* and *meta* position indicating that the protons have a different magnetic environment. The broadening of the peaks indicate that there is still some rotation present, if the phenyl was not rotating at all, sharp signals and splitting with the adjacent protons would be seen as well. The proton in *para* position gives a triplet, since the magnetic environment for this position would not change upon rotation around the C_{imine}-Ph bond. The broadening of the peaks is also observed in the ^{13}C-NMR spectrum. **Figure 30** shows the ^{1}H-NMR spectra of **8** upon decreasing the temperature. When the temperature is decreased the phenyl rotates more slowly, and at 1 ^{o}C all the peaks of the phenyl have sharpened up and show full splitting with the adjacent protons.

The ^{1}H-NMR spectra of **8** with increasing temperature are shown in **Figure 31**. Upon raising the temperature further a faster rotation is observed. The peaks get broader until they get so broad that they are no longer visible. At 66 ^{o}C the coalesced peak at 7.44 ppm of the two peaks of the *meta* protons is observed. Due to solvent limitations it was not possible to reach high enough temperatures to see the coalesced peak for the protons in *ortho* position.

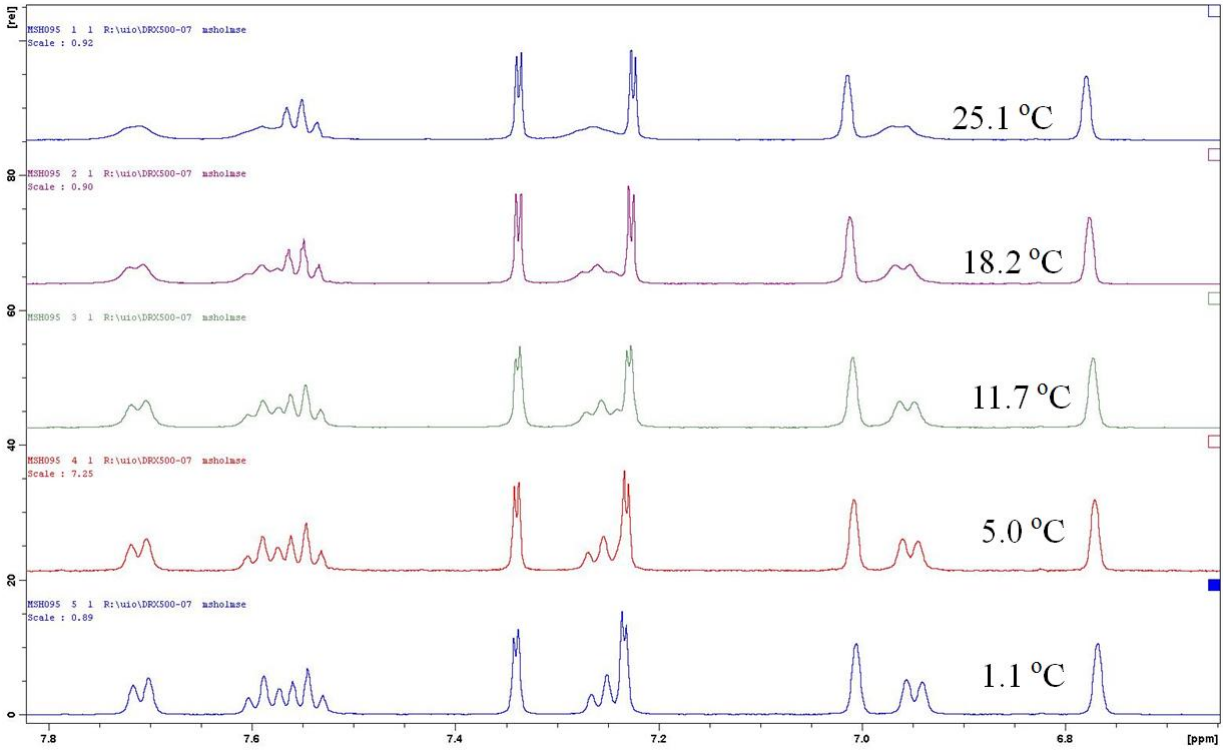

Figure 30: The ^{1}H-NMR spectra of **8** with decreasing temperature.

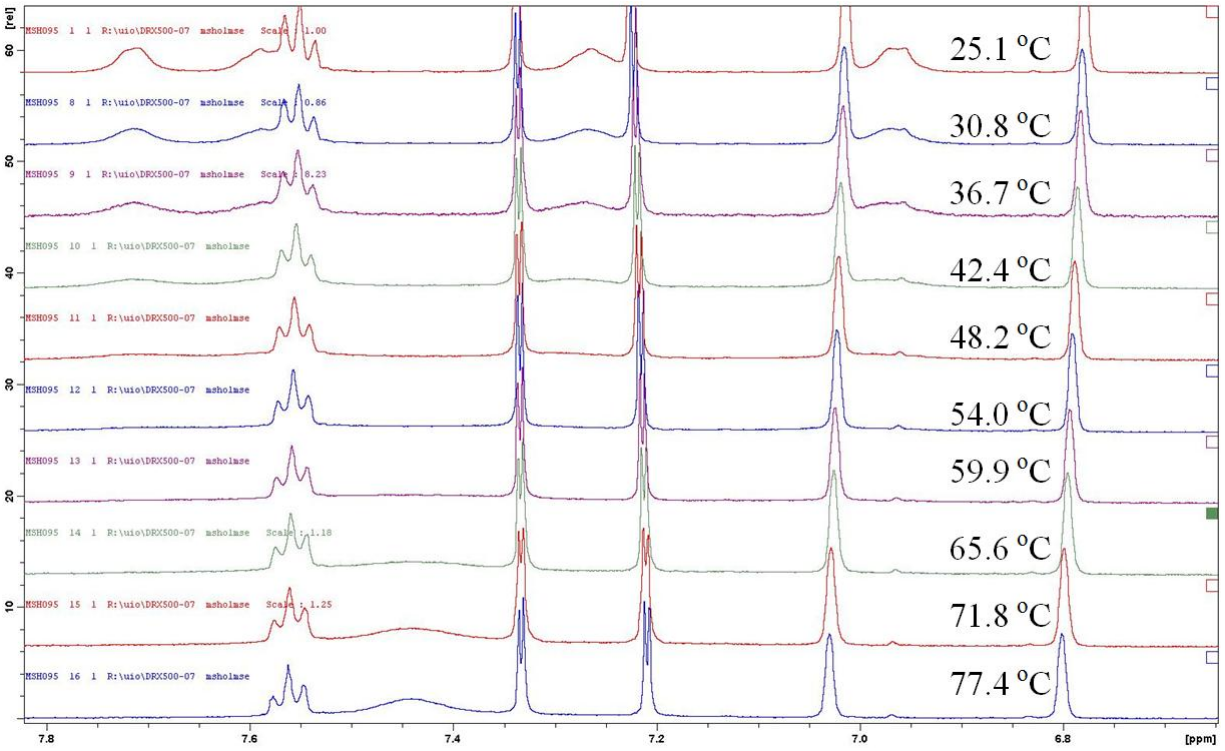

Figure 31: The ^{1}H-NMR spectra of **8** with increasing the temperature.

The rotation of the phenyl can be regarded as an exchange between the two protons in the *meta* position and an exchange between the two protons in the *ortho* position. Such exchange can be seen in a NOE-experiment. The NOESY spectrum of **8** is shown in **Figure 32**. Off-diagonal peaks in the NOESY spectrum that have the same phase (colour) as the peaks on the diagonal may be either peaks due to a COSY correlation or due to an exchange process.[48] In the NOESY spectrum of **8**, such peaks are seen. These peaks are not observed in the COSY spectrum of **8** indicating that they probably occur due to an exchange process. COSY peaks in a NOESY spectrum will also have a multiplet appearance, and will not give such round peaks as seen in **Figure 32**.

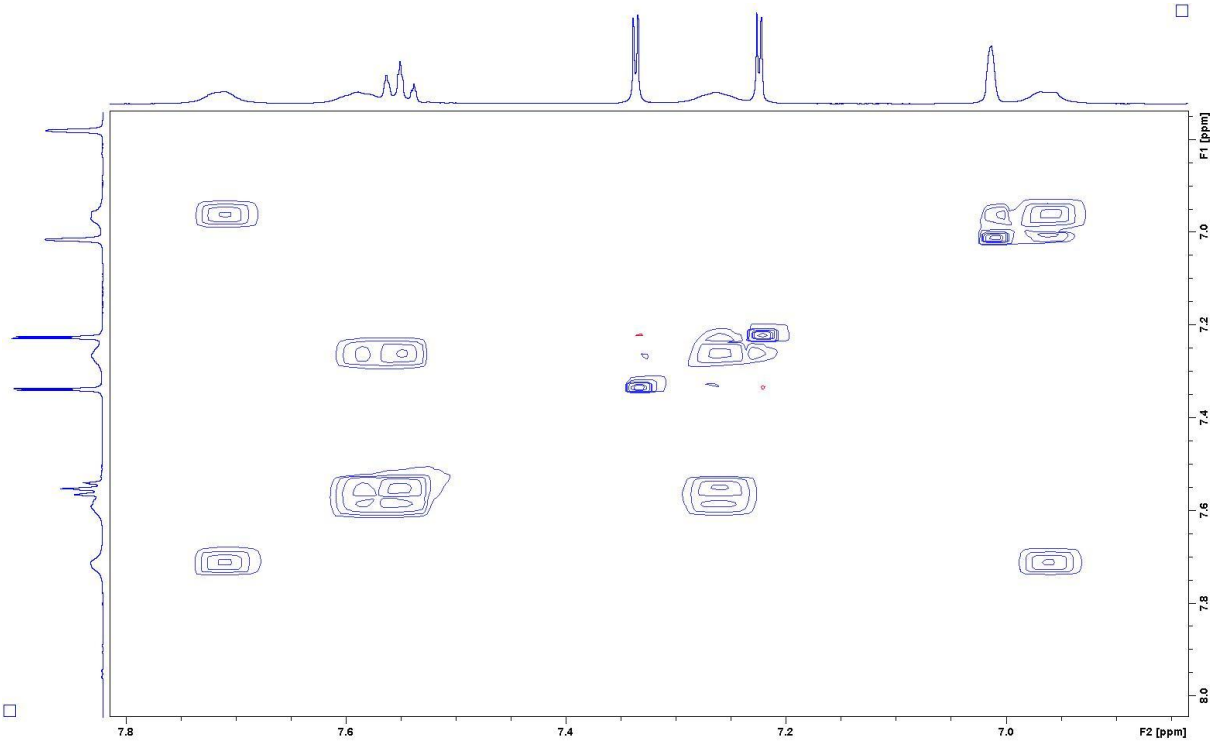

Figure 32: NOESY-spectrum (600 MHz, MeCN-d_3, mixing time = 900 ms) of **8**. The off-diagonal peaks with the same phase (colour) as the diagonal are likely due to the exchange process.

3.2.8.2 Variable temperature NMR of complex 9

The ^{1}H-NMR spectra of compound **9** upon decreasing the temperature are given in **Figure 33**. When the temperature is decreased the rotation slows down and at -9 ^{o}C the four different peaks for the four protons in *ortho* and *meta* position starts to show and they get more visible at -13 ^{o}C. At -27 ^{o}C the splitting of the peaks starts to show and at -39 ^{o}C the splitting gets even more visible. Due to solvent limitations, it was not possible to go low enough in temperature to observe full splitting.

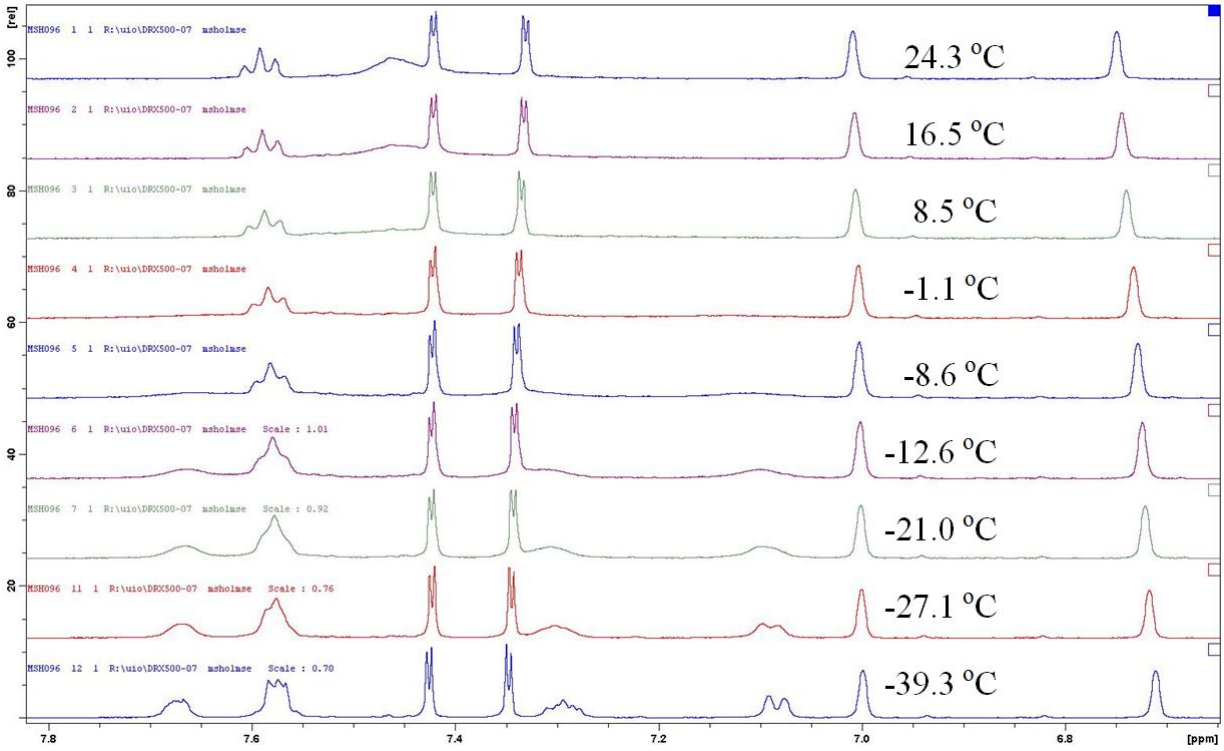

Figure 33: The ^{1}H-NMR spectra of **9** with decreasing temperature.

The ^{1}H-NMR spectra of **9** upon increasing the temperature are shown in **Figure 34**. Already at 9 ^{o}C the coalesced peak of the two *meta* protons is starting to show and at 31 ^{o}C the coalesced peak of the two protons in *ortho* position starts to show. At 54 ^{o}C the peak for the two protons in *meta* position has sharpened and at 66 ^{o}C the peak for the two protons in *ortho* position is nearly sharpened, and the phenyl group is approaching free rotation. No broadening of the peaks of the two *meta* protons on the mesityl substituent was observed upon increasing the temperature, indicating a high barrier to rotation for this substituent.

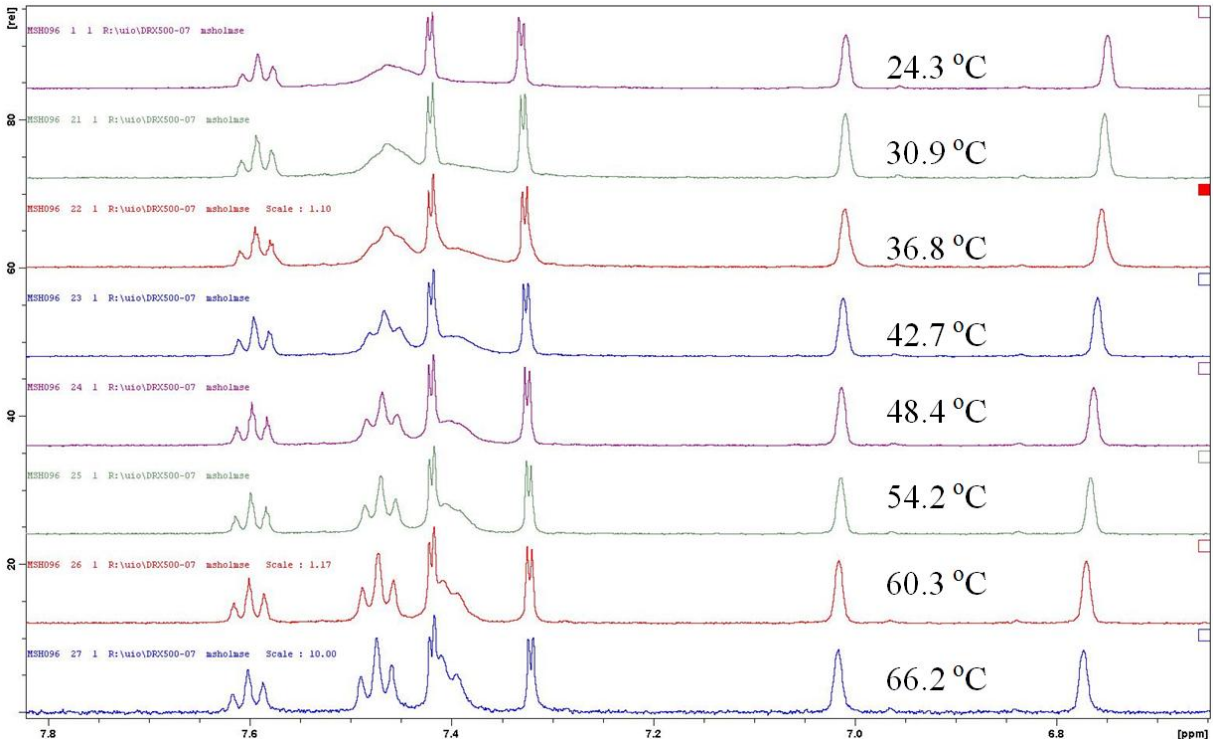

Figure 34: The ^{1}H-NMR spectra of **9** with increasing temperature.

3.2.8.2 Comparison of the dynamic behavior of 8 and 9

At room temperature, the phenyl substituent of compound **9** shows a faster rotation compared to compound **8**. The ^{1}H-NMR spectrum of compound **9** at 24 ^{o}C resembles the ^{1}H-NMR spectrum of compound **8** at 77 ^{o}C indicating that there is a substantially difference in the barrier to rotation of the phenyl substituent for the two complexes. Compound **9** carries the less sterically demanding Cp ligand compared to the large Cp* in complex **8**, which may explain the more freely rotating phenyl in complex **9**. For both complexes **8** and **9** no sign of rotation of the mesityl substituent within the NMR-timescale was observed, indicating a large barrier to rotation of this substituent.

3.2.9 Barrier to rotation: Lineshape analysis of Rh(III) complex 8

The ^{1}H-NMR spectrum of Rh(III) complex **8** was recorded at 14 different temperatures ranging from 1.1 ^{o}C to 77.4 ^{o}C. The exact temperature inside the NMR probe was measured for each experiment. It was originally planned to perform a full lineshape analysis of the data, but due to overlaps between several peaks, this was impractical. Instead, a lineshape analysis was performed in which the goodness of fit was optimized by visual inspection. A model of the spin system of the phenyl at low temperature was modeled in gNMR 5.0.[44] The ^{1}H-NMR spectrum of complex **8** at 1.1 ^{o}C was simulated in gNMR so that it resembled the experimentally acquired spectrum. Then an exchange between the two protons in *ortho* position and an exchange between the two protons in *meta* position was modeled. The rate of the exchange was changed so that one simulated spectrum that matches each of the real ones visually at all the different temperatures was obtained. The simulated spectra together with the experimental spectra are given in **Figure 35**.

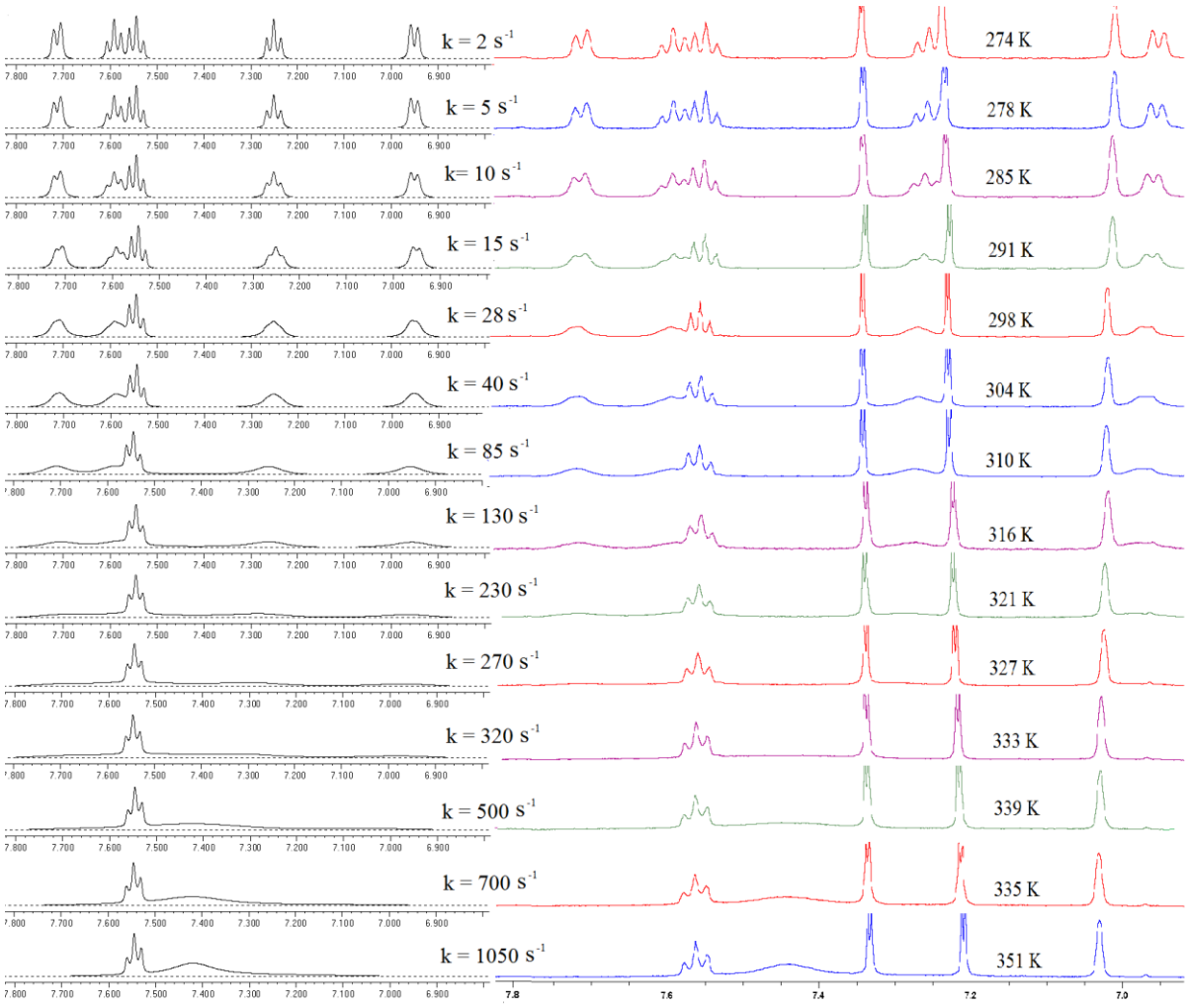

Figure 35: The simulated spectra of **8 (**left) and the experimental spectra (right).

An Eyring plot, a plot of ln(k/T), where k is the rate constant and T is the temperature in Kelvins, versus 1/T was performed.[15] Linear least square fitting of the data points were done to obtain a straight line and the enthalpy and entropy of rotation were calculated from the slope and the intercept of the linear fit (for more details see Appendix). The plot and the linear fit are given in **Figure 36**. The values obtained for the enthalpy and entropy of activation are listed in **Table 9**.

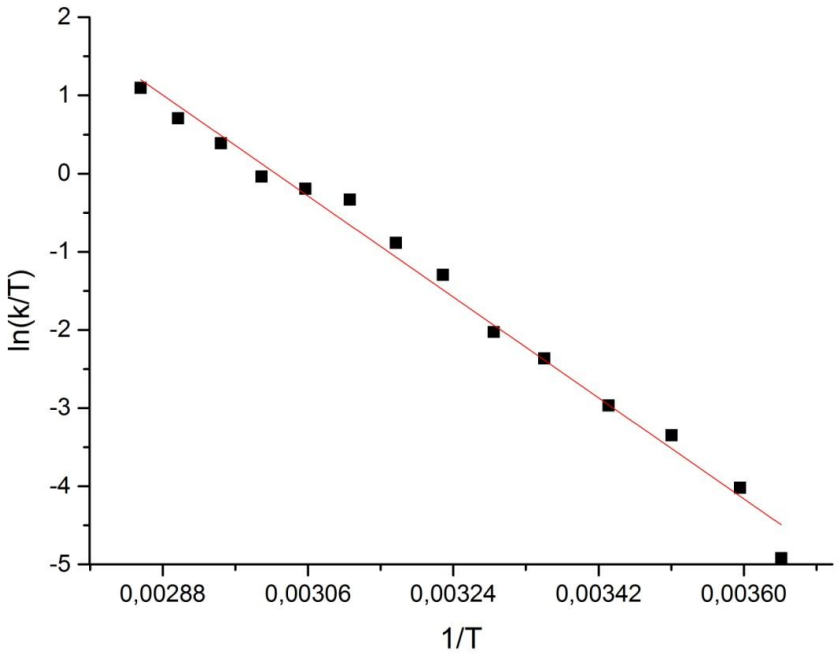

Figure 36: Eyring plot of the rotation process of the phenyl substituent in Rh(III) complex **8**. In this figure, comma is used instead of full stop to indicate the decimal points of the numbers on the axes.

Table 9: Enthalpy and entropy of rotation obtained from the visual lineshape analysis

$\Delta H^{\#}$	59.7 ± 0.4 kJ mol^{-1}
$\Delta S^{\#}$	-17.4 ± 1.4 J $K^{-1}mol^{-1}$

The enthalpy of rotation obtained from the visual lineshape analysis was 59.7 ± 0.4 kJ mol^{-1}. In comparison, the rotation of ethane from the more stable staggered form to the eclipsed form has an rotation barrier of 13 kJ mol^{-1}.[15] The entropy of rotation obtained for **8** is close to zero, as expected for such a unimolecular process as rotation. The slightly negative entropy

of rotation indicates a more ordered transition state for the rotation process. This suggests that there may be a correlated motion that involves the phenyl rotation and the conformation of the mesityl group. The mesityl group must assume a particular orientation in order to allow the rotation of the neighboring phenyl group.

Since this linshape analysis was performed only visually, there is a substantial uncertainty to the data obtained. Nevertheless, the data are consistent with such an unimolecular process as rotation.

3.2.10 Computational studies: DFT optimization of Rh(III) complex 8

The structure of the cationic part of Rh(III) complex **8** was optimized with density functional theory (DFT) calculations. For more details on how the calculations were carried out, see computational details. The optimized structure together with the experimental structure of complex **8** is given in **Figure 37**. The DFT optimization was performed with help from Dr. David Balcells.

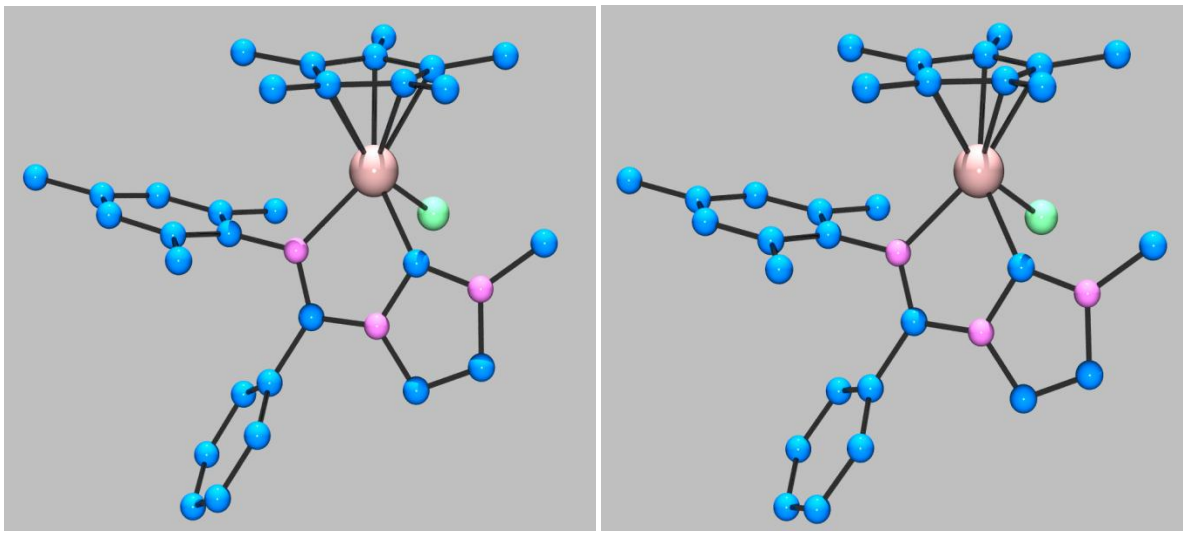

Figure 37: The DFT optimized (left) and the experimental (right) structure of complex **8**.

Selected bond lengths and angles were compared with the experimentally obtained structure, these values are listed in **Table 10** and **Table 11**.

Table 10: Selected bond lengths found in the structure based on the X-ray analysis and in the DFT optimized structure of Rh(III) complex **8**. The numbering of the atoms corresponds to the numbering scheme in **Figure 23**.

Bond	**Experimental structure Bond length [Å]**	**DFT optimized structure Bond length [Å]**
Rh(11)-C(101)	2.014(4)	1.9979
Rh(11)-N(103)	2.137(3)	2.1336
Rh(11)-Cl(11)	2.4058(11)	2.3946
Rh(11)-C(121)	2.166(4)	2.1846
Rh(11)-C(122)	2.241(4)	2.2673
Rh(11)-C(123)	2.229(4)	2.2472
Rh(11)-C(124)	2.163(4)	2.1747
Rh(11)-C(125)	2.183(4)	2.1889
Rh(11)-Cp(avg.)	2.196	2.2125
C(105)-N(103)	1.289(5)	1.2930
C(101)-N(101)	1.328(5)	1.3398
C(101)-N(102)	1.375(5)	1.3718
C(121)-C(122)	1.453(7)	1.4535
C(122)-C(123)	1.400(6)	1.4108
C(123)-C(124)	1.450(6)	1.4578
C(124)-C(125)	1.423(6)	1.4318
C(125)-C(121)	1.434(6)	1.4365

Table 11: Selected bond angles found in the experimental structure and in the DFT optimized structure of Rh(III) complex **8**.

Angle	Experimental structure Degrees [°]	DFT optimized structure Degrees [°]
C(101)-Rh(11)-N(103)	76.01(15)	76.7190
C(101)-Rh(11)-Cl(11)	79.07(12)	79.3396
N(103)-Rh(11)-Cl(11)	91.21(10)	90.8050
N(101)-C(101)-N(102)	104.9(4)	104.6532

The calculated values correspond well with the experimental values as seen from **Table 10** and **Table 11**. The root-mean square deviations from the experimental structure are given in **Table 12** indicating a good agreement between the two data sets. A slight difference in the orientation of the phenyl in the DFT-optimized structure compared to the experimental structure was observed (see **Figure 37**). The experimental values are from the complete structure of **8**, containing both the cation and the anion, while the DFT optimized structure is of only the cation, indicating that the counteranion do not have much effect on the structure of **8**.

Table 12: The root-mean square deviations[a] from the experimental structure of the DFT optimization of **8**. Only the selected bond lengths and angles in **Table 10** and **Table 11** were taken into consideration.

M-ligand distances [Å]	Other distances [Å]	Bond angles [°]
0.016	0.007	0.45

a: $\sqrt{(\frac{1}{n}\sum_{i=1}^{n}(x_i - y_i))}$

where:

x = n X-ray parameters

y = n DFT optimized parameters

3.2.11 Attempt at preparing a new Rh(I) *N*-heterocyclic carbene complex

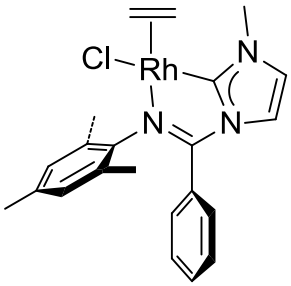

Figure 38: The desired Rh(I) *N*-heterocyclic carbene complex.

An attempt at preparing a Rh(I) complex from Rh(I) dimer **7** by reaction of the Ag(I) carbene **4a** with **7** was made. At first try the experiment was performed on an NMR scale. As soon as the solvent was vacuum-transferred into the NMR tube, the colour of the solution changed from pale orange to deep red followed by a rapid change to dark green. The crude ^{1}H-NMR of the reaction showed that all the starting materials had been consumed, but the spectrum contains a forest of peaks, and it does not look like there has been any formation of the desired Rh(I) complex.

Based on the colour changes of the reaction mixture in the NMR tube, it looks like there was a product formed initially, which then decomposes to the dark green solution. Therefore, the same reaction was performed at a laboratory scale at -78 ^{o}C to see if that would make it possible to observe what the initially formed product was.

Upon performing the reaction at -78 ^{o}C, the solution also goes deep red, however, in this case, it takes 3-4 hours before it reaches this deep red colour. A sample was taken out from the reaction mixture to be investigated by ^{1}H-NMR, but as soon as the reaction mixture was out of the cooling bath, it turned dark green. Upon investigation of this solution by ^{1}H-NMR, it was again seen that the starting materials were consumed, but no sign of formation of the desired complex.

In order to investigate what the deep red solution formed at low temperatures consists of, it was decided to perform a low temperature NMR experiment and monitor the reaction by ^{1}H-NMR. An NMR tube fitted with a septum containing the Ag(I) carbene **4a** dissolved in CD_2Cl_2 was cooled inside the NMR probe. When the solution had reached -60 ^{o}C the tube was taken out of the NMR probe and put into a cooling bath at -78 ^{o}C while the Rh(I) complex **7** was added in excess. The tube was shaken once, and then put back into the NMR probe. The ^{1}H-NMR spectra for the reaction is given in **Figure 39**. A close-up on the aromatic section is given in **Figure 40.**

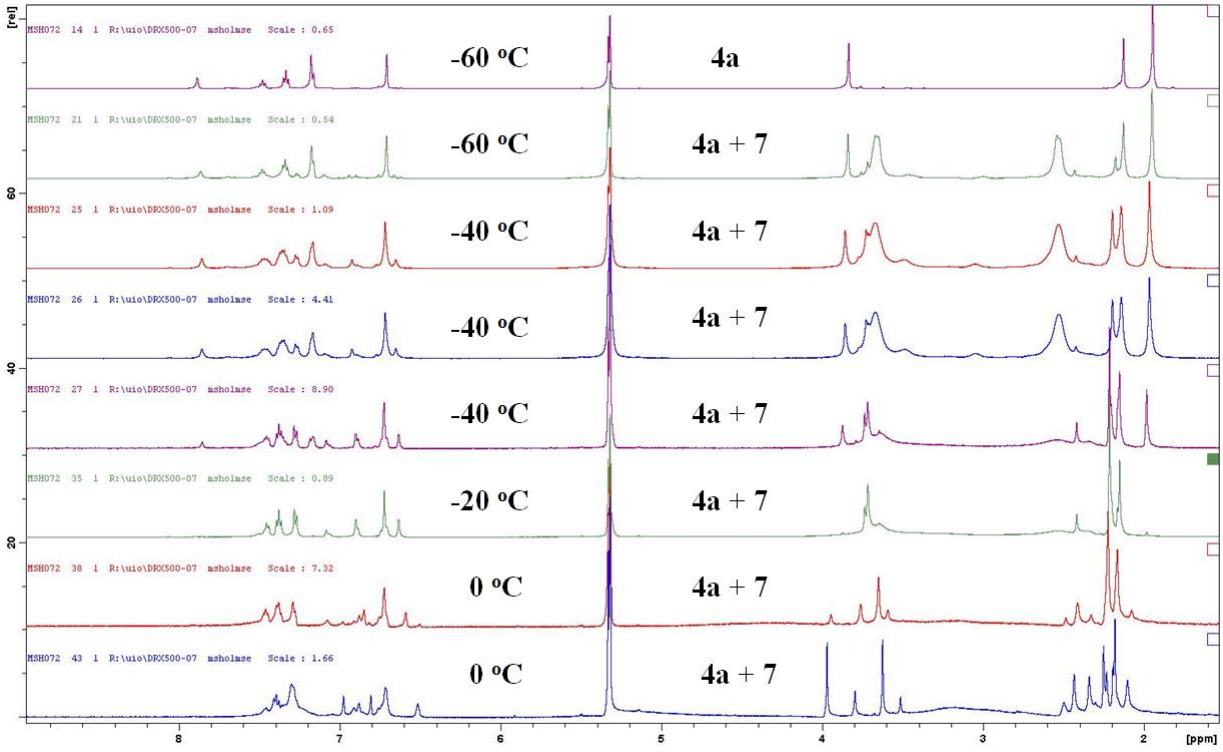

Figure 39: ^{1}H-NMR spectra for the reaction between **4a** and **7** at low temperatures.

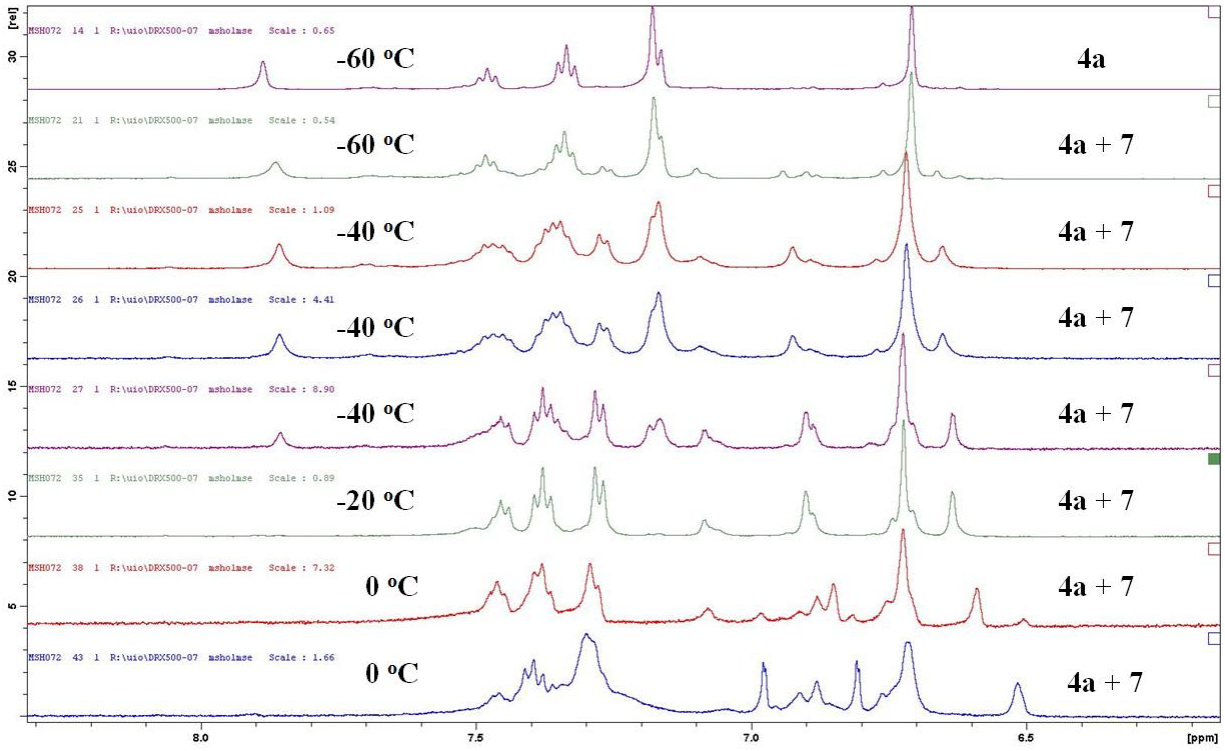

Figure 40: ^{1}H-NMR spectra for the reaction between **4a** and **7** at low temperatures, close-up of the aromatic region.

The uppermost spectrum shows only the Ag(I) carbene **4a** at -60 ^{o}C. In the second spectrum Rh(I) dimer **7** has been added, as is seen from the two broad peaks at 2.7 and 3.7 ppm. Already here, it can be seen that an extra set of signals starts to appear, and when the temperature is raised to -40 ^{o}C, this becomes more evident. For every signal from the Ag(I) carbene **4a**, a new signal appears nearby, except for the new signal for the two protons from the backbone of the imidazolylidene, which are shifted more upfield. While observing the reaction at -40 ^{o}C it is seen that the starting materials are gradually consumed.

At -20 ^{o}C, all of the Ag(I) carbene **4a** has been consumed as is seen by the disappearance of the leftmost peak. From the ^{1}H-NMR spectrum at -20 ^{o}C, it looks as if there is a new compound formed. No 2D characterization was attempted at low temperature. As seen before, upon raising the temperature to 0 ^{o}C, decomposition starts to occur.

One possible explanation is that at low temperatures there is first a cleavage of the Rh(I) dimer **7** by coordination of the carbene, followed by a displacement of one of the ethylenes by N_{imine} forming a chelate giving the 16 electron d^{8} square planar compound **a**, shown in **Figure**

41. Since there is no clear ethylene peak in the ^{1}H-NMR spectra, the ethylene may be labile, and thus the peak broadened. It must been kept in mind that ethylene may be hard to observe by ^{1}H-NMR if the signal is broadened by such a fluxional process and the presence of ethylene can not be ruled out solely because of the lack of its signals in the ^{1}H-NMR spectrum.

To support this theory, an experiment where CO(g) is bubbled through the reaction mixture of presumably **a** may be performed. If the complex **b** is obtained (see **Figure 41**) this may support the presence of **a**. A very close analogue of **b** has already been reported by our group, the only difference being that the aryl substituent is a 2,6-dimethylphenyl, instead of the 2,4,6-trimethylphenyl in this case.[8] Since we already know that complex **b** is stable, bubbling CO through the solution of **a** may give **b**. Unfortunately, there was not enough time to perform this within the time limitations of this master thesis.

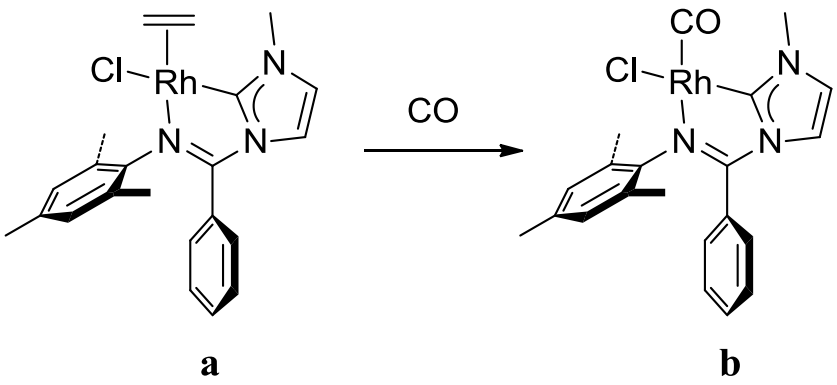

a **b**

Figure 41: Complex **a**, a possible complex formed at low temperatures in the reaction between **4a** and **7** and complex **b** which may be a resulting product of treating **a** with CO(g).

Upon adding CpNa x DME to the deep red solution, formation of $CpRh(CH_2Cl_2)_2$ was observed, together with recovery of a compound resembling the Ag(I) carbene **4a**, indicating that the process leading to the complex formed in the red solution is a reversible process. Since none of these compounds are the desired compound, this path was abandoned.

3.3 Conclusion and future work

The new Rh(III) *N*-heterocyclic carbene complexes **8** and **9** have been synthesized by a carbene transfer reaction from their corresponding Ag(I) *N*-heterocyclic carbenes in good yields. A thorough characterization of **8** and **9** were performed and some of their properties were investigated. Rh(III) complexes **8** and **9** show interesting dynamic behavior in the ^{1}H-NMR spectra which was further investigated by advanced NMR techniques. Good structures in agreement with the other spectroscopic data of both **8** and **9** were obtained by single crystal X-ray diffraction analysis. A DFT optimization of **8** was performed and gave good agreement with the experimentally obtained data of **8**. An unsuccessful attempt on preparing a new Rh(I) *N*-heterocyclic carbene complex was performed.

In the future, a catalytic testing of the new Rh(III) complexes would be desired. Testing of their performance in catalytic processes such hydrogenation, hydroformylation, ethylene dimerization or C-H functionalization may be performed.

Chapter 4

Attempts at preparing new Ru(II), Co(I) and Co(III) *N*-heterocyclic carbene complexes

4.1 The scope of the chapter

In this chapter, several attempts at preparing Ru(II), Co(I) and Co(III) *N*-heterocyclic carbene complexes are described without any of them leading to the desired complexes. The desired complexes are listed in **Figure 42**.

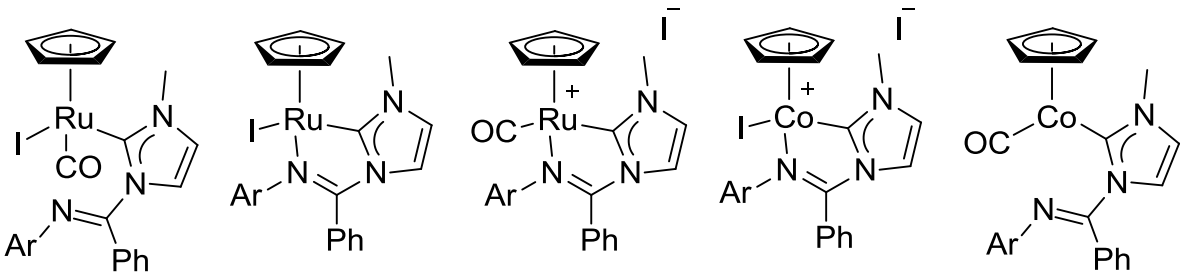

Figure 42: The desired Ru(II), Co(I) and Co(III) complexes

4.2 Results and discussion

4.2.1 Synthesis of Ru complexes 10, 11 and 12

Ru complexes **10**-**12** were prepared according to **Scheme 10** by previously reported procedures.[60-62] Isolation of Ru(II) hydride **10** from the heptane solution in which it is formed is not easy to achieve due to its instability, but in this solution, it is readily available for subsequent reaction.[60]

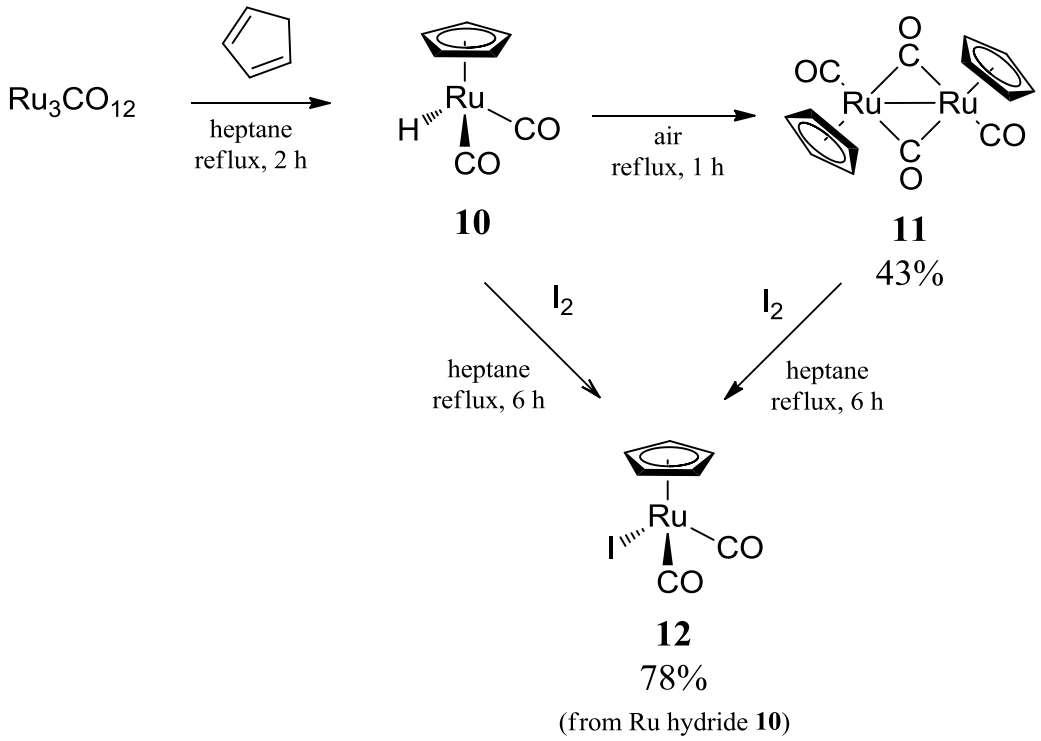

Scheme 10: Synthesis of compounds **10**-**12**.[60-62]

The Ru(II) iodo complex **12** can be synthesized either by reacting Ru(I) dimer **11** with I_2 or by directly reacting the *in situ* generated Ru(II) hydride **10** with I_2.[62] The latter method was preferred, since it requires a shorter work-up and gives **12** in good yield.

4.2.2 Characterization of Ru complexes 10, 11 and 12

^{1}H-NMR, MS and IR data corresponded with the reported data on compound **10**-**12**.[60-62] For all compounds **10**-**12** the characteristic singlet of the Cp was observed in the ^{1}H-NMR spectra. For compound **11** the characteristic ν_{CO} for the bridging carbonyl ligand was observed at 1772 cm^{-1} supporting the bridged structure of **11** in solution. Compound **10** was not isolated and was only characterized by ^{1}H-NMR and IR spectra of the crude mixture. Its most prominent spectroscopic feature was the hydride singlet at -10.69 ppm in the ^{1}H-NMR spectrum.

4.2.3 Attempts at preparing a new Ru(II) *N*-heterocyclic carbene complex

It was attempted to prepare the Ru(II) *N*-heterocyclic carbene complexes in an analogous way as their phosphine analogues. It has been shown that phosphines and phosphites are able to substitute one of the carbonyls or the iodide in $CpRu(CO)_2X$ (M=Fe; X=Cl, Br, I M=Ru; X=I) complexes.[63-65] For example, as depicted in **Scheme 11**, the substitution of one of the carbonyl ligands in $CpRu(CO)_2I$ with a phosphite giving $CpRu(CO)[P(OR)_3]$ has been performed.[66]

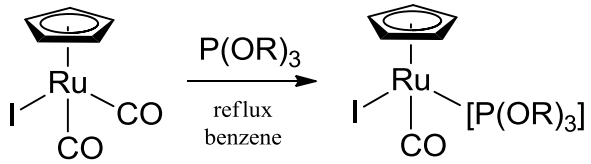

12 R=Me, Ph

Scheme 11: Substitution of one of the carbonyl ligands in $CpRu(CO)_2I$.

Upon reacting triphenylphosphine with $CpFe(CO)_2I$, which is a close analogue of $CpRu(CO)_2I$, it is the iodide which is substituted (see **Scheme 12**).[65]

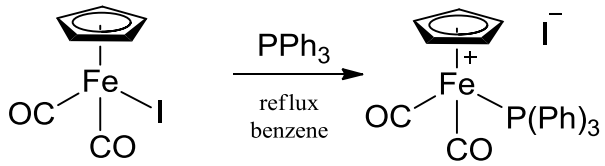

Scheme 12: Substitution of the iodide in $CpFe(CO)_2I$ with triphenylphosphine.

A substitution of one or two of the carbonyl ligands or the iodide in the Ru(II) complex **12** with the *N*-heterocyclic carbene of interest by doing a carbene transfer reaction from Ag(I) carbene **4b** was desired. Substitution of carbonyl ligands and iodides in this way in complexes like **12** has, to the best of our knowledge, not been observed before, however, it was hoped that the driving force of creating AgCl would contribute to make the reaction sufficiently favorable.

When attempting the carbene transfer from Ag(I) carbene **4b** to Ru(II) complex **12** (see **Scheme 13**) no substitution of either carbonyl ligands or iodide occurs. No change in the ν_{CO} or any shift of the Cp resonance in the ^{1}H-NMR spectrum was observed. The reaction was also performed in an NMR tube sealed on the vacuum line to make sure that the reaction was performed under an inert atmosphere, as well as being able to monitor the reaction by ^{1}H-

NMR. No reaction was observed in this case either. We suspect that the substitution of the carbonyl ligands or the iodide in $CpRu(CO)_2I$ requires a considerably thermal activation in order to proceed. However, increased temperatures seem to lead to decomposition of the Ag(I) carbenes used as the carbene source (see **4.2.6**). This synthesis strategy was clearly not a good choice for the system of interest.

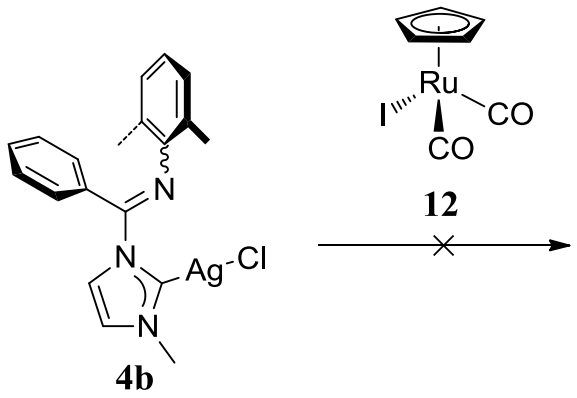

Scheme 13: Attempt at preparing a new Ru(II) *N*-heterocyclic complex from Ru(II) complex **12** and Ag(I) carbene **4b**.

Since it is not possible to isolate the free carbene of the ligand system of interest, an attempt was made to prepare the free carbene *in situ* and see if it could substitute a carbonyl ligand or iodide in **12** before the carbene had time to undergo rearrangement.[35] This has been performed previously in the Tilset-group with the same ligand system, but with a different metal (see **Scheme 14**).[7]

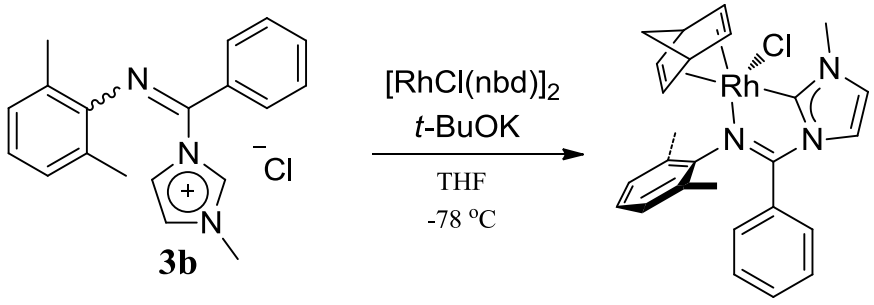

Scheme 14: Synthesis of Rh(I) *N*-heterocyclic carbene complex by generation of the free carbene *in situ.*[7]

Upon attempting to make the free carbene *in situ* and reacting it with Ru(II) complex **12** (see **Scheme 15**) the only reaction observed was decomposition of imidazolium salt **3a**. Ru(II) complex **12** remained unchanged, as was seen from ^{1}H-NMR.

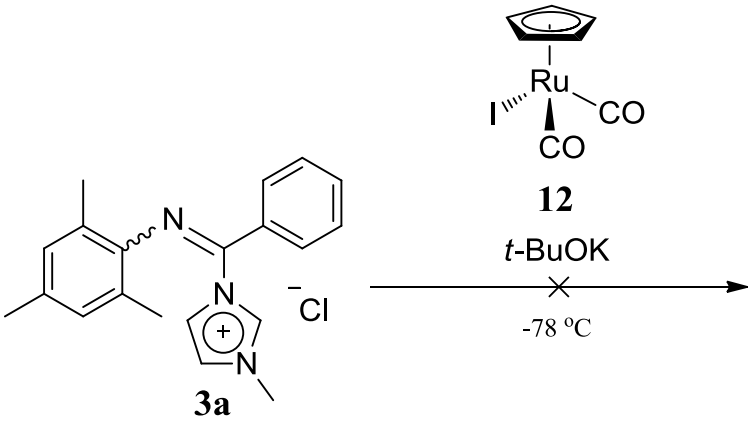

Scheme 15: Attempt at generating the free carbene *in situ* and reacting it with Ru(II) complex **12**.

An attempt at reacting Ru(II) complex **12** with the imidazolium salt **4b** directly was performed; this resulted in no observable reaction of Ru(II) complex **12**.

These results indicate that it is not favorable to substitute a carbonyl group or iodide in Ru(II) complex **12** when using the Ag(I) *N*-heterocyclic carbene as a carbene transfer reagent. At this point, it was decided to leave this strategy.

4.2.4 Synthesis of Co(III) complex 13

Co(III) complex **13** was prepared according to **Scheme 16** by a previously reported procedure.[43, 67] An oxidative addition of I_2 to $CpCo(CO)_2$ gave **13** in good yield.

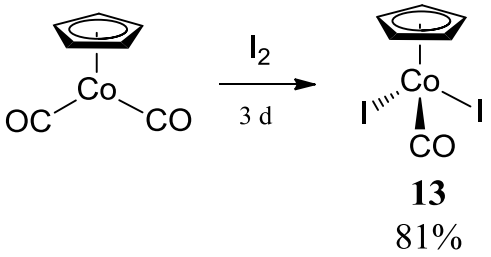

Scheme 16: Synthesis of Co(III) complex **13**.[43, 67]

4.2.5 Characterization of Co(III) complex 13

^{1}H-NMR, MS and IR data corresponded with the reported data on Co(III) complex **13**.[43, 67] The characteristic Cp resonance was observed as a singlet at 4.34 ppm in the ^{1}H-NMR spectrum of **13**. The observed ν_{co} of 2077 cm^{-1} is a substantial increase compared to that of $CpCo(CO)_2$ which has ν_{CO} of 2028 and 1967 cm^{-1}, this indicates that the carbonyl ligand is more loosely bonded in **13** than the carbonyl ligands in $CpCo(CO)_2$.[42]

4.2.6 Attempts at preparing new Co(I) and Co(III) *N*-heterocyclic carbene complexes

Some cyclopentadienyl Co(I) and Co(III) complexes of *N*-heterocyclic carbenes have previously been synthesized in the Tilset-group. One example, CpCo(IMes)(CO), is shown in **Scheme 17**.[32]

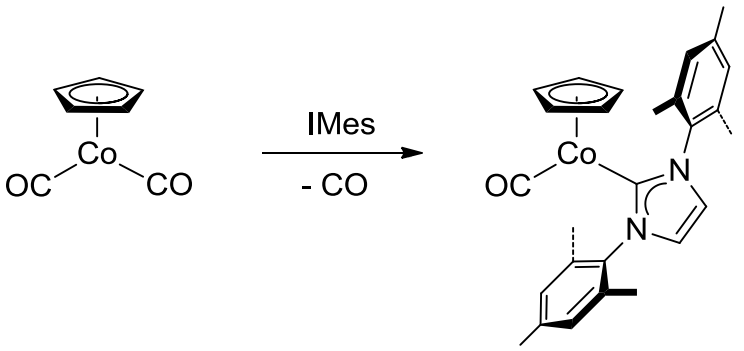

Scheme 17: One of the previously reported Co(I) *N*-heterocyclic carbene complexes synthesized in the Tilset-group.[32]

CpCo(IMes)(CO) was prepared by substituting one of the carbonyl ligands in $CpCo(CO)_2$ with the free carbene of IMes.[32] Based on this, it was desired to investigate if it would be possible to do the same with our *N*-heterocyclic carbene ligand system. Since it is not possible to generate the free carbene of the *N*-heterocyclic carbene of interest, it was decided to try to substitute the carbonyl ligand by a carbene transfer reaction from the Ag(I) carbene **4a**.[35] It was hoped that the driving force of forming AgCl would make the reaction favorable.

Upon reacting $CpCo(CO)_2$ with Ag(I) carbene **4a** no reaction occurred. Upon heating the reaction mixture the Ag(I) carbene **4a** decomposed. No change of the Cp resonance in the ^{1}H-NMR spectrum was observed, indicating that there was no reaction occurring. The reaction was also performed in an NMR tube sealed on the vacuum line to make sure that the reaction was performed under an inert atmosphere, as well as being able to monitor the reaction by ^{1}H-NMR. No reaction was observed in this case either.

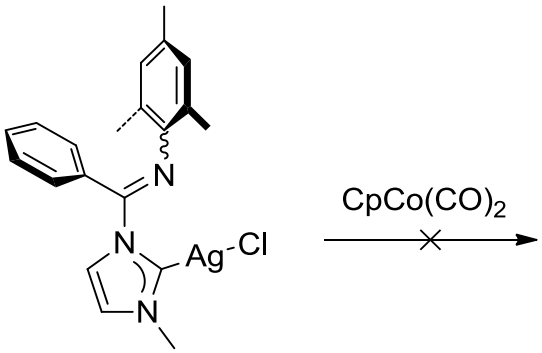

4a

Scheme 18: Attempt on preparing a new Co(I) *N*-heterocyclic carbene complex.

One explanation of the failure of the experiment may be that the free carbene is needed in order to substitute the carbonyl ligands in $CpCo(CO)_2$. Therefore an attempt to make the free carbene *in situ* was performed with the hope that the free carbene will substitute one of the carbonyl ligands before it undergoes rearrangement (see **Scheme 19**). This was however also unsuccessful. Only decomposition of the imidazolium salt **3a** was observed. No shift in the ^{1}H-NMR resonance of the Cp was observed.

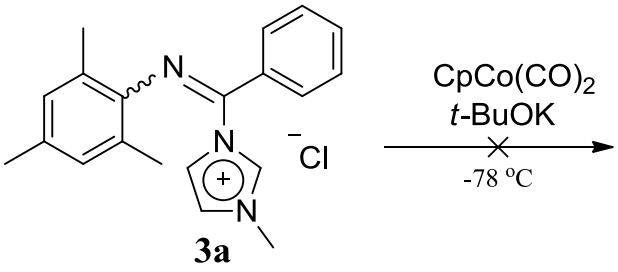

3a

Scheme 19: Attempt on preparing a new Co(I) *N*-heterocyclic carbene complex.

The Co precursor was changed to Co(III) complex **13**. As mentioned earlier, the ν_{CO} of Co(III) complex **13** is significantly higher than for $CpCo(CO)_2$ indicating that the CO is more loosely bonded to the metal.[12] This indicates that it might be easier to substitute the COs in this complex. It has been reported that substitution of the CO in Co(III) complex **13** readily occurs with both triphenylphosphine and pyridine.[43] It was therefore hoped that substitution of the carbonyl in **13** would proceed successfully.

The reaction between **13** and **4a** was performed in an NMR tube sealed on the vacuum line to make sure that the reaction was performed under an inert atmosphere and to enable monitoring of the reaction by ^{1}H-NMR. Upon performing the reaction, a rapid colour change was observed. Inspection of the reaction by ^{1}H-NMR, showed that the signal of the Cp had

changed to more upfield, from 5.66 ppm to 5.28 ppm. However, no sign of formation of any desired Co(III) *N*-heterocyclic carbene complex was observed.

At this point, due to the time limitations of the master thesis and the more interesting results obtained in the Rh project described in Chapter 3, the work on the Co(I) and Co(III) *N*-heterocyclic carbene complexes was discontinued.

4.3 Conclusion

Several attempts on preparing new Ru(II), Co(I) and Co(III) *N*-heterocyclic carbene complexes have been performed. However, none of them led to any of the desired complexes. Based on the experience gained from the work presented in this chapter and the previous chapter it seems like that in order to transfer a *N*-heterocyclic carbene from the Ag(I) carbene to the desired metal, it is required to have a readily available coordination site. It appears that in the complexes selected for these reactions, the ligands (CO, I) that need to be removed in order to provide the vacant sites are probably too strongly bonded. When using Ag(I) carbenes, it seems like one is not able to perform substitutions of carbonyl ligands, such as substituting the carbonyl ligands in complex **12**, **13** and $CpCo(CO)_2$ indicating that the driving force of forming AgCl is not enough to make the reaction take place.

Experimental

General

All glassware was dried in an oven and cooled under argon prior to use. CH_2Cl_2, THF and Et_2O were dried using a MB SPS-800 solvent purifying system from MBraun. MeOH was dried over molecular sieves. Heptane was distilled and dried over molecular sieves. All reactions were performed under an inert argon atmosphere with stirring unless otherwise noted. Vacuum line (1×10^{-3} mbar) was used for removal of solvents unless otherwise noted. NMR spectra were recorded on Bruker Avance DPX200, AVII400, DRX500 and AV600 at 25 ^{o}C unless otherwise noted. The peaks in the ^{1}H-NMR and ^{13}C-NMR spectra of all new compounds were assigned using 2D NMR techniques such as HSQC/HMQC, HMBC, COSY and NOESY. IR spectra (in solution) were recorded on a Perkin Elmer Spectrum One FT-IR spectrometer. An Ar-filled glovebox of the type HE-493 from VAC was used. The X-ray structure analysis was performed by Sigurd Øien and Professor Carl Henrik Gørbitz on a Bruker APEX II CCD diffractometer. Mass spectra were obtained on a Micromass QTOF II spectrometer (ESI) and on a Fision VG Prospec sector instrument at 70 eV (EI) by Osamu Sekiguchi. The different isotopes observed by MS are listed as for example: ^{35}Cl/^{37}Cl ((rel.%(^{35}Cl)/(rel. %(^{37}Cl)). Ru has 7 stable isotopes, which give complicated MS spectra, therefore only MS data for the most abundant isotope, ^{102}Ru, is given.[56] All new reactions were performed with Schlenk and glove box techniques and dry and degassed solvents the first time they were performed to make sure that no valuable unstable compounds were lost

Synthesis of amide 1a[45-46]

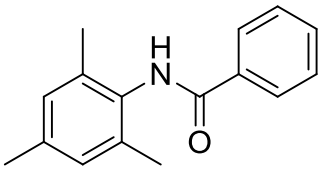

1a

Benzoyl chloride (4.60 mL, 39.6 mmol, 1.1 equiv.) in 21.0 mL CH_2Cl_2 was added dropwise to a stirred solution of 2,4,6-trimethylaniline (5.00 mL, 35.6 mmol, 1.0 equiv.) and Et_3N (5.50 mL, 39.5 mmol, 1.1 equiv.) in 35.0 mL CH_2Cl_2 and heated at reflux for 48 h. 150 mL CH_2Cl_2 was added and the reaction mixture was washed with distilled H_2O (100 mL), saturated $NaHCO_3$ (aq, 100 mL) and 3M HCl (aq, 100 mL). The product was dried over $MgSO_4$, filtrated and the solvent was removed by rotary evaporation yielding **1a** (7.81 g, 92%) as a cream white solid. **1a** was pure by ^{1}H-NMR.

^{1}H-NMR (200 MHz, $CDCl_3$): δ 2.23 (s, 6H, 2 *o*-Ar**Me**), 2.28 (s, 3H, *p*-Ar**Me**), 6.92 (s, 2H, Ar**H**), 7.30 (br. s, 1H, N**H**), 7.40-7.60 (m, 3H, Ph**H**), 7.90 (m, 2H, Ph**H**).

MS (EI, MeCN) *m/z*(rel.%): 239(M^+, 63), 134(25), 105(100), 77(33).

Synthesis of amide 1b[45-46]

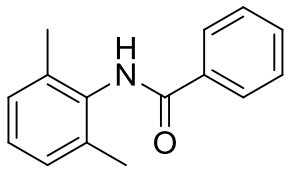

1b

Benzoyl chloride (4.60 mL, 39.6 mmol, 1.1 equiv.) in 25.0 mL CH_2Cl_2 was added dropwise to a stirred solution of 2,6-dimethylaniline (4.45 mL, 36.1 mmol, 1.0 equiv.) and Et_3N (5.40 mL, 39.5 mmol, 1.1 equiv.) in 35.0 mL CH_2Cl_2 and heated at reflux for 48 h. 50 mL CH_2Cl_2 was added and the reaction mixture was washed with distilled H_2O (100 mL), saturated $NaHCO_3$ (aq, 100 mL) and 3M HCl (aq, 100 mL). The product was dried over $MgSO_4$, filtrated and solvent was removed by rotary evaporation yielding **1b** (7.78 g, 96%) as a cream white solid. **1b** was pure by ^{1}H-NMR.

^{1}H-NMR (200 MHz, $CDCl_3$): δ 2.27 (s, 6H, Ar**Me**), 7.12 (m, 3H, Ar**H**), 7.36 (br. s, 1H, N**H**), 7.43-7.61 (m, 3H, Ph**H**), 7.87-7.94 (m, 2H, Ph**H**).

MS (EI, MeCN) *m/z*(rel.%): 225(M^+, 54), 120(14), 105(100), 77(45).

Synthesis of iminochloride 2a[46-47]

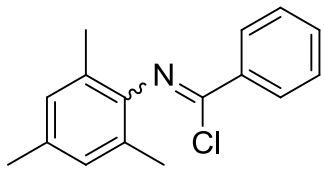

2a

$SOCl_2$ (1.50 mL, 20.7 mmol, 1.4 equiv.) was added to **1a** (3.472 g, 14.51 mmol, 1.0 equiv.). The reaction mixture was heated at reflux for 4 h. HCl and excess $SOCl_2$ was removed *in vacuo* yielding **2a** (3.556 g, 95 %) as a brown oil. **2a** was pure by ^{1}H-NMR.

^{1}H-NMR (200 MHz, $CDCl_3$): δ 2.07 (s, 6H, 2 *o*-Ar**Me**), 2.30 (s, 3H, *p*-Ar**Me**), 6.91 (s, 2H, Ar**H**), 7.40-7.60 (m, 3H, Ph**H**), 8.20 (m, 2H, Ph**H**).

MS (EI, MeCN) *m/z*(rel.%): 257/259(M^+, 28/9), 222(100), 207(16), 119(11), 104(11), 91(14), 77(10).

Synthesis of imine chloride 2b[46-47]

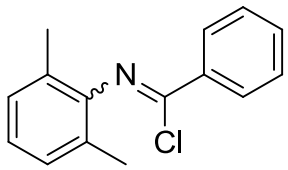

2b

$SOCl_2$ (1.80 mL, 25.6 mmol, 1.4 equiv.) was added to **1b** (4.15 g, 18.4 mmol, 1.0 equiv.). The reaction mixture was heated at reflux for 4 h. HCl and excess $SOCl_2$ was removed *in vacuo* yielding **2b** (4.41 g, 98%) as a brown oil. **2b** was pure by ^{1}H-NMR.

^{1}H-NMR (200 MHz, $CDCl_3$): δ 2.12 (s, 6H, Ar**Me**), 6.97-7.15 (m, 3H, Ar**H**), 7.44-7.63 (m, 3H, Ph**H**), 7.18-8.25 (m, 2H, Ph**H**).

MS (EI, MeCN) *m/z*(rel.%): 243/245(M^+, 30/10), 208(100), 193(11), 105(19), 103(14), 79(10), 77(18).

Synthesis of imidazolium salt 3a

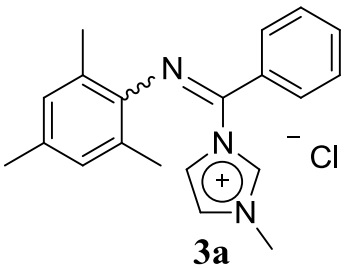

3a

1-Methylimidazole (0.70 mL, 8.8 mmol, 1.1 equiv.) was added dropwise to a stirred solution of **2a** (2.007 g, 7.788 mmol, 1.0 equiv) dissolved in 42.0 mL THF. The reaction mixture was stirred at ambient temperature for 48 h. The product precipitated from solution during the course of the reaction. The precipitated product was washed with THF (4 x 30 mL) and THF was removed by cannula filtration. The product was dried *in vacuo* yielding **3a** (1.781 g, 68%) as a white solid. **3a** was pure by ^{1}H-NMR.

^{1}H-NMR (500 MHz, $CDCl_3$): δ 1.95 (s, 6H, *o*-Ar**Me**), 2.18 (s, 3H, *p*-Ar**Me**), 4.33 (s, 3H, N-**Me**), 6.73 (s, 2H, Ar-**H**), 7.33 (d, 2H, *o*-Ph**H**, ^{3}J=7.5 Hz), 7.41 (t, 2H, *m*-Ph**H**, ^{3}J=7.5 Hz), 7.48 (t, 1H, *p*-Ph**H**, ^{3}J= 7.5 Hz), 7.70 (s, 1H, MeNC**H**CHN), 7.94 (s, 1H, MeNCHC**H**N), 10.39 (s, 1H, NC**H**NMe).

^{13}C-NMR (125 MHz, $CDCl_3$): δ 18.46 (*o*-Ar**Me**), 20.82 (*p*-Ar**Me**), 37.91 (N**Me**), 119.40 (MeNCH**C**HN), 124.22 (MeN**C**HCHN), 126.20 (*o*-**Ar**), 128.92 (*o*-Ph), 129.10 (*m*-**Ar**), 129.73 (*m*-**Ph**), 132.77 (*p*-**Ph**), 134.43 (*p*-**Ar**), 138.73 (br., N**C**HN), 140.78 (*i*-**Ar**), 148.08 (i-**Ph**). **C**=N was not observed.

MS (ESI, MeCN) *m/z*(rel.%): 304(M^+-Cl, 8), 222(100).

HRMS (MeCN): Found 304.1822, calculated for $C_{20}H_{22}N_3$ 304.1813.

IR (CH_2Cl_2): *ν*(C=N) 1674 cm^{-1}.

Synthesis of imidazolium salt 3b[1]

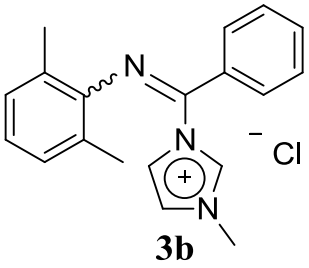

3b

1-Methylimidazole (0.60 mL, 7.6 mmol, 1.1 equiv.) was added dropwise to a stirred solution of **2b** (2.670 g, 6.853 mmol, 1.0 equiv) dissolved in 35.0 mL THF. The reaction mixture was stirred at ambient temperature for 48 h. The product precipitated from solution during the course of the reaction. The precipitated product was washed with THF (3 x 30 mL) and THF was removed by cannula filtration. The product was recrystallized from CH_2Cl_2/Et_2O and dried *in vacuo* yielding **3b** (0.890 g, 40%) as yellow crystals. **3b** was pure by ^{1}H-NMR, CH_2Cl_2 was observed in the ^{1}H-NMR spectrum.

^{1}H-NMR (200 MHz, $CDCl_3$): δ 2.00 (s, 6H, Ar**Me**), 4.33 (s, 3H, N**Me**), 6.93-8.89 (m, 3H, Ar**H**), 7.52-7.32 (m, 5H, Ph**H**), 7.68 (s, 1H, NC**H**CHNMe), 7.94 (s, 1H, NCHC**H**NMe), 10.38 (s, 1H, NC**H**N).

IR (CH_2Cl_2): *v*(C=N) 1674 cm^{-1}.

MS (ESI, MeCN) *m/z*(rel.%): 290(M^+-Cl, 100), 208(15).

Synthesis of Ag(I) carbene complex 4a

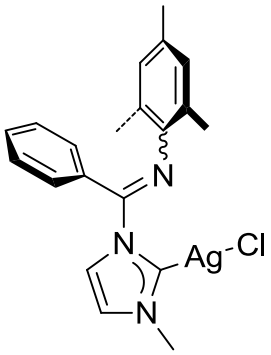

4a

Imidazolium salt **3a** (1.00 g, 2.97 mmol, 1.0 equiv.), Ag_2O (0.973 g, 4.20 mmol, 1.4 equiv.) and activated 3 Å molecular sieves were suspended in 20.0 mL CH_2Cl_2 and stirred at ambient temperature in the absence of light for 4 h. The solution was filtered off by cannula filtration and the solvent was removed *in vacuo* yielding **4a** (1.11 g, 84%) as a weakly yellow solid. **4a** was pure by ^{1}H-NMR. Crystals for single crystal X-ray diffraction analysis were obtained by layering a saturated solution of **4a** with Et_2O. CH_2Cl_2 was observed in the ^{1}H-NMR spectrum.

^{1}H-NMR (400MHz, $CDCl_3$): δ 1.99 (s, 6H, *o*-Ar**Me**), 2.17 (s, 3H, *p*-Ar**Me**), 3.88 (s, 3H, N**Me**), 6.71 (s, 2H, Ar**H**), 7.08-7.15 (m, 3H, *o*-Ph**H** and MeNCHC**H**N), 7.34 (t, 2H, *m*-Ph**H**, ^3J=7.6 Hz), 7.48 (t, 1H, *p*-Ph**H**, ^3J=7.6 Hz), 7.95 (s, 1H, MeNC**H**CHN).

^{13}C-NMR (100 MHz, $CDCl_3$): δ 18.52 (*o*-Ar**Me**), 20.81 (*p*-Ar**Me**), 40.09 (N**Me**), 120.98 (MeNCH**C**HN), 122.27 (MeN**C**HCHN), 126.11 (*o*-Ar), 128.82 (*m*-**Ar** or *o*-**Ph**), 128.90 (*m*-**Ar** or *o*-**Ph**), 129.17 (*m*-**Ph**), 130.79 (*i*-**Ph**), 131.98 (*p*-**Ph**), 133.46 (*p*-**Ar**), 142.00 (*i*-**Ar**), 152.59 (**C**=N), 184.21 (N**C**N).

IR (CH_2Cl_2): *ν*(C=N) 1663 cm^{-1}.

MS (ESI, MeCN) *m/z*(rel.%): 713/715($[Ag(NHC)_2]^+$, 14/14), 222(100), 207(29).

HRMS (MeCN): Found 713.2532, calculated for $C_{40}H_{42}N_6Ag$ 713.2521.

Synthesis of Ag(I) carbene complex 4b[1]

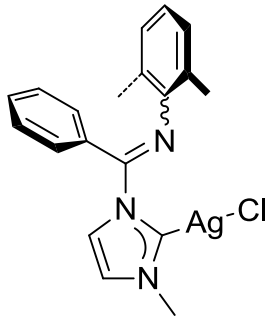

4b

Imidazolium salt **3b** (868 mg, 2.66 mmol, 1.0 equiv.), Ag_2O (871 mg, 3.76 mmol, 1.4 equiv.) and activated 3 Å molecular sieves were suspended in 20.0 mL CH_2Cl_2 and stirred at ambient temperature in the absence of light for 4 h. The solution was filtered off by cannula filtration and the solvent was removed *in vacuo* yielding **4b** (923.1 mg, 80%) as a grayish solid. **4b** was pure by ^{1}H-NMR. CH_2Cl_2 was observed in the ^{1}H-NMR spectrum.

^{1}H-NMR (200MHz, CD_2Cl_2): δ 2.06 (s, 6H, Ar**Me**), 3.88 (s, 3H, N**Me**), 6.96-6.82 (m, 3H, Ar**H**), 7.20-7.17 (m, 3H, NC**H**CHNMe and *o*-Ph**H**), 7.38-7.31 (m, 2H, *m*-Ph**H**), 7.51-7.44 (m, 1H, *p*-Ph**H**), 7.84 (s, 1H, NCHC**H**NMe).

IR (CH_2Cl_2): *ν*(C=N) 1674 cm^{-1}.

MS (ESI, MeCN) *m/z*(rel.%): 685/687($[Ag(NHC)_2]^+$, 90/100), 478/480(10/8), 437/439(7/7), 396/398(42/39).

Synthesis of Rh(III) complex 5[52]

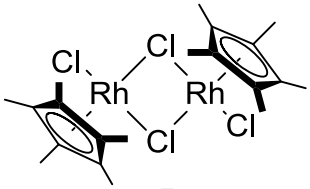

5

Pentamethylcyclopentadiene (0.15 mL, 0.96 mmol, 1.2 equiv) was added to a stirred and degassed solution of $RhCl_3$ x $3H_2O$ (205.8 mg, 0.7816 mmol, 1.0 equiv.) in 6.0 mL MeOH. The solution was heated at reflux for 21 h, the product precipitated out of the solution during the course of the reaction. The solution was filtrated off by cannula filtration and the solid was washed with Et_2O (3x5 mL) yielding **5** as a red solid (200.5 mg, 83%). **5** was pure by ^{1}H-NMR.

^{1}H-NMR (200 MHz, $CDCl_3$): δ 1.60 (s, Cp**Me**).

MS (ESI, MeCN) *m/z* (rel.%): 581/583/585(M^+-Cl, 100/86/11), 314/316(26/4), 273/275(73/13).

Synthesis of Rh(III) complex 6[53]

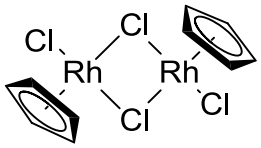

6

Dicyclopentadiene was cracked over iron fillings and freshly distilled cyclopentadiene (bp. ca 42 ^oC) was collected on an ice bath. Freshly distilled cyclopentadiene (0.26 mL, 3.1 mmol, 4.2 equiv.) was added to a stirred and degassed solution of $RhCl_3$ x $3H_2O$ (199.3 mg, 0.7569 mmol, 1.0 equiv) in 6.0 mL MeOH. The solution was heated at reflux for 16 h, the product precipitated out of solution during the course of the reaction. The solution was filtered off by cannula filtration and the solid was washed with MeOH (5 mL) and Et_2O (3x5 mL) yielding **6** (38.2 mg, 21%) as a red solid. Upon suspending some of the solid into DMSO-d_6 a ^{1}H-NMR of presumably [$CpRhCl_2$(DMSO-d_6)] was obtained. **6** was pure by ^{1}H-NMR.

^{1}H-NMR (400 MHz, DMSO-d_6) δ 6.02 (s, **Cp**).

^{13}C-NMR (100 MHz, DMSO-d_6) δ 88.56 (d, **Cp**, $^1J(^{103}Rh\text{-}^{13}C)$=6.9 Hz)).

Synthesis of Rh(I) complex 7[54]

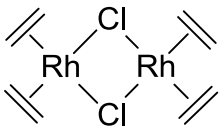

7

CH_2CH_2 was bubbled through a stirred and degassed solution of $RhCl_3$ x $3H_2O$ (420.3 mg, 1.519 mmol) in 20.0 mL MeOH and 0.85 mL distilled water in a Schlenk flask for 8 h. Product precipitated out of solution during the course of the reaction. The solvent was removed by cannula filtration and the product was washed with of MeOH (2x5 mL) while kept in an ice bath yielding **7** (82 mg, 28%) as an orange solid. The product was dried *in vacuo* for 1 h. **7** is thermally unstable and should be stored in a freezer, it can be handled at room temperature for short periods only. **7** was pure by ^{1}H-NMR.

^{1}H-NMR (200 MHz, C_6D_6): δ 2.84 (s, br, C**H_2**).

Synthesis of Rh(III) complex 8

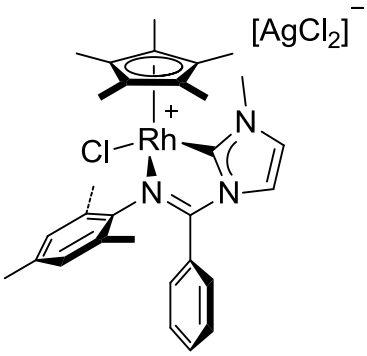

8

Rh(III) complex **5 (**27.1 mg, 0.0438 mmol, 1.0 equiv.) in 20.0 mL CH_2Cl_2 was added dropwise to a stirred dry-ice/acetone-cooled solution of Ag(I) carbene **4a** (43.3 mg, 0.0974 mmol, 2.2 equiv.) in 10.0 mL CH_2Cl_2 in the absence of light. The reaction mixture was allowed to warm to ambient temperature over night. The reaction mixture was stirred in the presence of light for a few hours to make any excess of **4a** decompose and the crude mixture was filtrated by cannula filtration. Solvent was removed *in vacuo* yielding an orange solid which was recrystallized from CH_2Cl_2/Et_2O to obtain **8** (54.4 mg, 82%) as an orange solid. **8** was pure by ^{1}H-NMR. CH_2Cl_2 was observed in the ^{1}H-NMR spectrum. Crystals for X-ray analysis were grown by layering a saturated solution of **8** with Et_2O.

The reaction was also performed with 100.0 mg of **5** and 157.8 mg of **4a** yielding **8** (164.5 mg, 67%).

^{1}H-NMR (500 MHz, MeCN-d_3): δ 1.49 (s, 15H, Cp**Me**), 1.82 (s, 3H, *o*-Ar**Me**), 2.20 (s, 3H, *p*-Ar**Me**), 2.44 (s, 3H, *o*-Ar**Me**), 4.00 (s, 3H, N**Me**), 6.78 (s, 1H, Ar**H**), 6.96 (br. s, 1H, *o*-Ph**H**), 7.01 (s, 1H, Ar**H**), 7.22 (d, 1H, MeNCHC**H**N, ^3J=2.2 Hz), 7.26 (br. s, 1H, *m*-Ph**H**), 7.34 (d, 1H, MeNC**H**CHN, ^3J=2.2 Hz), 7.55 (t, 1H, *p*-Ph**H**, ^3J=7.5 Hz), 7.59 (br. s, 1H, *m*-Ph**H**), 7.71 (br. s, 1H, *o*-Ph**H**).

^{1}H-NMR (500 MHz, MeCN-d_3, 1.1 ^{o}C): δ 1.47 (s, 15H, Cp**Me**), 1.79 (s, 3H, *o*-Ar**Me**), 2.19 (s, 3H, *p*-Ar**Me**), 2.42 (s, 3H, *o*-Ar**Me**), 4.99 (s, 3H, N**Me**), 6.77 (s, 1H, Ar**H**), 6.95 (d, 1H, *o*-Ph**H**, ^3J=7.6 Hz), 7.01 (s, 1H, Ar**H**), 7.23 (d, 1H, MeNCHC**H**N, ^3J=2.2 Hz), 7.25 (t, 1H, *m*-Ph**H**, ^3J=7.6 Hz), 7.34 (d, 1H, MeNC**H**CHN, ^3J=2.2 Hz), 7.55 (t, 1H, *p*-Ph**H**, ^3J=7.6 Hz), 7.59 (t, 1H, *m*-Ph**H**, ^3J=7.6 Hz), 7.70 (d, 1H, *o*-Ph**H**, ^3J=7.6 Hz).

^{13}C-NMR (125 MHz, MeCN-d_3): δ 9.65 (Cp**Me**), 19.78 (*o*-Ar**Me**), 20.74 (*p*-Ar**Me**), 21.07 (*o*-Ar**Me**), 38.69 (N**Me**), 101.35 (d, Cp, $^1J(^{103}Rh\text{-}^{13}C)$=6.9 Hz), 121.00 (MeN**C**HCHN), 127.16 (MeNCH**C**HN), 128.05 (*i*-**Ph**), 129.84-130.50 (br., *o*-**Ph** and *m*-**Ph**), 130.07 (m-**Ar**), 130.62 (*o*-**Ar**), 130.88 (m-**Ar**), 133.69 (*p*-**Ph**), 134.50 (*o*-**Ar**), 138.17 (*p*-**Ar**), 141.77 (*i*-**Ar**), 163.32 (**C**=N), 184.46 (d, N**C**N, $^1J(^{103}Rh\text{-}^{13}C)$=51 Hz).

IR (CH_2Cl_2): *v*(C=N) 1615 cm^{-1}.

MS (ESI, MeCN) *m/z* (rel %): 576/578(M^+-Cl, 100/18).

HRMS (MeCN): Found 576.1664, calculated for $C_{30}H_{36}N_3ClRh$ 576.1652.

MS (ESI^-, MeCN) *m/z*(rel.%): 177/179/181/183($[AgCl_2]^-$, 46/100/26/1).

HRMS (MeCN): Found 176.8436, calculated for $AgCl_2$ 176.8428.

Synthesis of Rh(III) complex 9

Ag(I) carbene **4a** (ca 80 mg, 0.18 mmol, 2.4 equiv.)* in 10.0 mL CH_2Cl_2 was added dropwise to a stirred dry-ice/acetone-cooled suspension of Rh(III) complex **6** (36.5 mg, 0.0764 mmol, 1.0 equiv.) in 10.0 mL CH_2Cl_2. The reaction mixture was stirred in the absence of light over night followed by stirring in the presence of light for a few hours to decompose any excess of **4a**. The reaction mixture was filtered by cannula filtration. Solvent was removed *in vacuo* yielding an orange solid which was recrystallized from CH_2Cl_2/Et_2O to obtain **9** (69.2 mg, 65%) as an orange solid. **9** was pure by ^{1}H-NMR except one unknown impurity in which has not been removed. Et_2O was observed in the ^{1}H-NMR spectrum. Crystals of **9** were grown by the vapor diffusion-diffusion technique.[59] A small capped vial with a small opening on the top containing a nearly saturated solution of **9** in CH_2Cl_2 was placed into a larger vial containing Et_2O. The crystals were formed within 24 h.

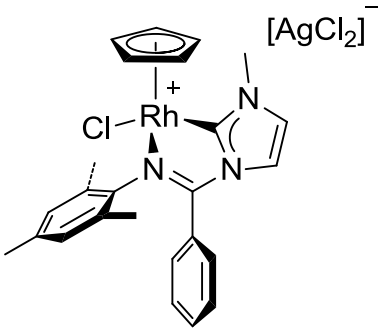

9

^{1}H-NMR (600 MHz, $CDCl_3$): δ 1.94 (s, 3H, *o*-Ar**Me**, near Cp), 2.21 (s, 3H, *p*-Ar**Me**), 2.59 (s, 3H, *o*-Ar**Me**), 4.25 (s, 3H, N**Me**), 5.68 (s, 5H, Cp**H**), 6.66 (s, 1H, Ar**H**, near Cp), 6.91 (s, 1H, Ar**H**), 7.19 (d, 1H, MeNCHC**H**N, ^3J=2.2 Hz), 7.30 (d, 1H, MeNC**H**CHN, ^3J=2.2 Hz), 7.41 (br. s, 2H, *m*-Ph**H**), 7.51 (t, 1H, *p*-Ph**H**, ^3J=7.6 Hz)**.

^{1}H-NMR (500 MHz, MeCN-d_3, -21°C): δ 1.82 (s, 3H, *o*-Ar**Me**, near Cp), 2.20 (s, 3H *p*-Ar**Me**), 2.56 (s, 3H, *o*-Ar**Me**), 3.99 (s, 3H, N**Me**), 5.52 (s, 5H, Cp**H**), 6.72 (s, 1H, Ar**H**, near Cp), 7.00 (s, 1H, Ar**H**), 7.10 (s br., 1H, *o*-Ph**H**), 7.30 (s br., 1H, *m*-Ph**H**), 7.34 (d, 1H, MeC**H**CHN or MeCHC**H**N, ^3J=2.3 Hz), 7.42 (d, 1H, MeNC**H**CHN or MeNCHC**H**N, ^3J=2.3 Hz), 7.58 (m, 2H, *m*-Ph**H** and *p*-Ph**H**), 7.66 (s br., 1H, *o*-Ph**H**).

^{13}C-NMR (100 MHz, $CDCl_3$): δ 19.18 (*o*-Ar**Me**), 20.85 (*o*-Ar**Me**), 20.93 (*p*-Ar**Me**), 39.87 (N**Me**), 89.78 (**Cp**, $^1J(^{103}Rh\text{-}^{13}C)$=5.8 Hz)), 120.05 (MeNCH**C**HN), 125.50 (*i*-**Ph**), 126.05 (MeN**C**HCHN), 128.17 (*o*-**Ar**), 129.41-129.44 (s br., *m*-**Ph**) 129.68 (m-**Ar**), 130.16 (m-**Ar**),

132.58 (*o*-**Ar**), 133.39 (*p*-**Ph**), 137.91 (*p*-**Ar**), 145.79 (*i*-**Ar**), 163.29 (**C**=N), 181.75 (N**C**N, $^{1}J(^{103}Rh\text{-}^{13}C)$=46.8 Hz)**.

IR (CH_2Cl_2): *v*(C=N) 1616 cm^{-1}.

MS (ESI, MeCN): *m/z*(rel.%) 506/508(M^+-Cl, 100/20).

HRMS (MeCN): Found 506.0854, calculated for $C_{25}H_{26}N_3ClRh$ 506.0870.

MS (ESI^-, MeCN): *m/z*(rel.%) 177/179/181/183($[AgCl_2]^-$, 66/100/53/5).

*Due to a problem with the balance, this mass could not be measured exactly.

** The two protons and carbons in *ortho* position on the phenyl are not observed due to the broadness of their peak at this temperature.

Attempt at preparing a Rh(I) complex: NMR-experiment

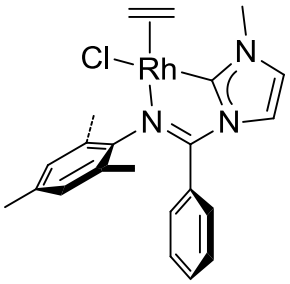

In the glovebox, an NMR tube was loaded with **7** (10 mg, 0.026 mmol, 1.0 equiv.) and **4a** (23 mg, 0.052mmol, 2.0 equiv). An adaptor was fitted onto the NMR tube and the NMR tube was closed and taken out of the glove box. On the vacuum line, CD_2Cl_2 was degassed by the freeze pump thaw method and ca 0.5 mL was vacuum-transferred into the NMR tube. The NMR tube was sealed by melting the top off, to prevent any air from entering. The reaction mixture first turned deep red, then it rapidly went dark green. No sign of formation of the desired product was observed by ^{1}H-NMR.

Attempt at preparing a Rh(I) complex: In round bottom flask at -78 ^{o}C

7 and **4a** were weighed out in the glove box. **4a** (75 mg, 0.17 mmol, 2.2 equiv.) in 19.0 mL THF was added dropwise to a stirred solution of **7** (30 mg, 0.077 mmol, 1.0 equiv.) at -78 ^{o}C. The reaction mixture was stirred in the absence of light. After 3 h, the solution had a deep red colour. Upon taking out a sample from the cooled reaction mixture, it rapidly turns dark green. The same is observed if allowed to slowly heat to room temperature. No sign of formation of the desired product was observed by ^{1}H-NMR.

Attempt at preparing a Rh(I) complex: Low temperature NMR experiment

The sample was prepared in the glovebox. A NMR tube fitted with an air tight septum was loaded with **4a** (5 mg, 0.01 mmol, 1.0 equiv) and ca 0.5 mL CD_2Cl_2. A solution of **7** in CD_2Cl_2 was prepared, the concentration was approx. 0.025 mg/μL. The NMR tube containing **4a** was cooled down in the NMR probe. At every 20 ^{o}C shimming of the magnetic field and tuning and matching of the probe were performed. When the sample was at -60 ^{o}C, it was taken out of the probe and put into a cooling bath at -78 ^{o}C and **7** (250 μL, 0.016 mmol, 1.6 equiv.) was added. The NMR tube was shaken once and then put back into the probe which still holds -60 ^{o}C. The temperature was raised gradually and the reaction was monitored by ^{1}H-NMR.

Attempt at preparing a Rh(I) complex: In round bottom flask at -78 °C II

7, **4a** and CpNa x DME were weighed out in the glove box. **7** (30 mg, 0.077 mmol, 1.0 equiv.) in 10.0 mL THF was added dropwise to a solution of **4a** (70 mg, 0.16 mmol, 2.2 equiv.) at -78 °C in 6.0 mL THF. The reaction mixture was stirred in the absence of light. After 3 h, the reaction mixture had reached a deep red colour. CpNa x DME (30 mg, 0.17 mmol, 2.2 equiv.) in 10.0 mL THF was added dropwise. The desired product was not formed, but $CpRh(CH_2CH_2)_2$ is seen by ^{1}H-NMR. The rest of the peaks resemble those of Ag(I) carbene **4a**, except that a few of the peaks are slightly shifted, however, this was a crude-NMR, so there might be some salts present causing the changes in the shifts.

^{1}H-NMR (200 MHz, C_6D_6): ($CpRh(CH_2CH_2)_2$) δ 1.10 (s br., 4H, C**H$_2$**), 2.88 (s br., 4H, C**H$_2$**), 4.83 (s, 5H, **Cp**).

^{1}H-NMR (200 MHz, C_6D_6): (presumably of **4a**) δ 1.92 (s, 6H, *o*-Ar**Me**), 2.01 (s, 3H, *p*-Ar**Me**), 2.66 (N**Me**), 5.68 (s, 1H, MeNC**H**CHN or MeNCHC**H**N), 6.60 (s, 2H, Ar**H**), 6.86-7.10 (m, 5H, Ph**H**), 7.37 (s, 1H, MeNC**H**CHN or MeNCHC**H**N).

Variable temperature ^{1}H-NMR of Rh(III) complex 8

A J-Young NMR tube was loaded with Rh(III) complex **8**, and the complex was dissolved in MeCN-d_3. The NMR tube was closed to prevent solvent from evaporating. The ^{1}H-NMR spectrum of compound **8** was recorded at 14 different temperatures ranging from 1.1 °C to 77.4 °C. At every temperature optimization of the magnetic field, shimming, and tuning and matching of the probe was performed. The exact temperature inside the probe, where the sample sits, was measured with a Delta OHM HD-9214 thermometer.

Variable temperature ^{1}H-NMR of Rh(III) complex 9

A J-Young NMR tube was loaded with Rh(III) complex **9**, and the complex was dissolved in MeCN-d_3. The NMR tube was closed to prevent solvent from evaporating. The ^{1}H-NMR spectrum of compound **9** was recorded at 16 different temperatures ranging from -39.3 °C to 66.2 °C. At every temperature, optimization of the magnetic field, shimming, and tuning and matching of the probe were performed. The exact temperature inside the probe, where the sample sits, was measured with a Delta OHM HD-9214 thermometer.

Synthesis of Ru(II) complex 10[60]

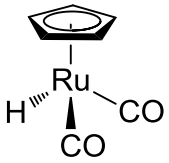

10

Dicyclopentadiene was cracked over iron fillings and freshly distilled cyclopentadiene (bp. ca 42 ^{o}C) was collected on an ice bath. A Schlenk flask was loaded with $Ru_3(CO)_{12}$ (297.2 mg, 0.4649 mg, 1.0 equiv.). 25.0 mL heptane was added and the solution was degassed by bubbling argon through. Freshly distilled cyclopentadiene (0.75 mL, 8.9 mmol, 19 equiv.) was added. The reaction mixture was heated at reflux until the reaction mixture had turned pale yellow, this is an indication that the hydride has been formed and it takes approximately 2 h. Ru(II) complex **10** was not isolated due to its instability.[60] A ^{1}H-NMR of the crude prepared in the absence of air and water on the vacuum line showed the characteristic hydride resonance.

^{1}H-NMR (of crude) (200 MHz, C_6D_6): δ -10.69 (s, Ru-**H**).

IR (of crude) (heptane): *ν*(CO) 2032 cm^{-1}, 1973 cm^{-1}.

Synthesis of Ru(I) complex 11[61]

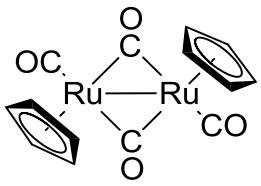

11

Dicyclopentadiene was cracked over iron fillings and freshly distilled cyclopentadiene (bp. ca 42 ^{o}C) was collected on an ice bath. A Schlenk flask was loaded with $Ru_3(CO)_{12}$ (297.2 mg, 0.4649 mg, 1.0 equiv.). 25.0 mL heptane was added and the solution was degassed by bubbling argon through. Freshly distilled cyclopentadiene (0.75 mL, 8.9 mmol, 19 equiv.) was added. The reaction mixture was heated at reflux until the reaction mixture had turned pale yellow. The flask was opened to air for a short time and the reaction mixture was heated at reflux for one more hour. Solvent was removed *in vacuo* and the resulting solid was dissolved in CH_2Cl_2:hexane (1:2) and filtered through alumina with CH_2Cl_2:hexane (1:2), the solvent was removed *in vacuo* yielding **11** (133.9 mg, 43%) as an orange crystalline solid. **11** was pure by ^{1}H-NMR.

^{1}H-NMR (200MHz, C_6D_6): δ 4.72 (s, **Cp**).

IR (heptane): *v*(CO) 2002 cm^{-1}, 1965 cm^{-1}, 1935 cm^{-1}, 1772 cm^{-1}.

MS (EI, Et_2O) *m/z*(rel.%): 446(M^+, 38), 418(17), 390(30), 362(24), 334(100).

Synthesis of Ru(II) complex 12[62]

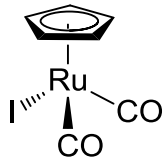

12

Dicyclopentadiene was cracked over iron fillings and freshly distilled cyclopentadiene (bp. ca 42 ^{o}C) was collected on an ice bath. A Schlenk flask was loaded with $Ru_3(CO)_{12}$ (304.7 mg, 0.4766, 1.0 equiv.) and 30.0 mL heptane, the reaction mixture was degasses by bubbling argon through. Freshly distilled cyclopentadiene (0.80 mL, 9.5 mmol, 20 equiv.) was added and the reaction mixture was heated at reflux until the reaction mixture had obtained a pale yellow colour. When the pale yellow colour had appeared a heated solution of I_2 (293.8 mg, 1.158 mmol, 2.4 equiv.) in 40.0 mL heptane was added dropwise and the reaction mixture turned red, then dark. The reaction mixture was heated at reflux for 6 h (over night may also be performed). Solvent and excess I_2 was removed *in vacuo* and the resulting solid was dissolved in CH_2Cl_2 and filtered through alumina. The solvent was removed *in vacuo* yielding **12** (390.8 mg, 78%) as a red solid. **12** was pure by ^{1}H-NMR except a few impurities in the grease-region.

^{1}H-NMR (200 MHz, C_6D_6): δ 4.29 (s, **Cp**).

IR (CH_2Cl_2): *ν*(CO) 2049 cm^{-1}, 1999 cm^{-1}.

MS (EI, Et_2O) *m/z*(rel.%): 350(M^+, 81), 322(53), 294(30), 229(10), 167(100).

Attempts at preparing new Ru(II) *N*-heterocyclic carbene complexes

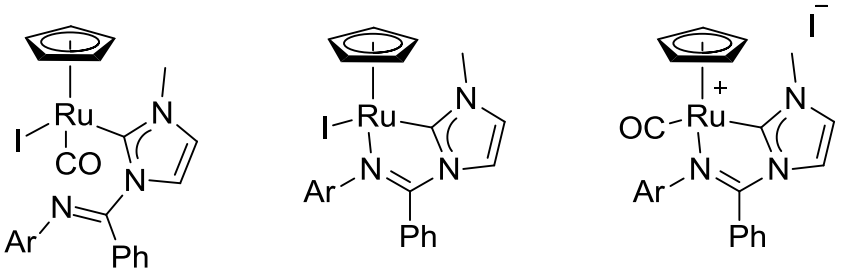

Several attempts on preparing a new Ru(I) *N*-heterocyclic carbene complex were performed. An overview of the different attempts is given in **Table 13**. The detailed procedures are given below.

Attempt at preparing a new Ru(II) *N*-heterocyclic carbene complex I

Imidazolium salt **3b** (115.1 mg, 0.3531 mmol, 1.2 equiv.) in 10.0 mL CH_2Cl_2 was added to a solution of Ru(II) complex **12** (100.6 mg, 0.2882, 1.0 equiv) in 5.0 mL CH_2Cl_2. The reaction mixture was heated at reflux for 4 h. After 4 h the reaction mixture was investigated by IR and no change in *v*(CO) was observed.

Attempt at preparing a new Ru(II) *N*-heterocyclic carbene complex II

A solution of Ag(I) carbene **4b** (140.4 mg, 0.325 mmol, 1.1 equiv.) at 0 ^{o}C in 11.0 mL CH_2Cl_2 was added dropwise to a solution of Ru(II) complex **12** (102.5 mg, 0.2935, 1.0 equiv) at 0 ^{o}C in 6.0 mL CH_2Cl_2. The reaction mixture was stirred in the absence of light and was warmed to room temperature over night. No change in the ν_{CO} was observed by IR and no change in ^{1}H-NMR shift of the Cp was observed.

Attempt at preparing a new Ru(II) *N*-heterocyclic carbene complex: NMR experiment I

An NMR tube was loaded with Ru(II) complex **12** (7.8 mg. 0.022 mmol, 1.0 equiv.) and Ag(I) carbene **4b** (10.8 mg, 0.025 mmol, 1.1 equiv) and fitted to the vacuum line via an adaptor. Dry $CDCl_3$ was degassed by the freeze pump thaw method and vacuum-transferred into the NMR tube. The NMR tube was sealed by melting the top off and the reaction was monitored by ^{1}H-NMR. No significant change of the ^{1}H-NMR signal of the Cp was observed.

Attempt at preparing a new Ru(II) *N*-heterocyclic carbene complex: NMR experiment II

A NMR tube was loaded with Ru(II) complex **12** (8.0 mg, 0.023 mmol, 1.0 equiv.) and Ag(I) carbene **4b** (10.4 mg, 0.0240 mmol, 1.0 equiv.) and fitted on the vacuum line via an adaptor. Dry CD_2Cl_2 was degassed by the freeze pump thaw technique and vacuum-transferred into the NMR tube. The NMR tube was sealed by melting the top off and the reaction was monitored by ^{1}H-NMR. No significant shift in the Cp ^{1}H- NMR resonance was observed.

Attempt at preparing a new Ru(II) *N*-heterocyclic carbene complex III

t-BuOK was weighed out in the glove box. *t*-BuOK (33.3 mg, 0.297 mmol, 1.2 equiv.) was dissolved in 20.0 mL THF, cooled down to -78 ^{o}C and added dropwise to a solution of Ru(II) complex **12** (86.3 mg, 0.247 mmol, 1.0 equiv.) and imidazolium salt **3a** (93.6 mg, 0.2770 mmol, 1.1 equiv.) at -78 ^{o}C in 10.0 mL THF over a period of 30 min. The reaction mixture was slowly heated to room temperature over night and investigated by ^{1}H-NMR the next day. No significant shift in the Cp ^{1}H- NMR resonance was seen. Decomposition of imidazolium salt **3a** was observed.

Table 13: Attempts at preparing a new Ru(I) *N*-heterocyclic carbene complex.

Reagent 1	Reagent 2	Reagent 3	Solvent	Conditions	Time	Result
12	**3b**	-	CH_2Cl_2	reflux	4 h	**12** unchanged
12	**4b**	-	CH_2Cl_2	0 ^{o}C	Over night	**12** unchanged
12	**4b**	-	$CDCl_3$[a]	Ambient temperature	Followed by ^{1}H-NMR	**12** unchanged
12	**4b**	-	CD_2Cl_2[a]	Ambient temperature	Followed by ^{1}H-NMR	**12** unchanged
12	**3a**	*t*-BuOK	THF	-78 ^{o}C, then ambient temperature	Over night	**12** unchanged **3a** decomposed

a: NMR experiment

Synthesis of Co-complex 13[43, 67]

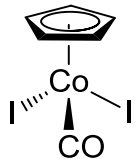

13

$CpCo(CO)_2$ is very air sensitive and was weighed out in the glove box. I_2 (570.0 mg, 2.246 mmol, 1.0 equiv) in 60.0 mL Et_2O was added dropwise to a solution of $CpCo(CO)_2$ (413 mg, 2.29 mmol, 1.0 equiv.) in a Schlenk flask at 0 °C in 10 mL Et_2O. The reaction mixture was stirred at room temperature for 3 d. The solvent was removed *in vacuo* and the solid was washed with 40 mL heptane yielding **13** (753 mg, 81 %) as a dark purple solid. **13** was pure by ^{1}H-NMR except a few impurities in the grease-region.

^{1}H-NMR (200 MHz, C_6D_6): δ 4.34 (s, **Cp**).

^{1}H-NMR (200 MHz, $CDCl_3$): δ 5.66 (s, **Cp**).

MS (EI, MeCN) *m/z* (rel.%): 406(M^+, 5), 378(6), 251(100), 186(10), 128(23), 127(14), 124(68), 65(12), 39(17).

IR (CH_2Cl_2) *ν*(CO) 2077 cm^{-1}.

Attempts at preparing new Co *N*-heterocyclic carbene complexes

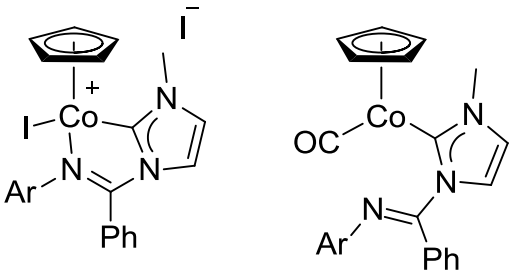

A few attempts at preparing new Co(I) and Co(III) *N*-heterocyclic complexes were performed, without any overwhelming results. An overview of the different procedures and their results are given in **Table 14**. The detailed procedures are given below.

Attempt at preparing a new Co(I) *N*-heterocyclic carbene complex: NMR experiment

All compounds were weighed out in the glove box. An NMR tube was loaded with $CpCo(CO)_2$ (13 mg, 0.072 mmol, 1.0 equiv.) and Ag(I) carbene **4a** (41 mg, 0.092 mmol, 1.3 equiv.). The NMR tube was fitted with an adapter, closed to prevent air from entering and taken out of the glove box. C_6D_6 was degassed by the freeze pump thaw method and was vacuum-transferred into the NMR tube. The NMR tube was sealed by melting the top off and the reaction was investigated by ^{1}H-NMR. No indication of any reaction was seen by ^{1}H-NMR. The solution was then refluxed for 1 h and was again investigated by ^{1}H-NMR. It was observed that the Ag(I) carbene **4a** had started to decompose while the ^{1}H-NMR signal of the Cp had not changed. Upon further heating, the Ag(I) carbene **4a** decomposed further.

Attempt at preparing a new Co(I) *N*-heterocyclic carbene complex

t-BuOK and $CpCo(CO)_2$ were weighed out in the glove box. Imidazolium salt **3a** (206.5 mg, 0.6111 mmol, 1.1 equiv.) in 10.0 mL THF was added to a solution of $CpCo(CO)_2$ (99 mg, 0.55 mmol, 1.0 equiv.) in 5.0 mL THF, the reaction mixture was cooled down to -78 ^{o}C and *t*-BuOK (74 mg, 0.66 mmol, 1.2 equiv.) in 20.0 mL THF was added dropwise over 30 min. The reaction mixture was stirred and warmed to ambient temperature over night. A sample was taken out from the reaction mixture, and an air free NMR sample was prepared on the vacuum line. No shift of the ^{1}H-NMR signal of the Cp was seen. Decomposition of the imidazolium salt **3a** was observed.

Attempt at preparing a new Co(III) *N*-heterocyclic carbene complex: NMR experiment

All reagents were weighed out in the glove box. An NMR tube was loaded with Co(III) complex **13** (11 mg, 0.027 mmol, 1.0 equiv.) and Ag(I) carbene **4a** (13 mg, 0.029 mmol, 1.1 equiv.). The NMR tube was fitted with an adapter, sealed to prevent air from entering and was taken out of the glove box. $CDCl_3$ was degassed on the vacuum line by the freeze pump thaw technique and vacuum-transferred into the NMR tube. The NMR tube was sealed by melting the top off and the reaction was investigated by ^{1}H-NMR. A colour change from the purple colour of Co(III) complex **13** to a deep red colour was observed. The ^{1}H-NMR shift of the Cp has now moved from 5.66 to 5.28 ppm, however, no indications of formation of the desired complex was seen.

Table 14: Attempts on preparing new Co(I) and Co(III) *N*-heterocyclic carbene complex

Reagent 1	Reagent 2	Reagent 3	Solvent	Conditions	Time	Result
$CpCo(CO)_2$	**4a**	-	C_6D_6[a]	Ambient temperature, then reflux	Followed by ^{1}H-NMR	**4a** decomposed. $CpCo(CO)_2$ unchanged
$CpCo(CO)_2$	**3a**	*t*-BuOK	THF	-78 ^{o}C, then ambient temperature	Over night	**3a** decomposed $CpCo(CO)_2$ unchanged
13	**4a**	-	$CDCl_3$[a]	Ambient temperature	Followed by ^{1}H-NMR	Starting material has disappeared, no desired compound formed

a: NMR-experiment

Computational details

DFT Structure optimization of Rh(III) complex 8

The structure of the cationic part of complex **8** was optimized with density functional theory calculations (DFT) by following the stepwise approach illustrated in **Figure 43.** The first steps were performed on a local desktop computer, whereas the last step was performed on the Abel supercomputer.[68] The first optimization was performed on a simplified model of **8**, in which the phenyl, mesityl and Cp* methyls were replaced by hydrogen atoms. After these initial calculations, the system was re-optimized by adding the Cp*-methyls. In the subsequent two steps, the mesityl and phenyl groups were added to have a full model of the system. This model was finally re-optimized at a higher level of theory on the Abel supercomputer.

All calculations were carried out at the DFT level with Gaussian09.[69] Structures were fully optimized in gas phase without any geometry and symmetry constraints. Vibrational frequencies were computed in order to verify that all stationary points were minima of the potential energy surface. The pure PBE functional was used to carry out the geometry optimizations on the desktop computer.[70-71] The Stuttgart-Dresden pseudopotentials were used for Rh and Cl with the associated basis sets.[72] C, N and H were described with the all-electron double-ζ 6-31G** basis set.[73] For the calculations performed on Abel, a higher level of theory was used, involving the hybrid PBE0 functional and the 6-31G* basis set for C, N and H.[74-75] The calculations were performed in collaboration with a postdoctoral researcher at the CTCC (Centre for Theoretical and Computational Chemistry) of the University of Oslo, Dr. David Balcells.

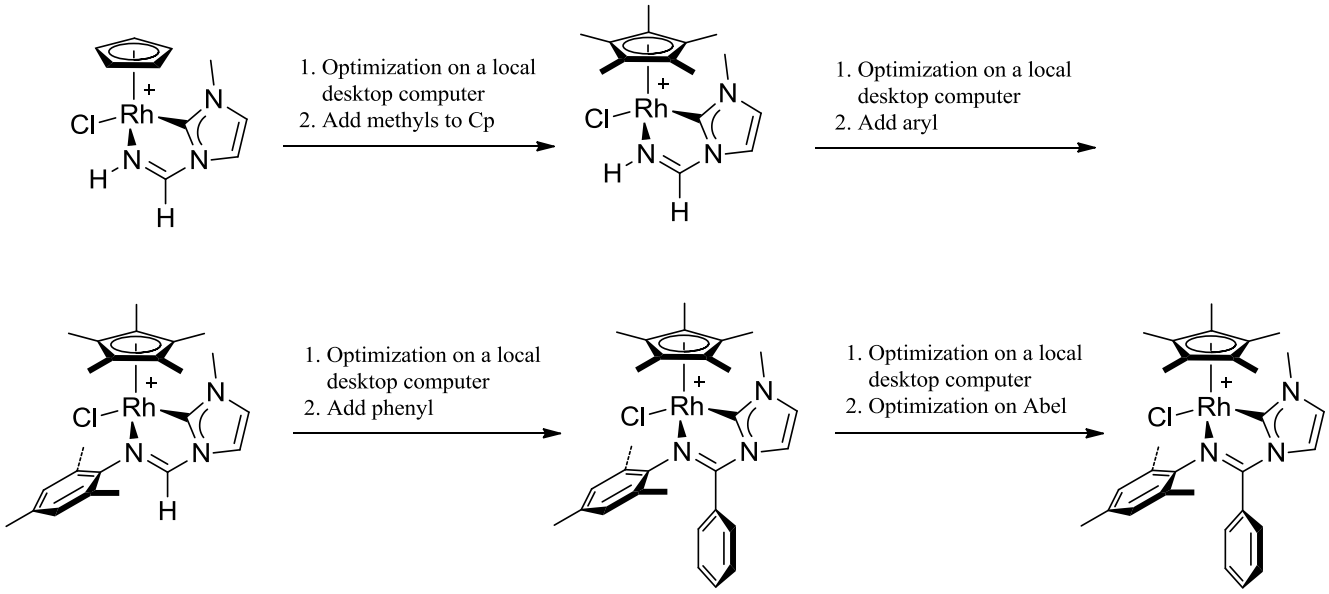

Figure 43: Strategy for optimization of the structure of the cationic part of Rh(III) complex **8**.

Appendix

Compound 1a

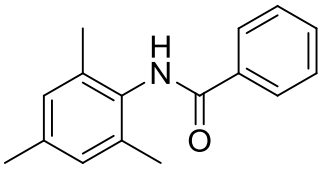

1a

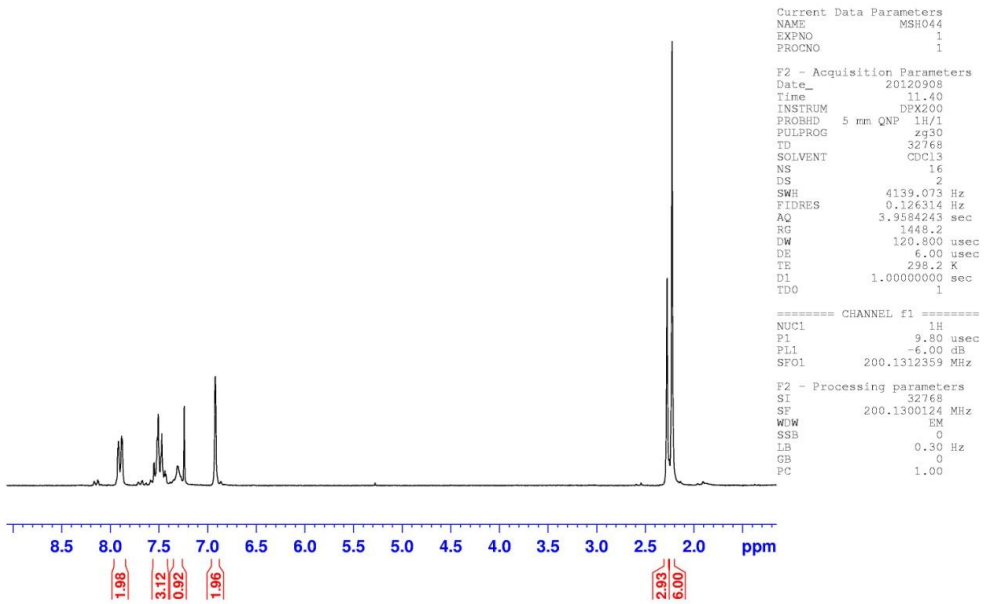

Figure 44: ^{1}H-NMR (200 MHz, $CDCl_3$) spectrum of 1a.

Compound 1b

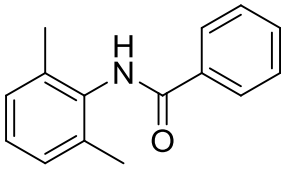

1b

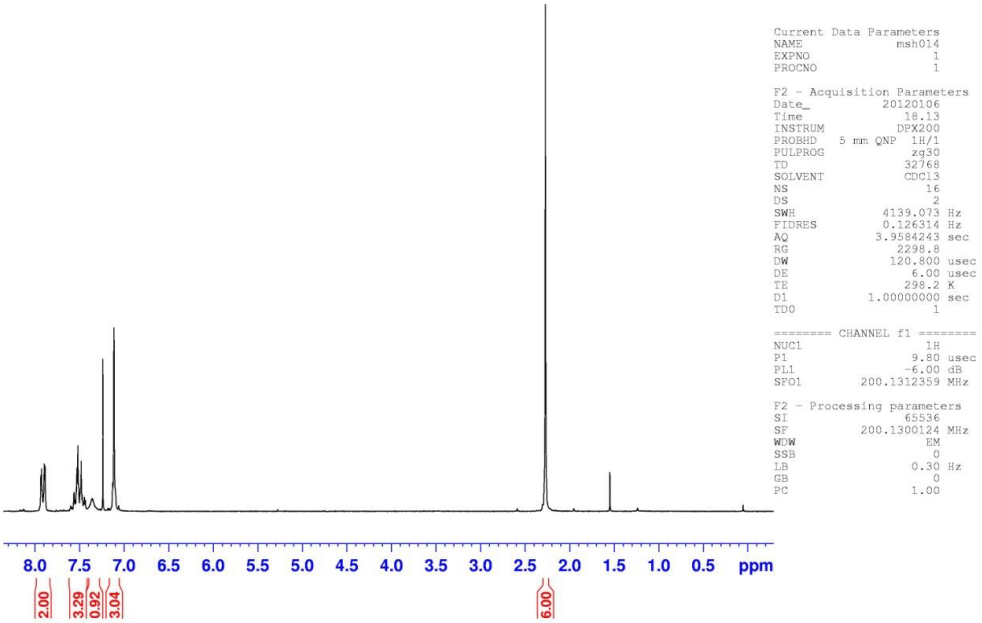

Figure 45: ^{1}H-NMR (200 MHz, $CDCl_3$) spectrum of 1b. The peak at ca 1.5 ppm is water from the NMR solvent.

Compound 2a

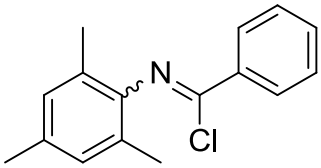

2a

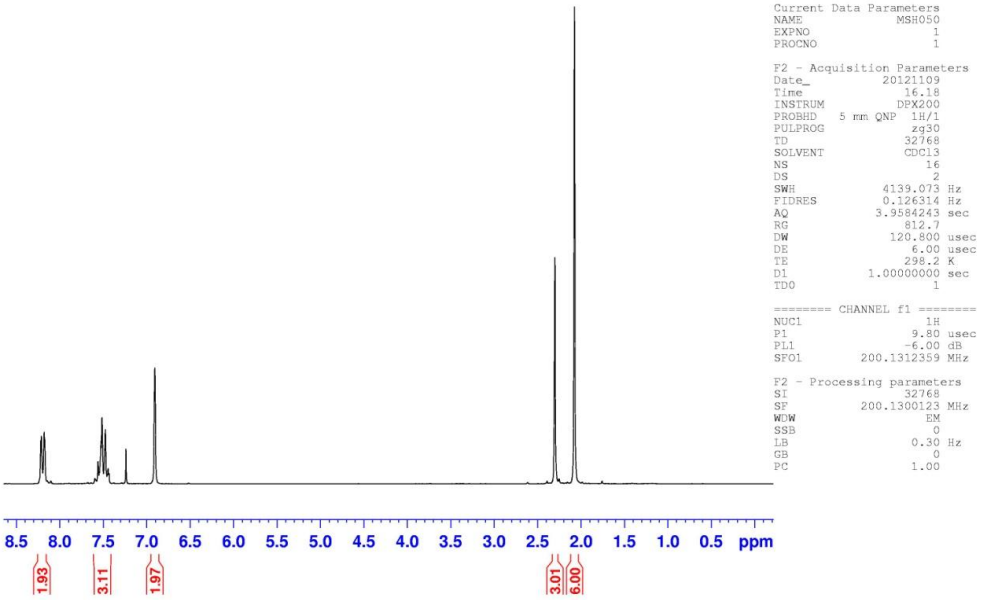

Figure 46: ^{1}H-NMR (200 MHz, $CDCl_3$) spectrum of **2a**.

Compound 2b

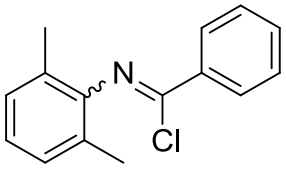

2b

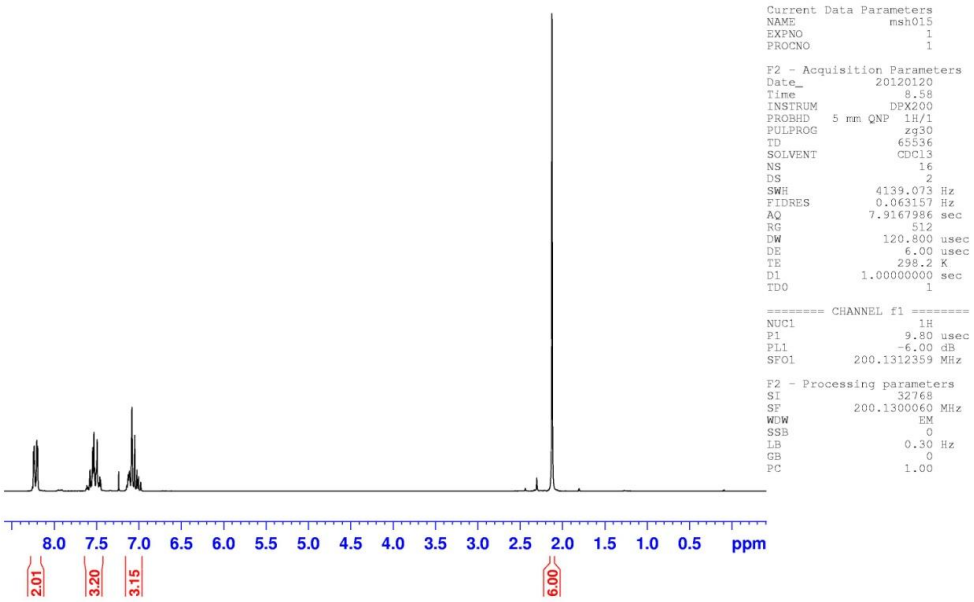

Figure 47: ^{1}H-NMR (200 MHz, $CDCl_3$) spectrum of **2b**.

Compound 3a

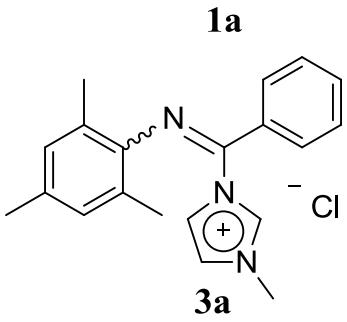

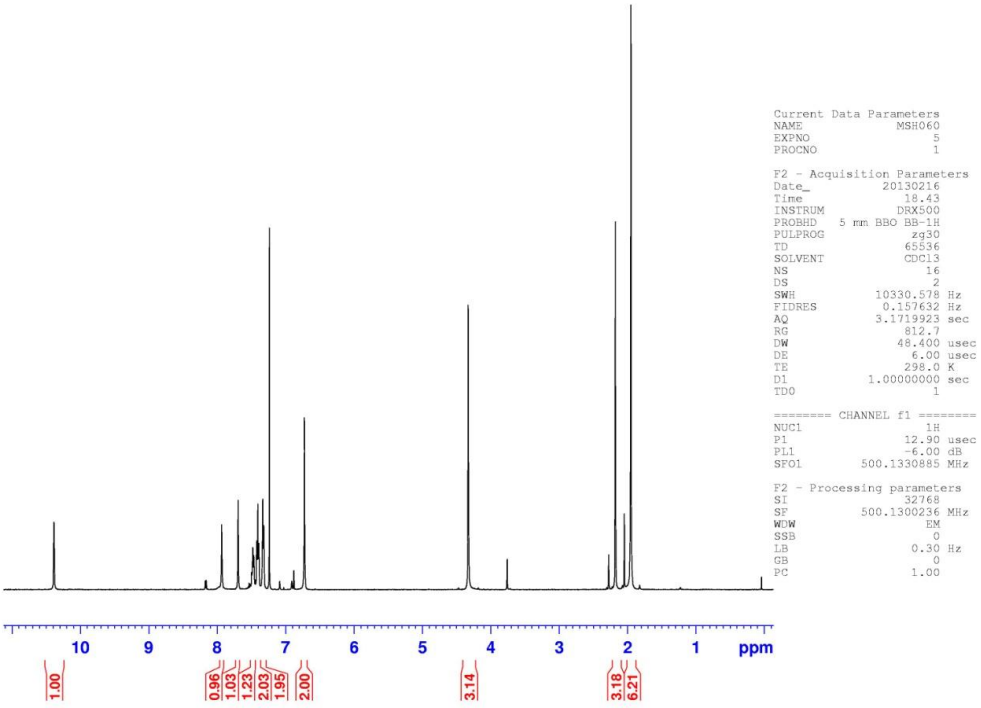

Figure 48: ^{1}H-NMR (500 MHz, $CDCl_3$) spectrum of **3a**.

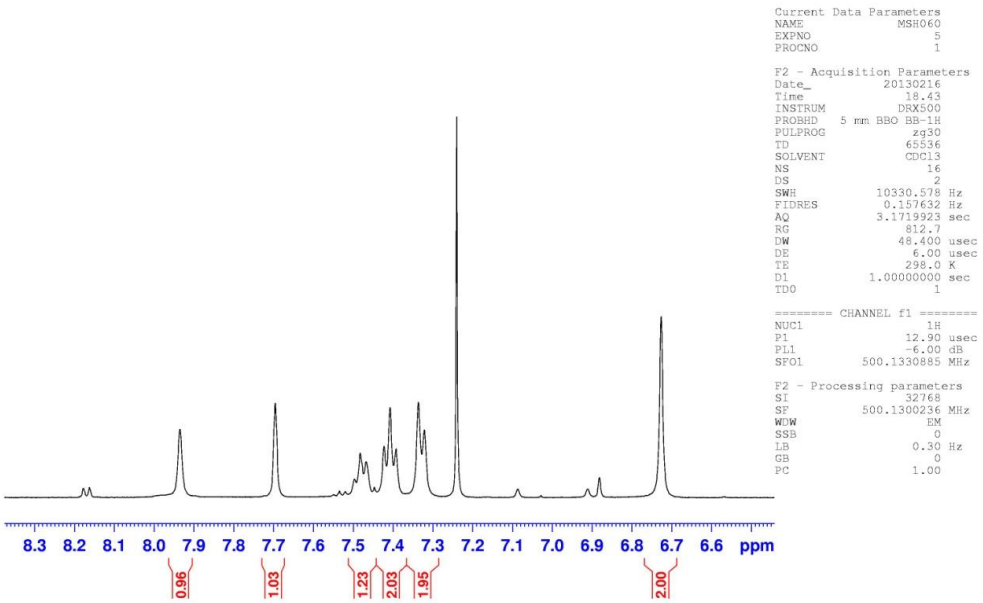

Figure 49: ^{1}H-NMR (500 MHz, $CDCl_3$) spectrum of **3a**. Close-up of the aromatic region.

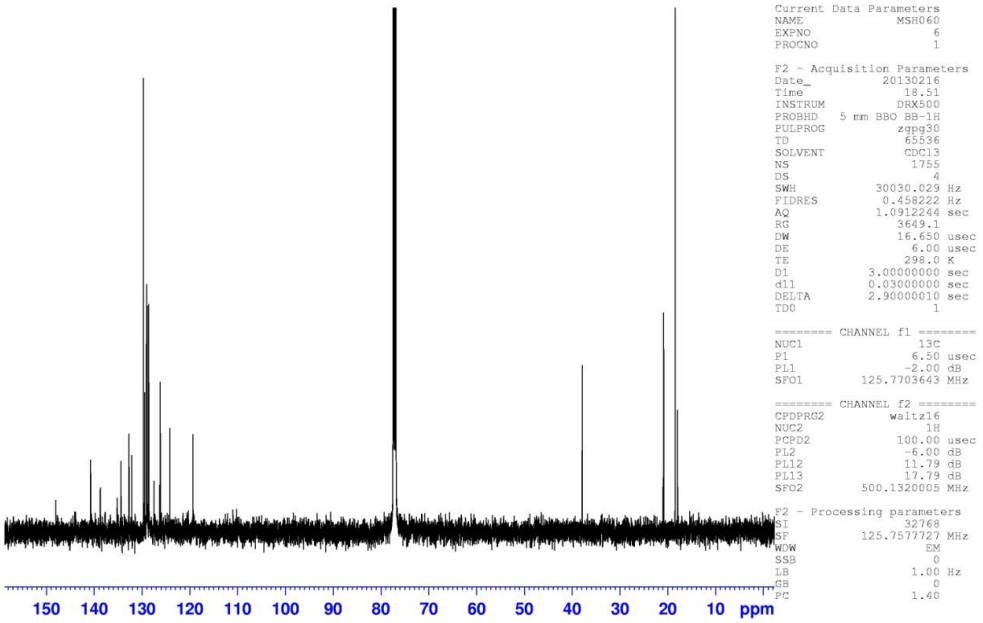

Figure 50: ^{13}C-NMR (125 MHz, $CDCl_3$) spectrum of **3a**.

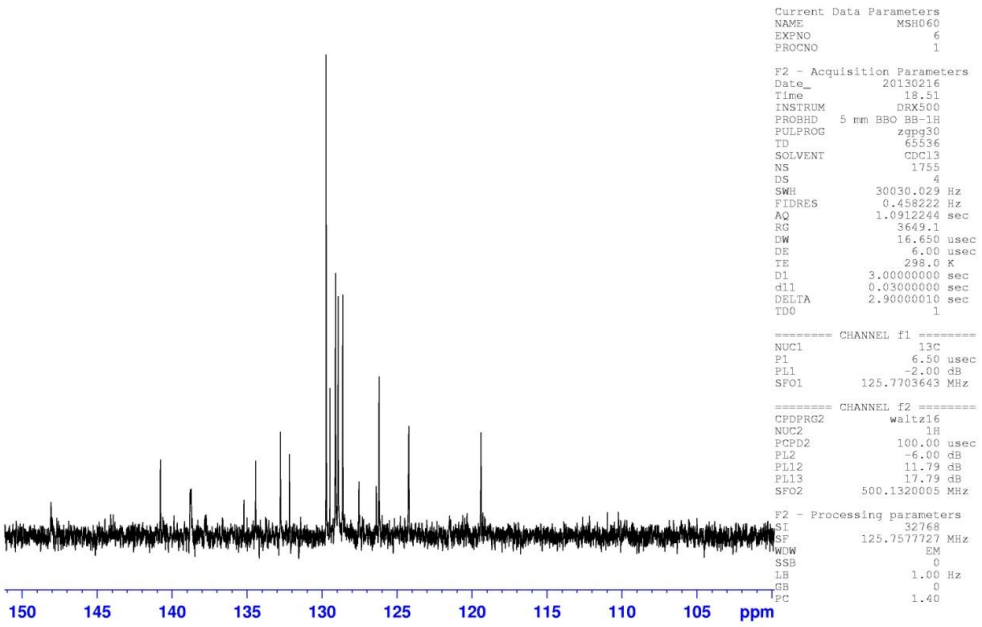

Figure 51: ^{13}C-NMR (125 MHz, $CDCl_3$) spectrum of **3a**. Close-up of the aromatic region.

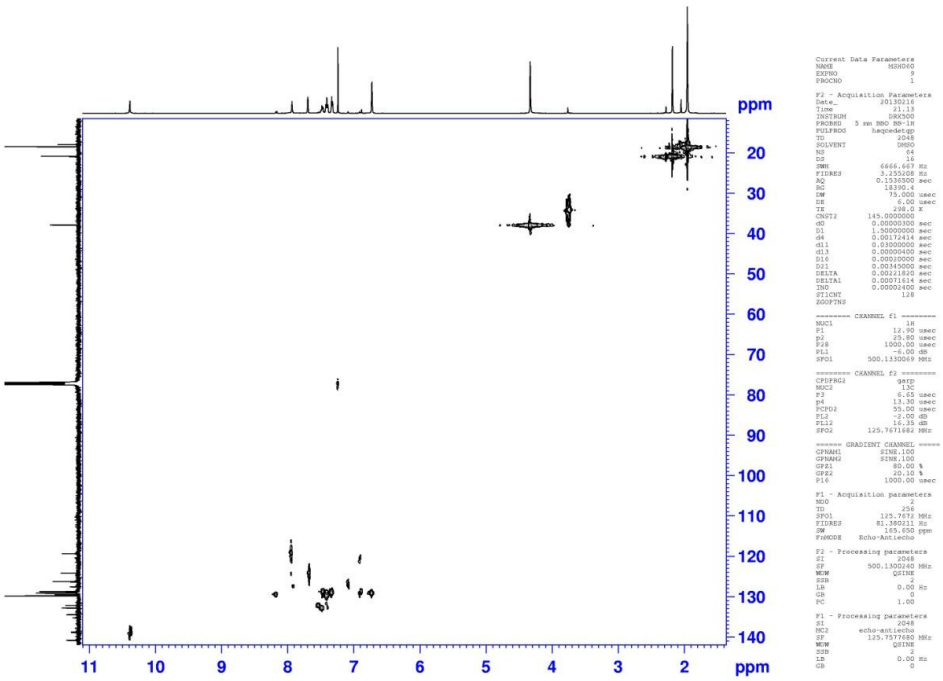

Figure 52: HSQC (500 MHz, $CDCl_3$) spectrum of **3a**.

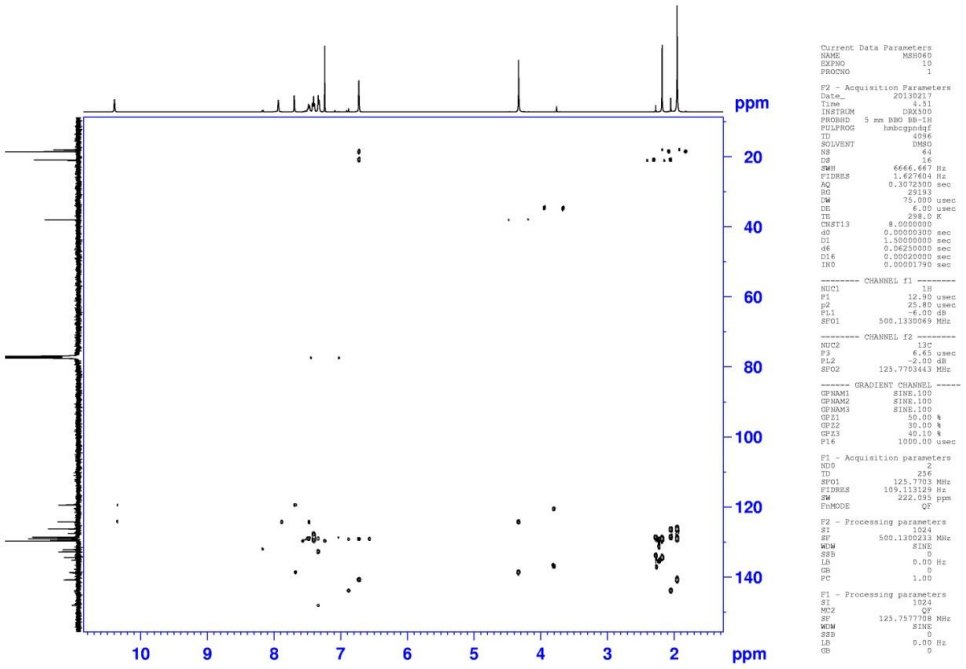

Figure 53: HMBC (500 MHZ, $CDCl_3$, no decoupling) spectrum of **3a**.

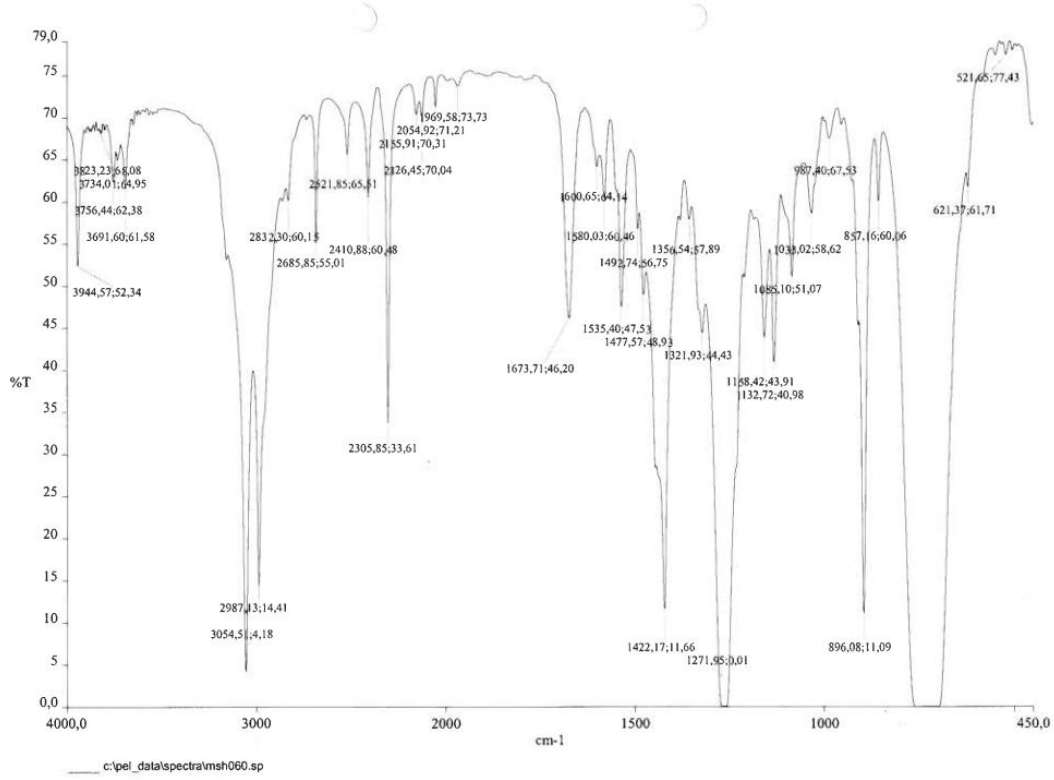

Figure 54: IR (CH_2Cl_2) spectrum of **3a**.

Compound 3b

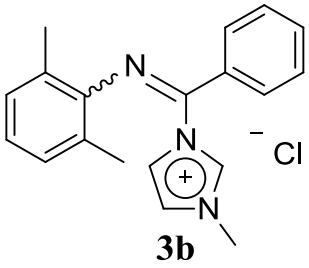

3b

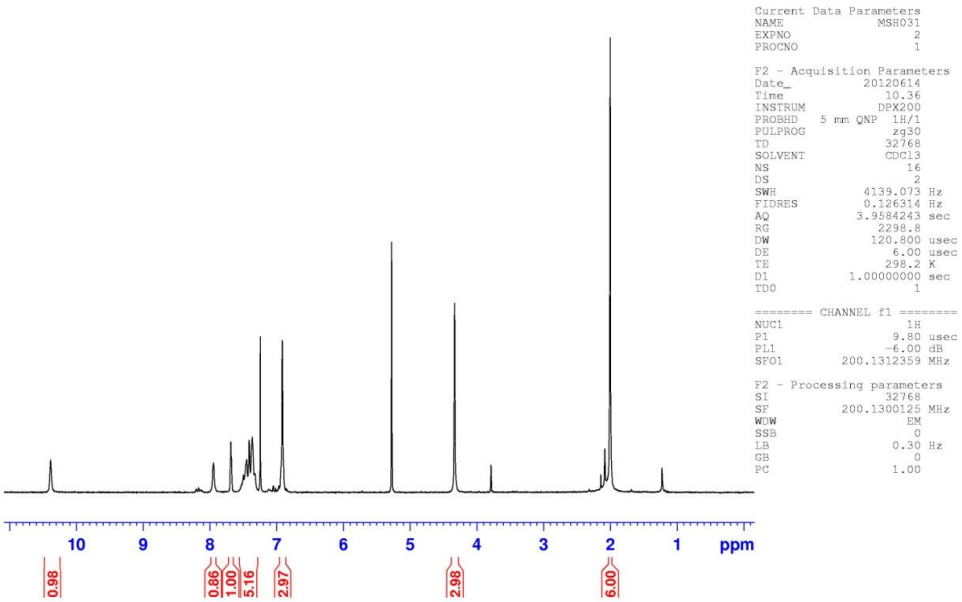

Figure 55: ^{1}H-NMR (200 MHz, $CDCl_3$) spectrum of **3b**. The peak at ca 5.3 is CH_2Cl_2.

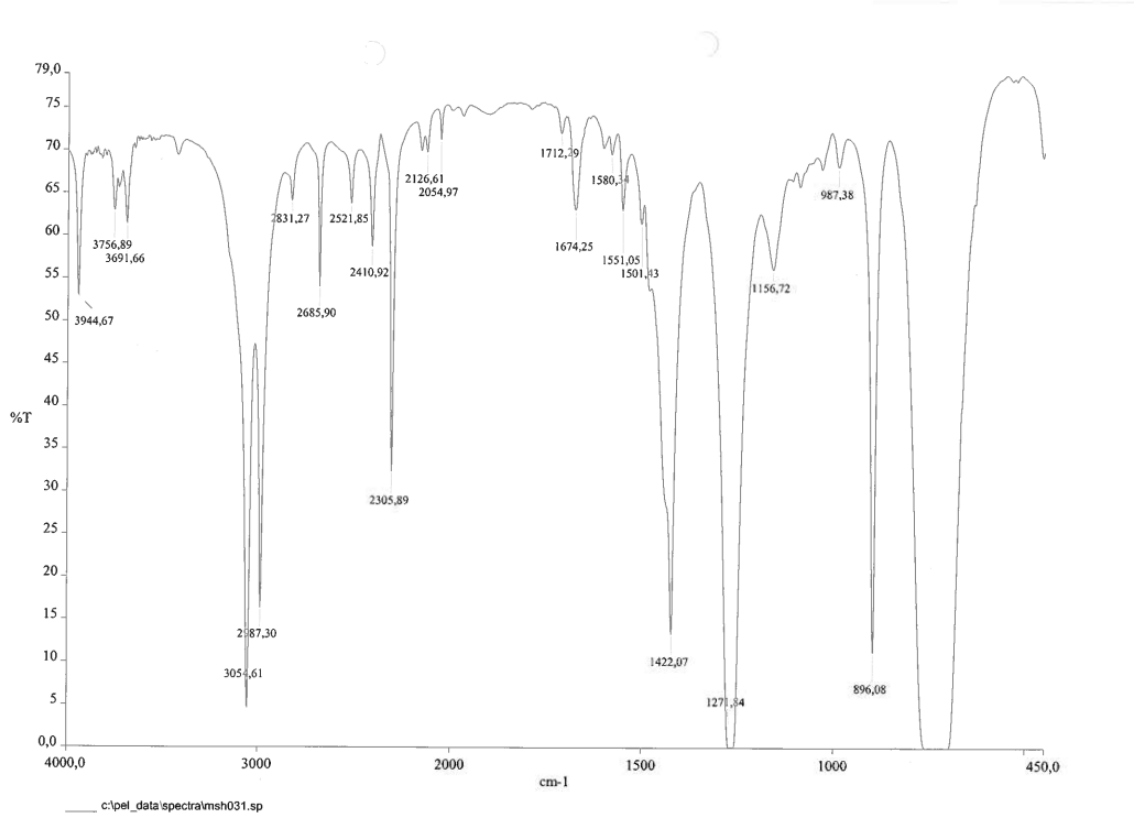

Figure 56: IR (CH_2Cl_2) spectrum of **3b**.

Compound 4a

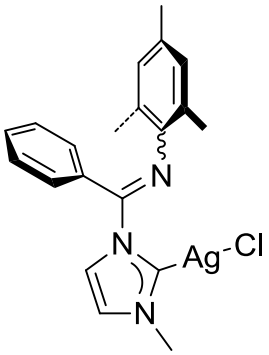

4a

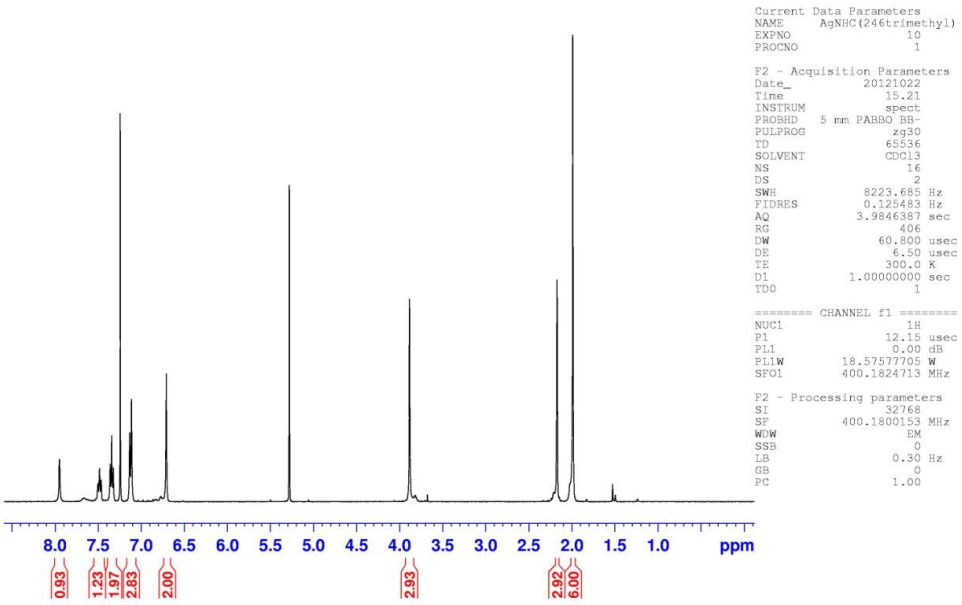

Figure 57: ^{1}H-NMR (400 MHz, $CDCl_3$) spectrum of **4a**. The peaks at ca 1.5 and 5.3 are due to CH_2Cl_2 and water.

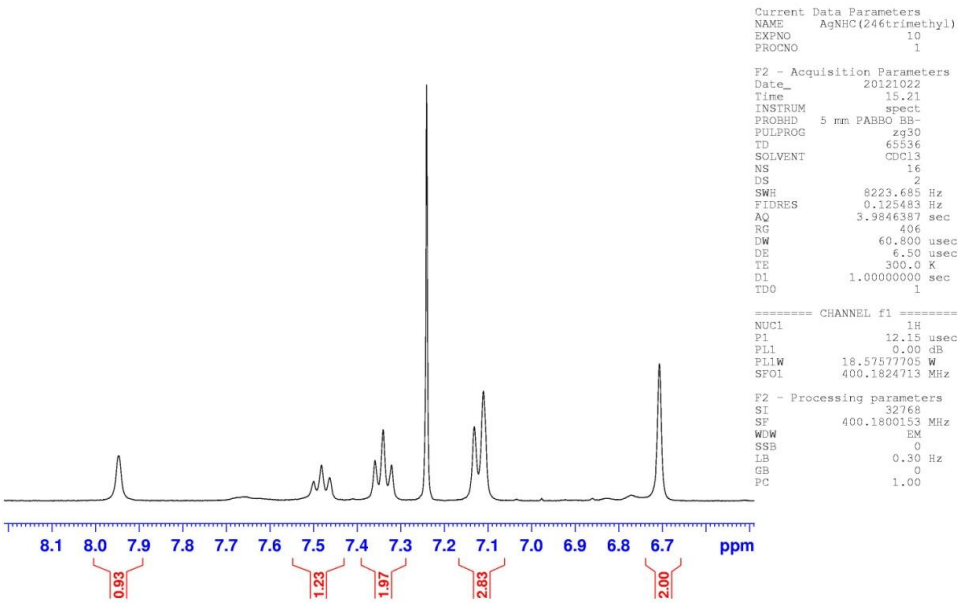

Figure 58: ^{1}H-NMR (400 MHZ, $CDCl_3$) spectrum of **4a**. Close-up of the aromatic region.

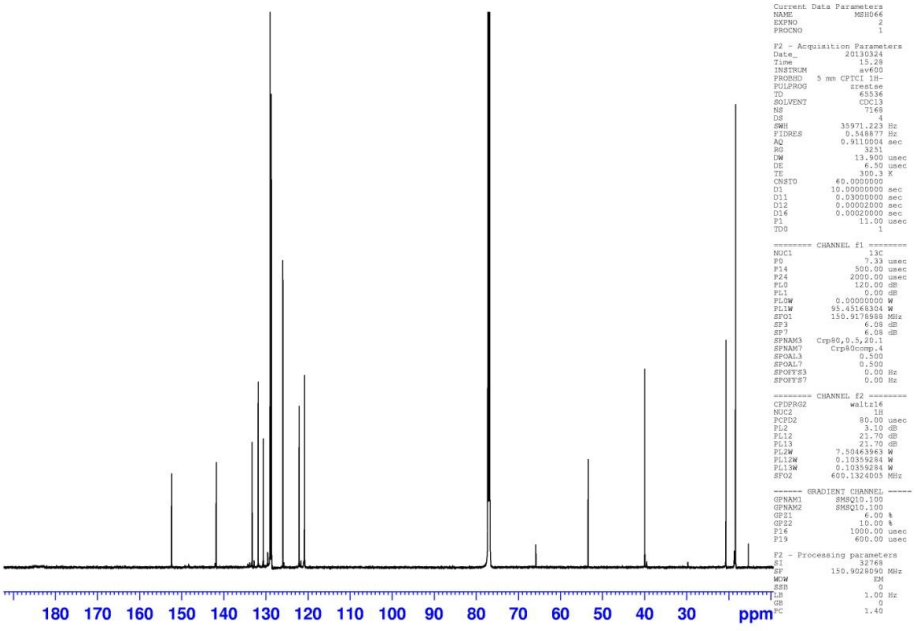

Figure 59: ^{13}C-NMR (150 MHz, $CDCl_3$, d1 = 10 s) spectrum of **4a**. The peak at ca 53 ppm is due to CH_2Cl_2.

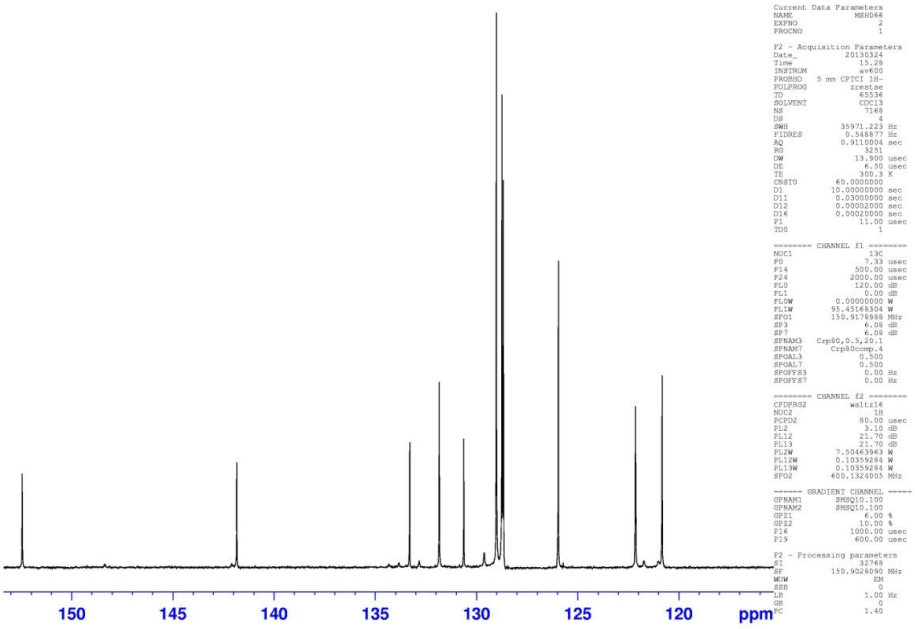

Figure 60: ^{13}C-NMR (150 MHz, $CDCl_3$, d1=10 s) spectrum of **4a**. Close-up of the aromatic region.

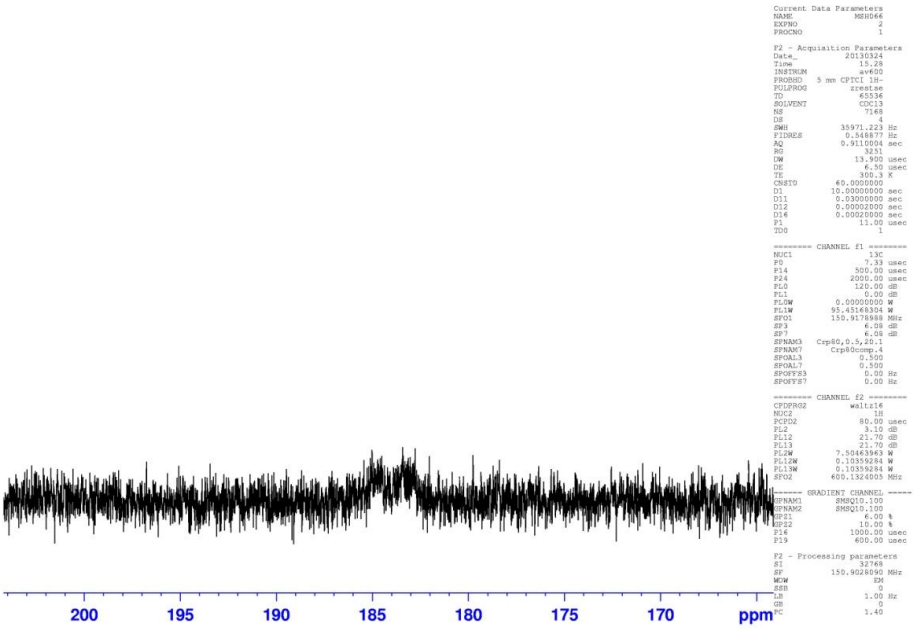

Figure 61: ^{13}C-NMR (150 MHz, $CDCl_3$, d1= 20 s) spectrum of **4a**. Close-up of $C_{carbene}$.

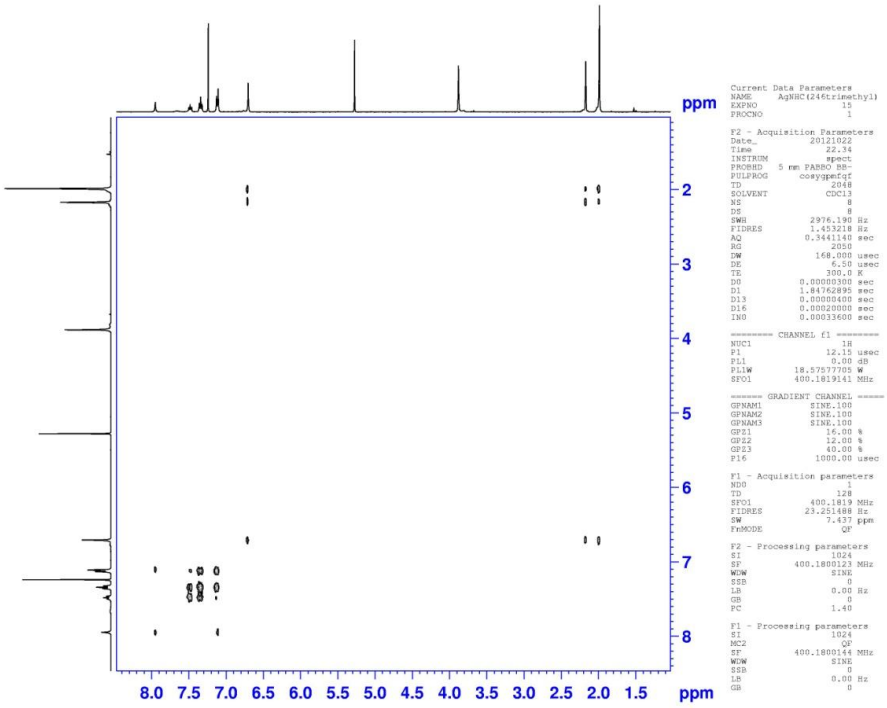

Figure 62: COSY (500 MHz, $CDCl_3$) spectrum of **4a**.

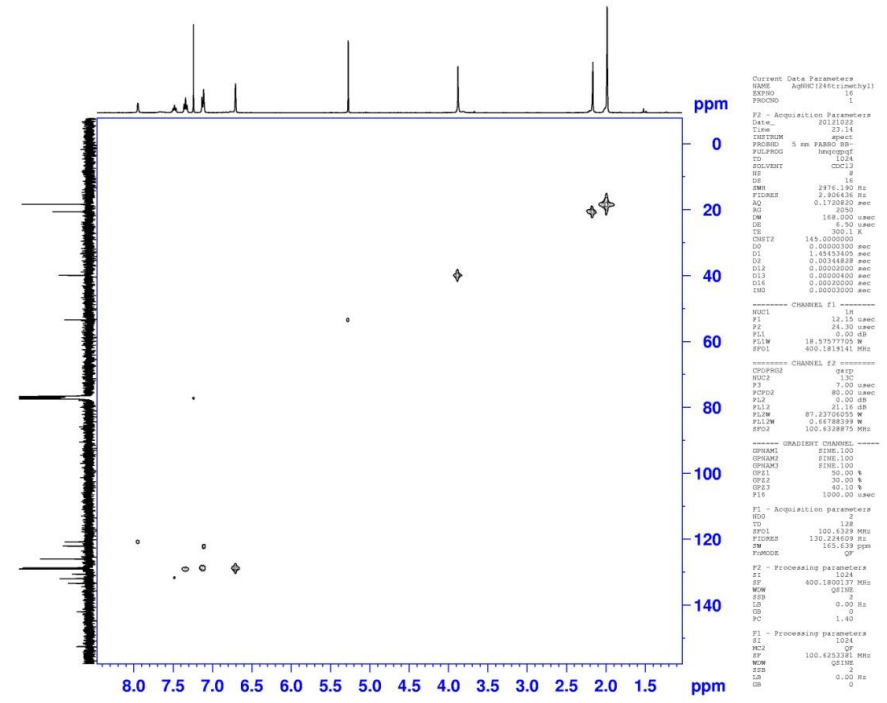

Figure 63: HMQC (400 MHz, $CDCl_3$) spectrum of **4a**.

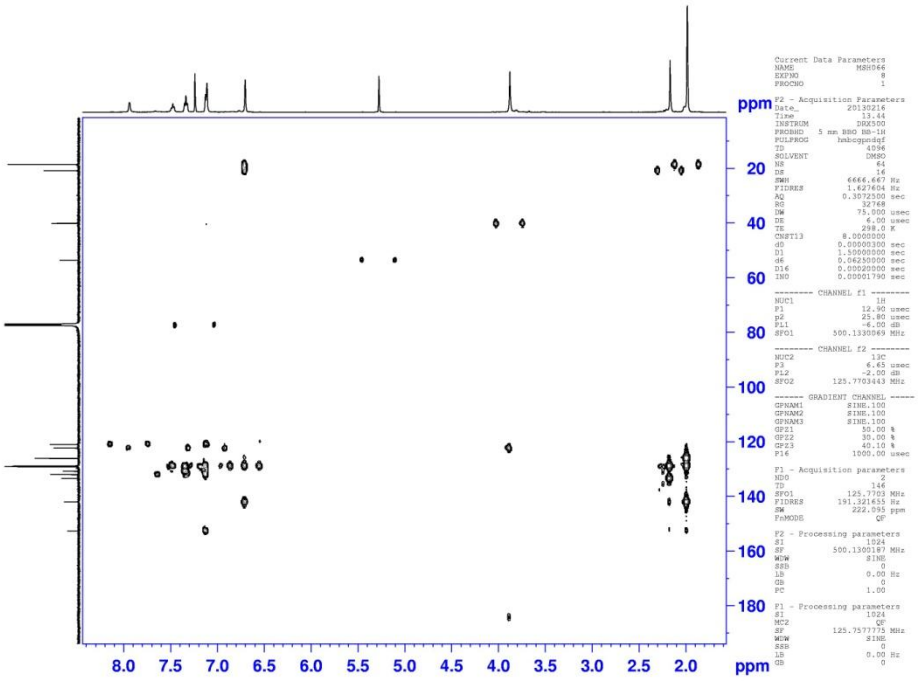

Figure 64: HMBC (500 MHz, $CDCl_3$, no decoupling) spectrum of **4a**.

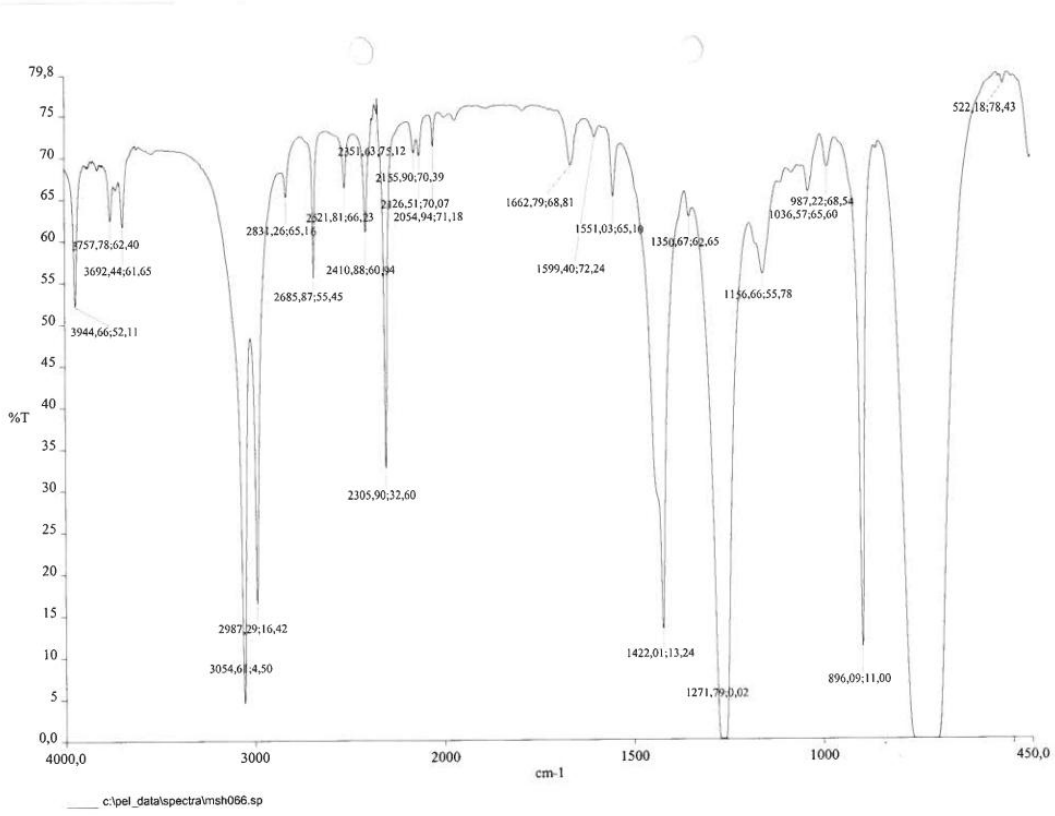

Figure 65: IR (CH_2Cl_2) spectrum of **4a**.

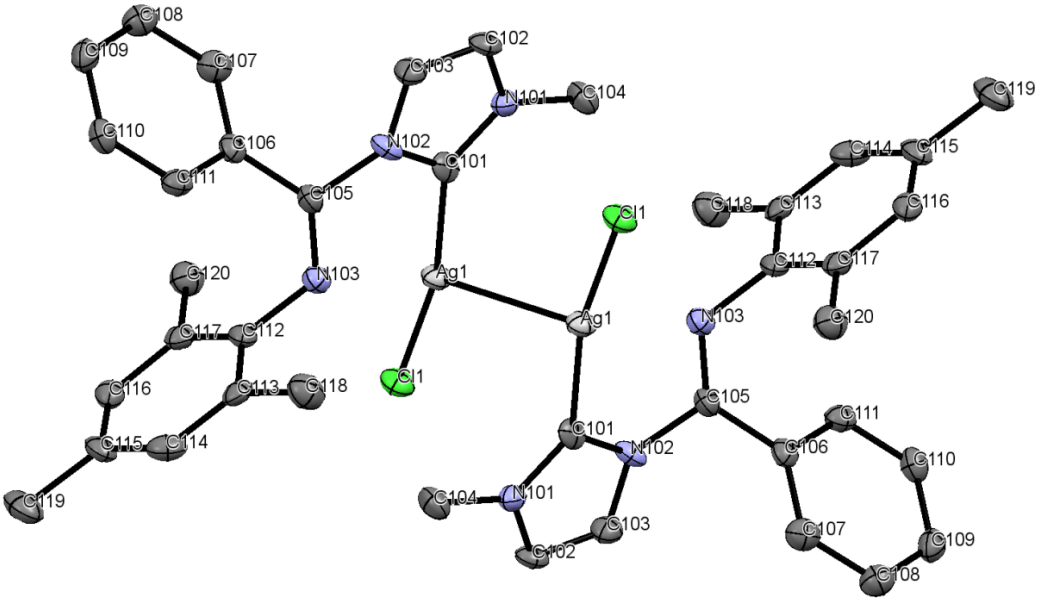

Figure 66: ORTEP-drawing of complex **4a**. Hydrogens and CH_2Cl_2 are omitted for clarity. Ellipsoids at 50% probability.

Table 15: Selected bond lengths from structure based on the X-ray analysis of **4a**.

Bond	Bond length [Å]
Ag(1)-C(101)	2.075(8)
Ag(1)-C(l1)	2.343(2)
Ag(1)-Ag(1)	3.073(2)
N(101)-C(101)	1.345(10)
N(102)-C(101)	1.349(11)
N(103)-C(105)	1.264(10)

Table 16: Selected bond angles from structure based on the X-ray analysis of **4a**.

Angle	Degrees [°]
C(101)-Ag(1)-Cl(1)	165.9(2)
C(101)-Ag(1)-Ag(1)	76.1(2)
Cl(1)-Ag(1)-Ag(1)	117.85(6)
N(101)-C(101)-N(102)	103.9(7)
N(101)-C(101)-Ag(1)	132.4(6)
N(102)-C(101)-Ag(1)	123.6(6)

Table 17: Crystallographic data for compound **4a**.

Crystal data	
Formula	$(C_{40}H_{42}N_6Ag_2Cl_2)$ $2(C\ Cl_2)$*
Formula weight	1059.34
Crystal size	0.35 x 0.25 x 0.003 mm
Colour, shape	Yellow, prism
Crystal system	Triclinic
Space group	$P\overline{1}$
b	9.265(6) Å
c	13.543(9) Å
α	92.527(7)^o
β	95.936(7)^o
γ	101.591(7)^o
V	11102.3(13)Å^3
Z	1
T	100 K
Radiation	Mo *K*α, λ=0.71073 Å
θ_{min}-θ_{max}	2.3-25.1^o
μ	1.29 mm^{-1}
D_x	1.614 Mg m^{-3}
Data Collection	
Instrument	Bruker Apex II CCD diffractiometer
Measured reflections	7828
Independent reflections	3843
Reflections with $I>2\sigma(I)$	3613
R_{int}	0.028
h	-10→10
k	-10→11
l	-16→16

Refinement	
Refinement on F^2	
$R[F^2>2\sigma(F^2)]$	0.063
$wR(F^2)$	0.172
S	1.61
Reflections	3842
Parameters	255
Restraints	0
w	$1/[\sigma^2(F_o^2)+(0.0257P)^2+9.P]$ where $P=(F_o^2+2F_c^2)/3$
$(\Delta/\sigma)_{max}$	<0.001
$\Delta\rho_{max}$	2.68 e $Å^3$
$\Delta\rho_{min}$	-1.17 e $Å^{-3}$
Hydrogen atoms treated by a mixture of independent and constrained refinement	

* No hydrogen atoms were added to the solvent molecules in this structure

Compound 4b

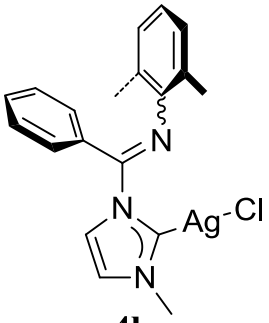

4b

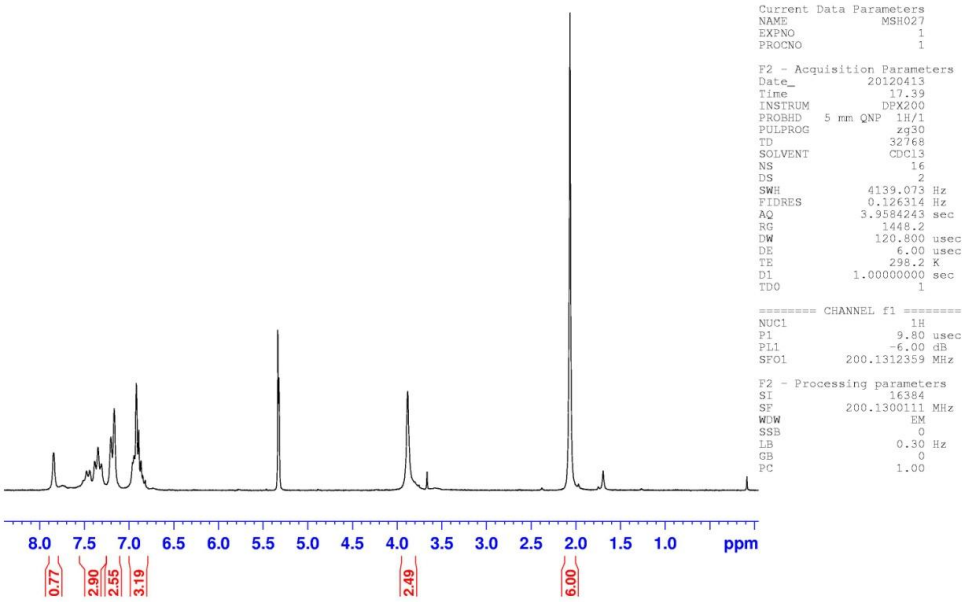

Figure 67: ^{1}H-NMR (200 MHz, CD_2Cl_2) spectrum of **4b**.

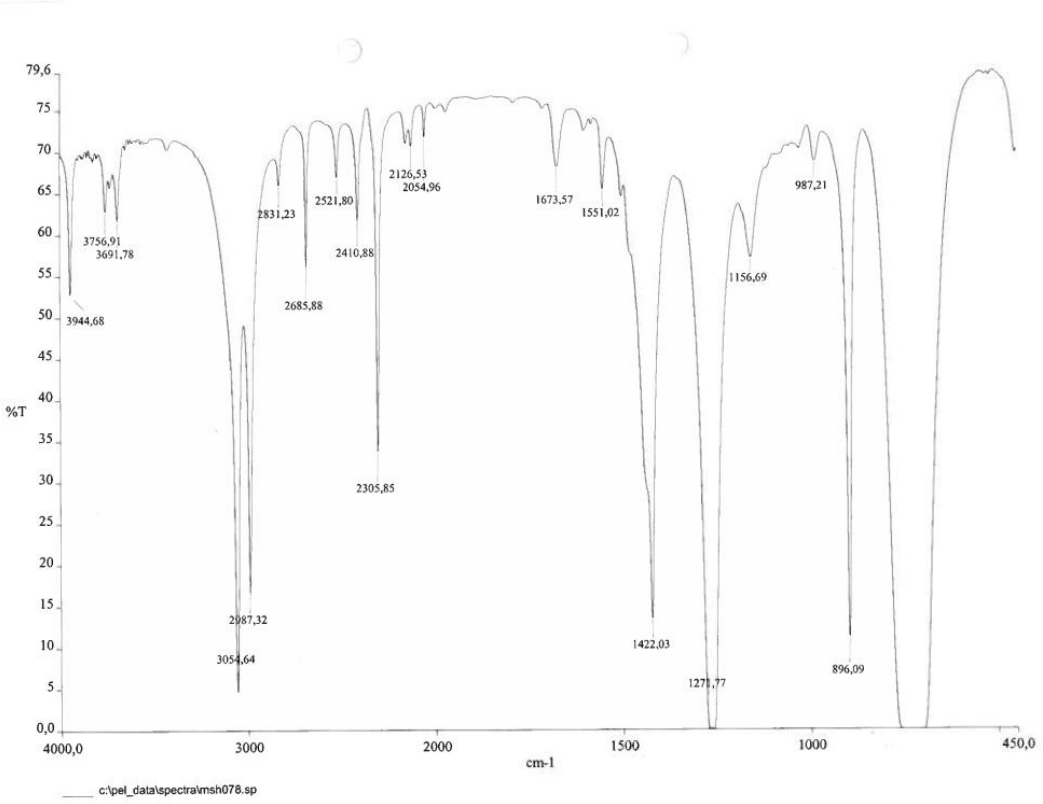

Figure 68: IR (CH_2Cl_2) spectrum of **4b**.

Compound 5

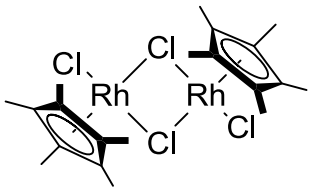

5

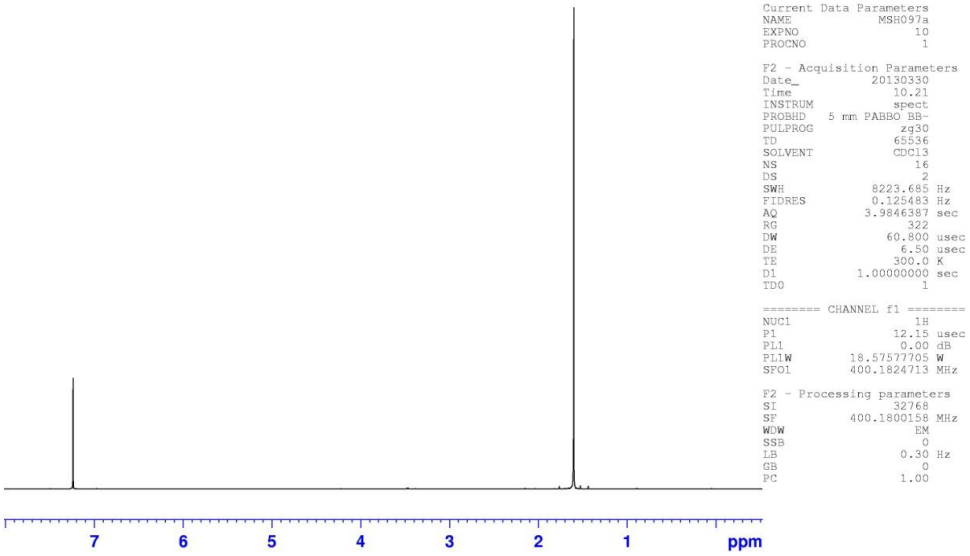

Figure 69: ^{1}H-NMR (400 MHz, $CDCl_3$) spectrum of **5**.

Compound 6

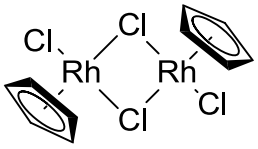

6

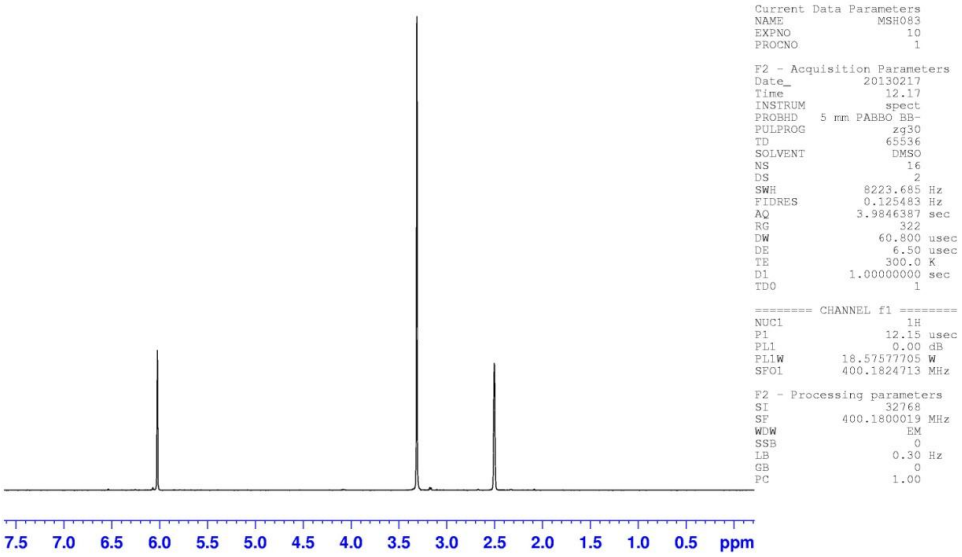

Figure 70: ^{1}H-NMR (400 MHz, DMSO-d_6) spectrum of **6**. The peak at ca 3.3 ppm is due to water in the NMR solvent.

Compound 7

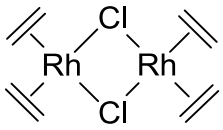

7

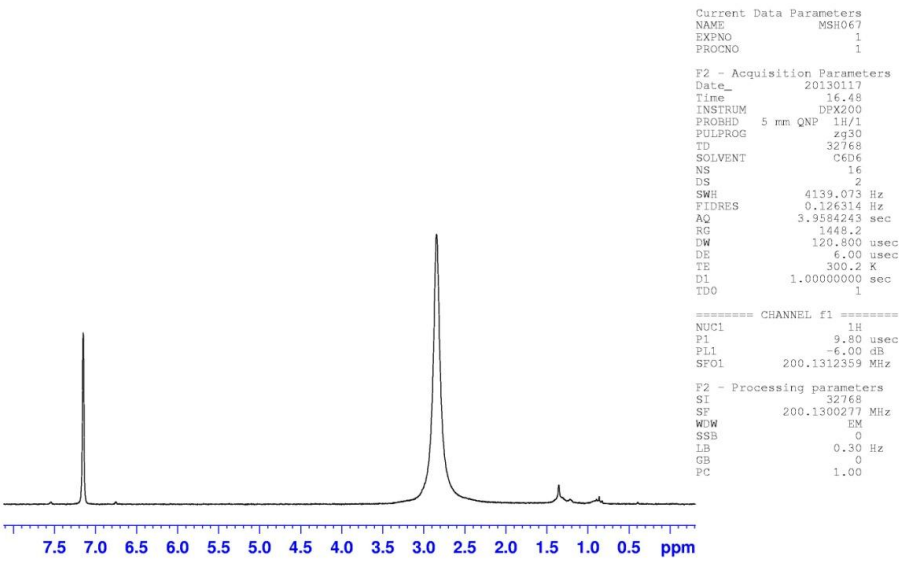

Figure 71: ^{1}H-NMR (200 MHz, C_6D_6) spectrum of **7**.

Compound 8

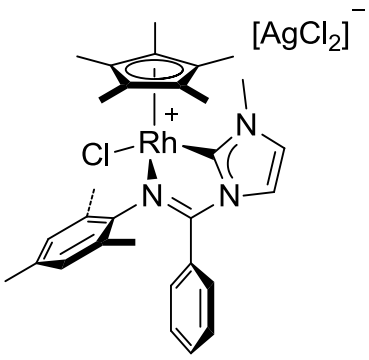

8

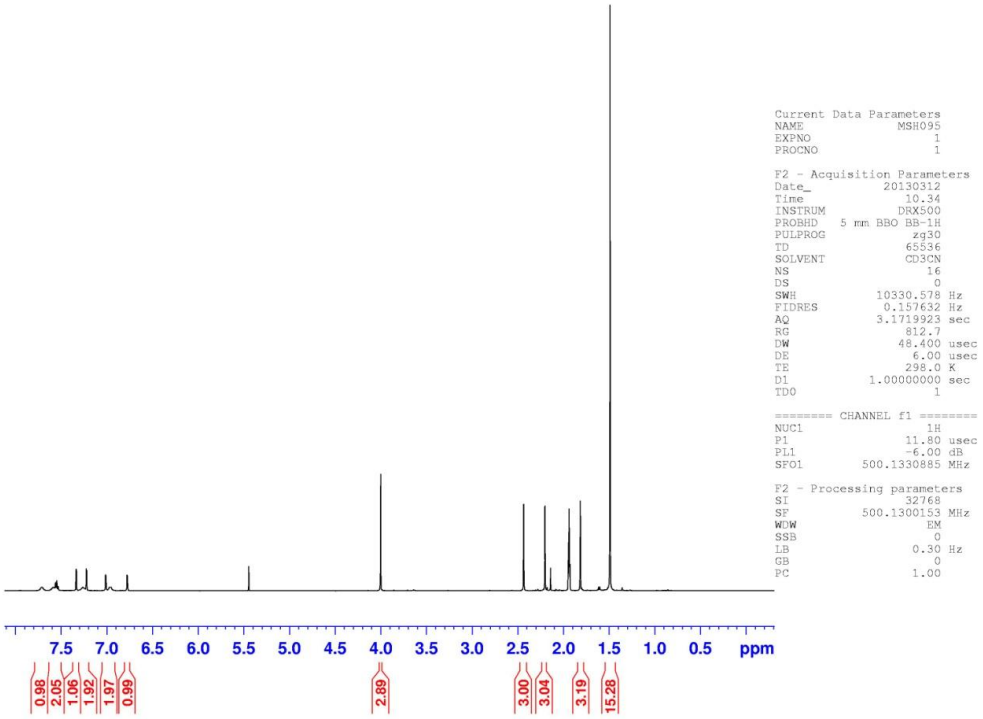

Figure 72: ^{1}H-NMR (500 MHz, MeCN-d_3) spectrum of **8**. The peaks at ca 2.1 and 5.5 are due to water and CH_2Cl_2.

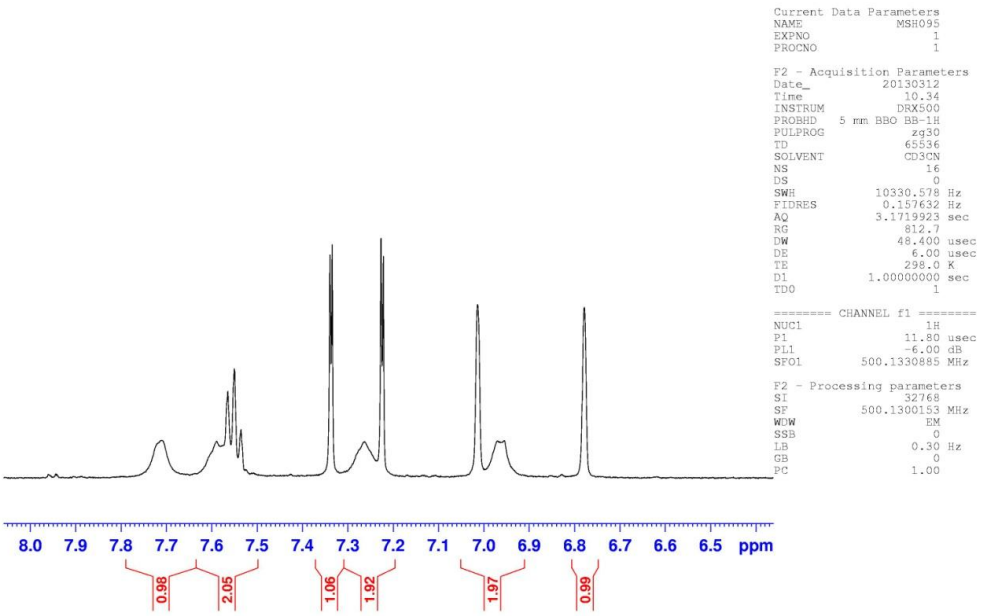

Figure 73: ^{1}H-NMR (500 MHz, MeCN-d_3) spectrum of **8**. Close-up of the aromatic region.

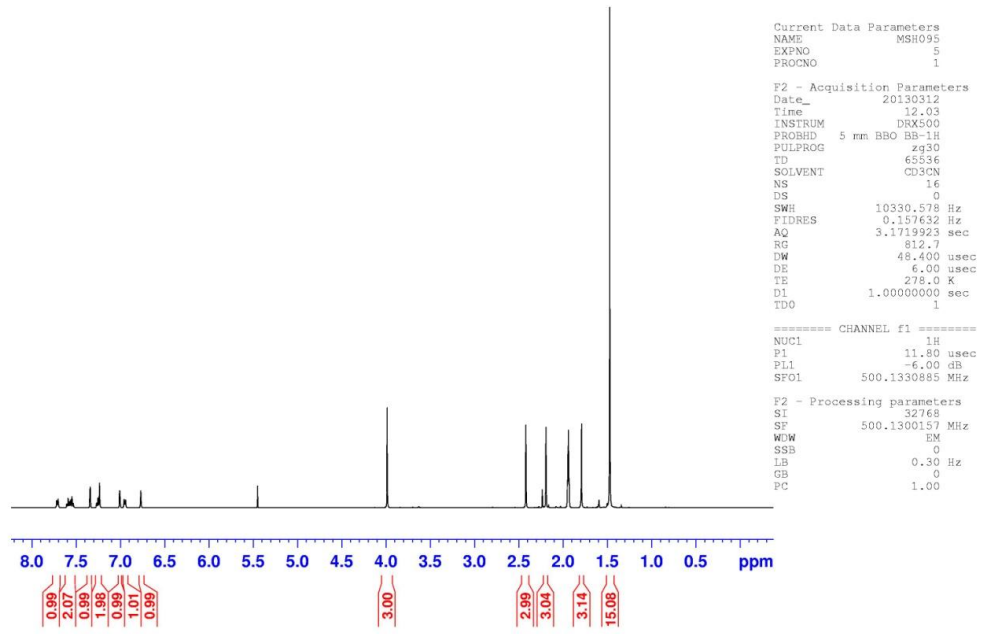

Figure 74: ^{1}H-NMR (500 MHz, MeCN-d_3, -1.1 ^{o}C) spectrum of **8**. The peaks at ca 2.2 and 5.5 ppm are due to water and CH_2Cl_2.

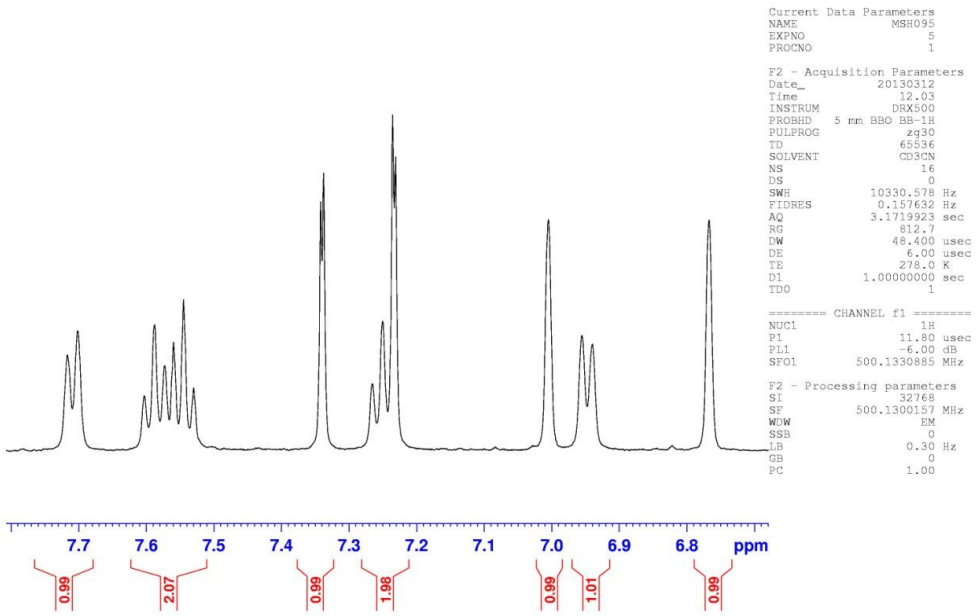

Figure 75: ^{1}H-NMR (500 MHz, MeCN-d_3, -1-1 ^{o}C) spectrum of **8**. Close-up of the aromatic region.

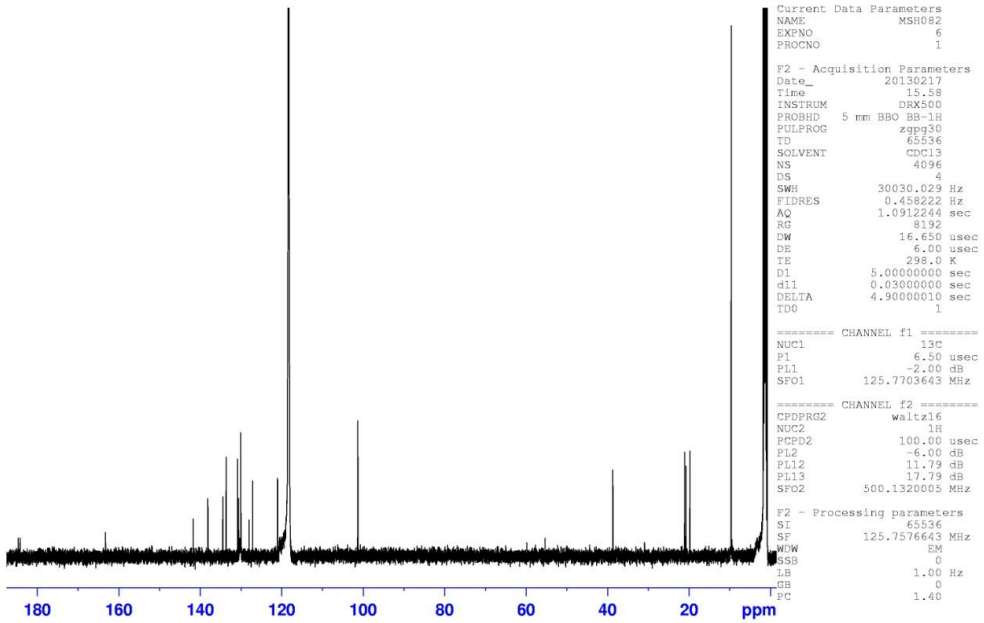

Figure 76: ^{13}C-NMR (125 MHz, MeCN-d_3, d1=5 s) spectrum of **8**. The peak at ca 40 ppm is due to CH_2Cl_2.

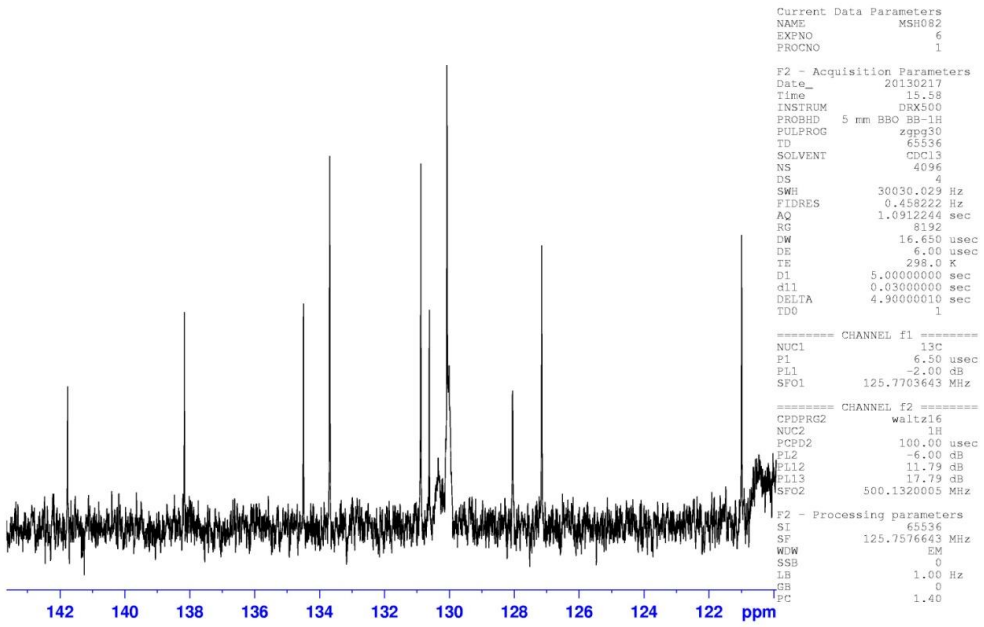

Figure 77: ^{13}C-NMR (125 MHz, MeCN-d_3, d1=5 s) spectrum of **8**. Close-up of the aromatic region.

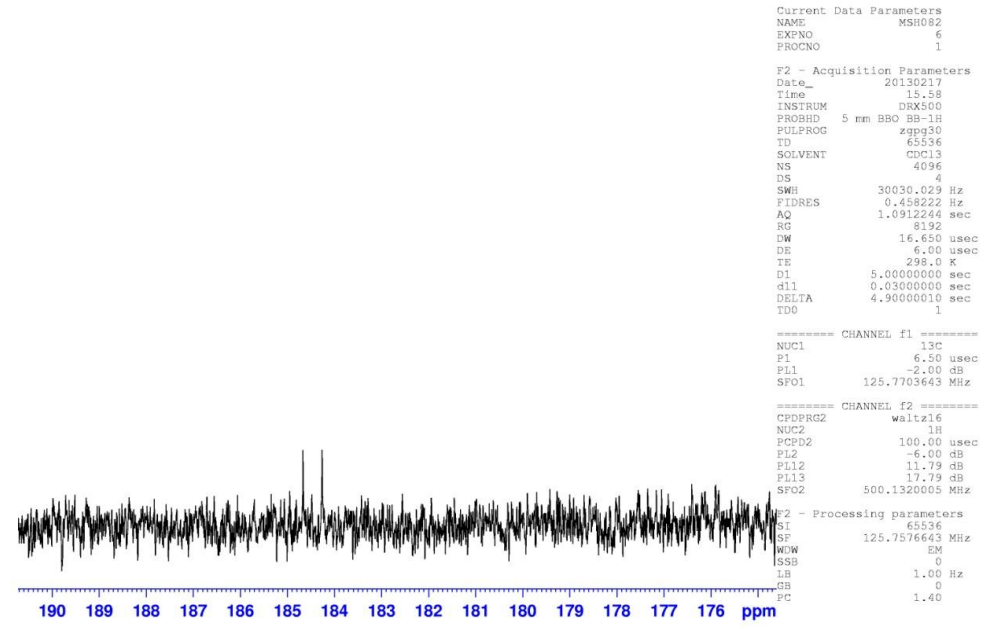

Figure 78: ^{13}C-NMR (125 MHz, MeCN-d_3, d1=5 s) spectrum of **8**. Close-up of $C_{carbene}$.

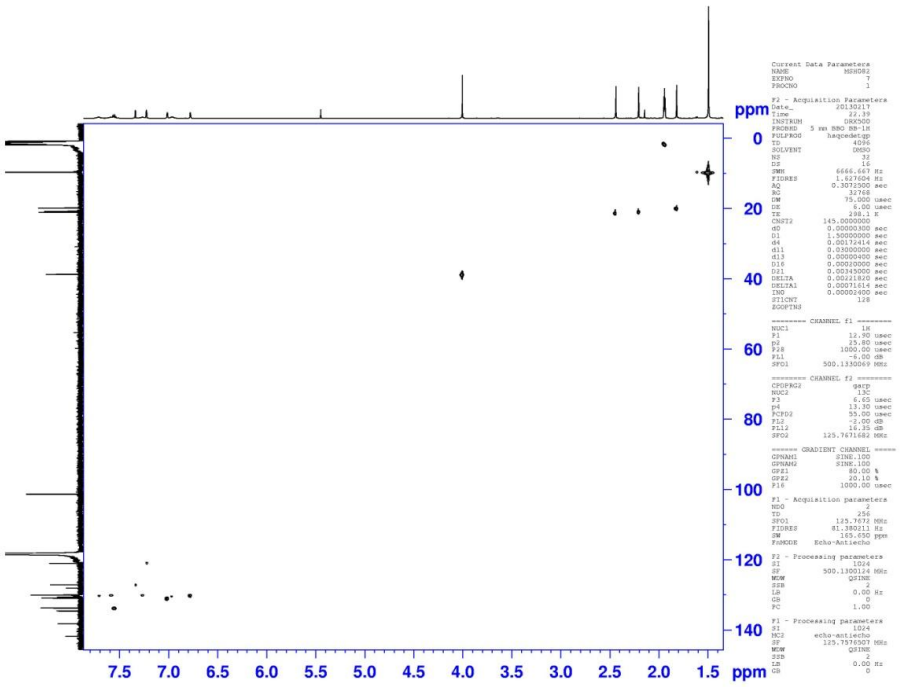

Figure 79: HSQC (500 MHz, MeCN-d_3) spectrum of **8**.

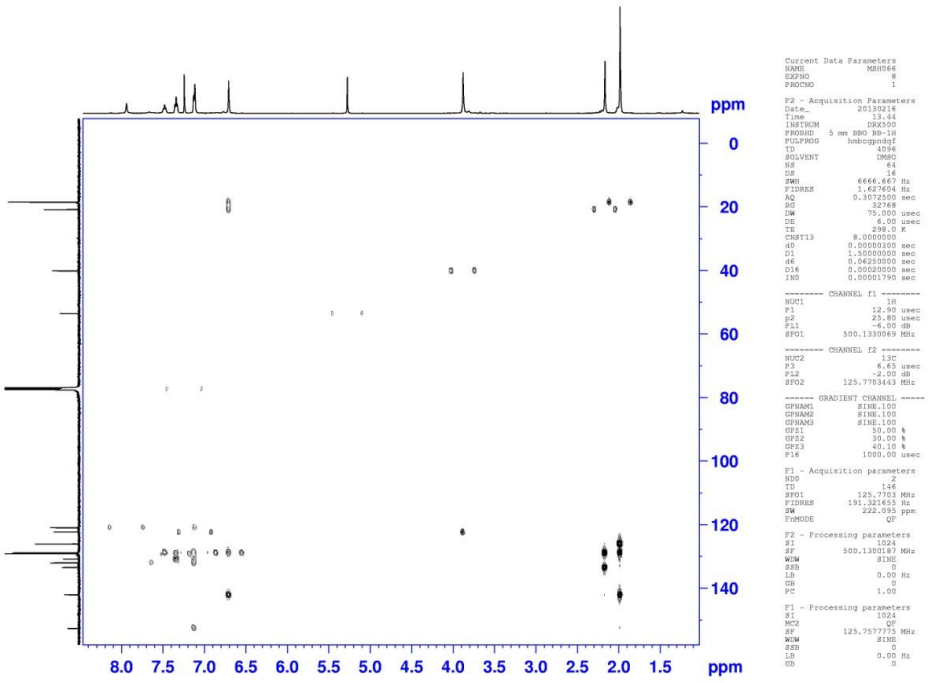

Figure 80: HMBC (500 MHz, MeCN-d_3) spectrum of **8**.

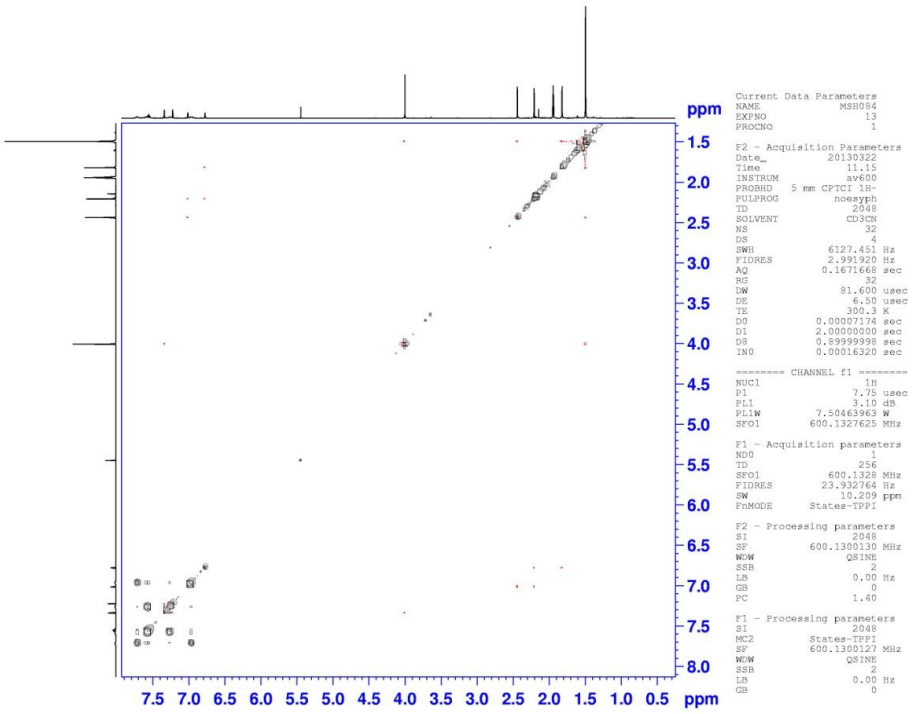

Figure 81: NOESY (600 MHz, MeCN-d_6, mixing time = 900 ms) spectrum of **8**.

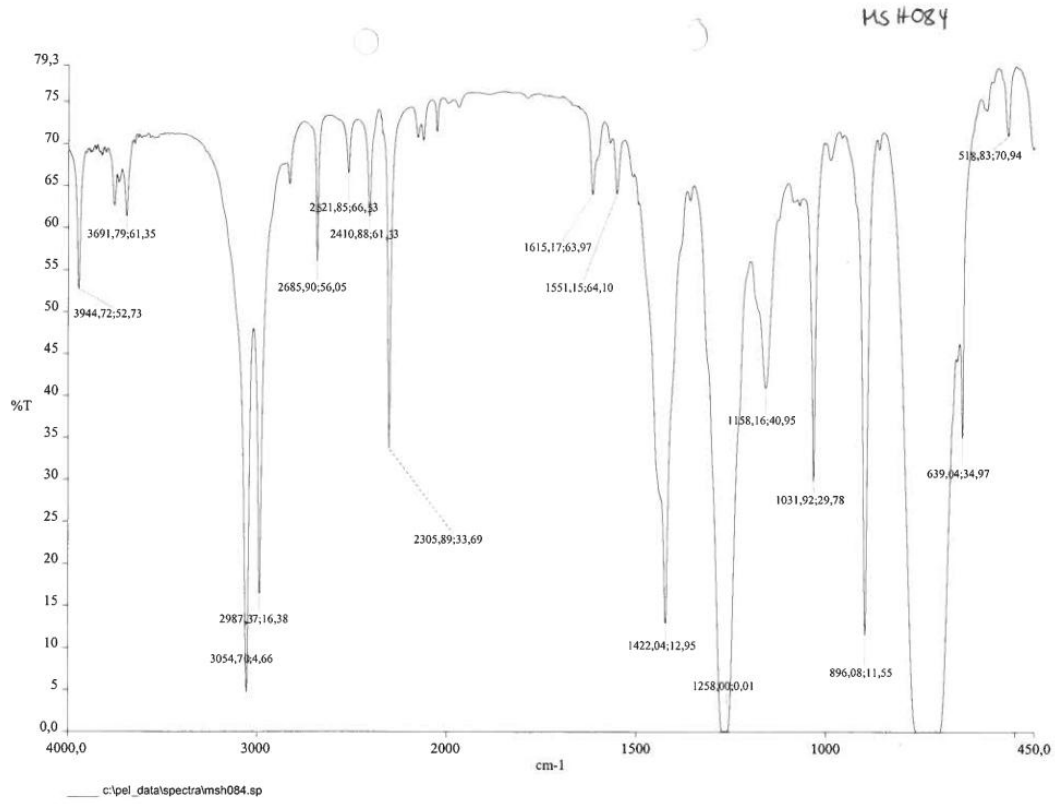

Figure 82: IR (CH_2Cl_2) spectrum of **8**.

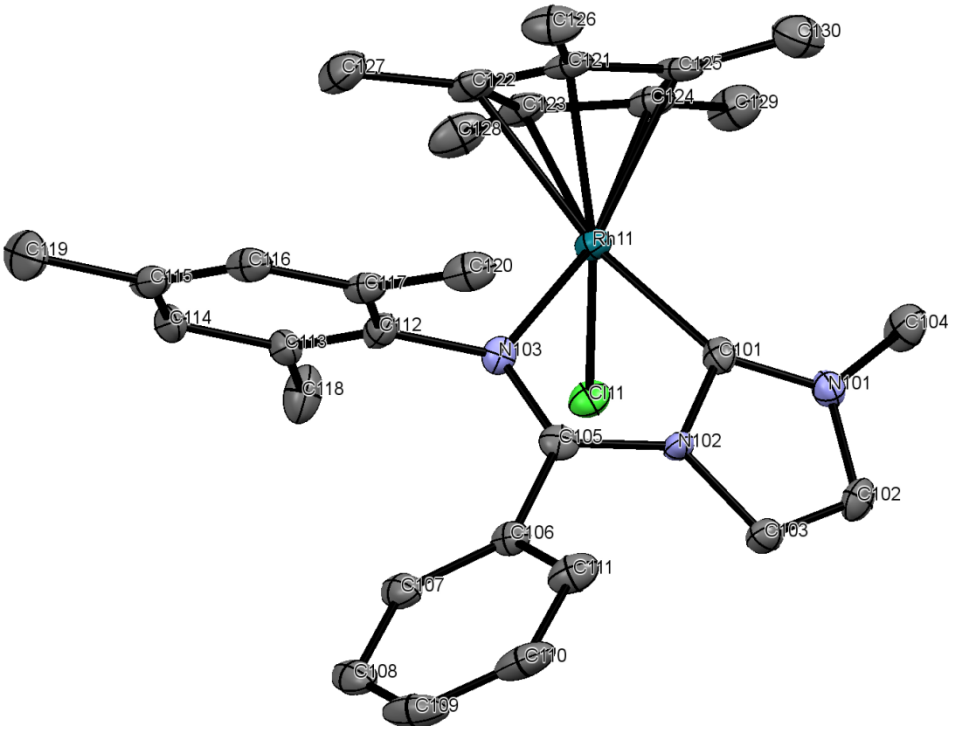

Figure 83: ORTEP-drawing of compound **8**. Hydrogens, the anions and CH_2Cl_2 are omitted for clarity. Ellipsoids at 50% probability.

Table 18: Selected bond lengths from the structure based on the X-ray analysis of compound **8**.

Bond	Bond length [Å]	Bond	Bond length [Å]
Rh(11)-C(101)	2.014(4)	C(105)-N(103)	1.289(5)
Rh(11)-N(103)	2.137(3)	C(101)-N(101)	1.328(5)
Rh(11)-Cl(11)	2.4058(11)	C(101)-N(102)	1.375(5)
Rh(11)-C(121)	2.166(4)	C(121)-C(122)	1.453(7)
Rh(11)-C(122)	2.241(4)	C(122)-C(123)	1.400(6)
Rh(11)-C(123)	2.229(4)	C(123)-C(124)	1.450(6)
Rh(11)-C(124)	2.163(4)	C(124)-C(125)	1.423(6)
Rh(11)-C(125)	2.183(4)	C(125)-C(121)	1.434(6)
Rh(11)-Cp(avg.)	2.196		

Table 19: Selected bond angles from the structure based on the X-ray analysis of compound **8**.

Angle	Bond angle [^{o}]
C(101)-Rh(11)-N(103)	76.01(15)
C(101)-Rh(11)-Cl(11)	79.07(12)
N(103)-Rh(11)-Cl(11)	91.21(10)
N(101)-C(101)-N(102)	104.9(4)
N(101)-C(101)-Rh(11)	136.6(3)
N(102)-C(101)-Rh(11)	115.5(3)

Table 20: Crystallographic data for compound **8**.

Crystal data	
Formula	$4(C_{30}H_{36}ClN_3Rh)\ 0.5(Ag_6Cl_{12})$ $3.5(CH_2Cl_2)\ (AgCl_2)$
Formula weight	3320.23
Crystal size	0.22 x 0.07 x 0.03 mm
Colour, shape	Orange, needle
Crystal system	Triclinic
Space group	$P\overline{1}$
a	11.0118(12) Å
b	17.349(2) Å
c	18.737(2) Å
α	72.434(1)^o
β	81.111(1)^o
γ	83.571(1)^o
V	3363.6(6)Å^3
Z	4
T	100 K
Radiation	Mo *K*α, λ=0.71073 Å
θ_{min}-θ_{max}	1.9-28.7^o
μ	1.48 mm^{-1}

D_x	1.639 Mg m^{-3}

Data Collection

Instrument	Bruker Apex II CCD diffractometer
Measured reflections	30745
Independent reflections	15795
Reflections with $I>2\sigma(I)$	10672
R_{int}	0.048
h	-14→14
k	-23→23
l	-25→25

Refinement

Refinement on F^2	
$R[F^2>2\sigma(F^2)]$	0.051
$wR(F^2)$	0.102
S	1.01
Reflections	15795
Parameters	852
Restraints	31
w	$1/[\sigma^2(F_o^2)+(0.0336P)^2+1.190.P]$ where $P=(F_o^2+2F_c^2)/3$
$(\Delta/\sigma)_{max}$	0.003
$\Delta\rho_{max}$	1.14 e $Å^3$
$\Delta\rho_{min}$	-1.01 e $Å^{-3}$
Hydrogen atoms treated by a mixture of independent and constrained refinement.	

Compound 9

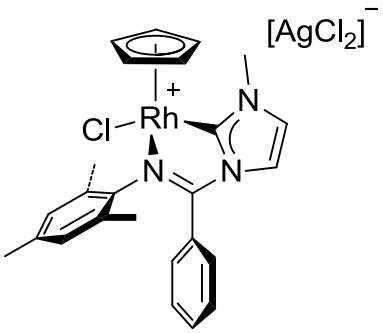

9

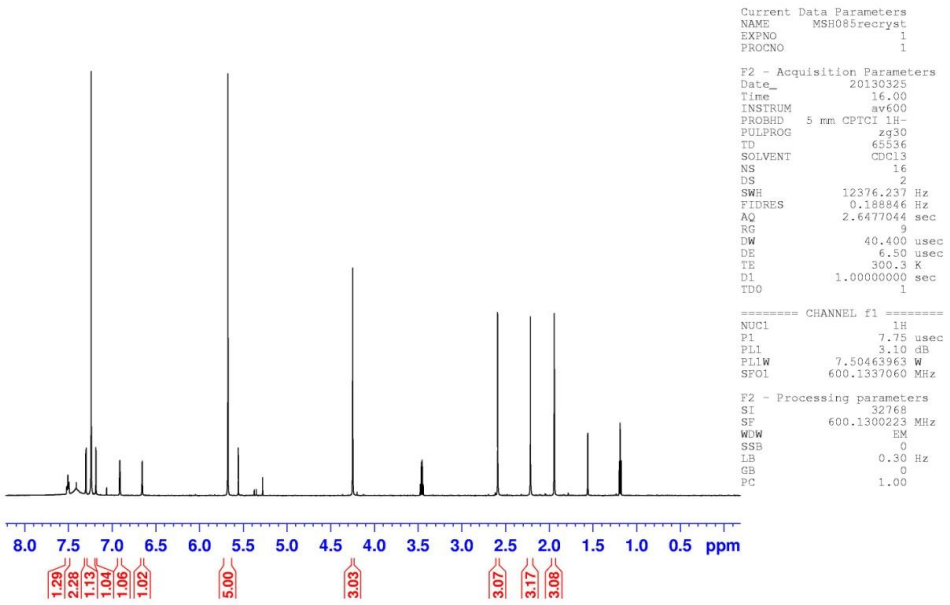

Figure 84: ^{1}H-NMR (600 MHz, $CDCl_3$) spectrum of **9**. The peaks at ca 1.2, 1.5 and 3.5 ppm are due to water and Et_2O. The peak at 5.6 ppm is due to an unknown impurity that has not been removed yet. The satellites of $CDCl_3$ are visible in the spectrum.

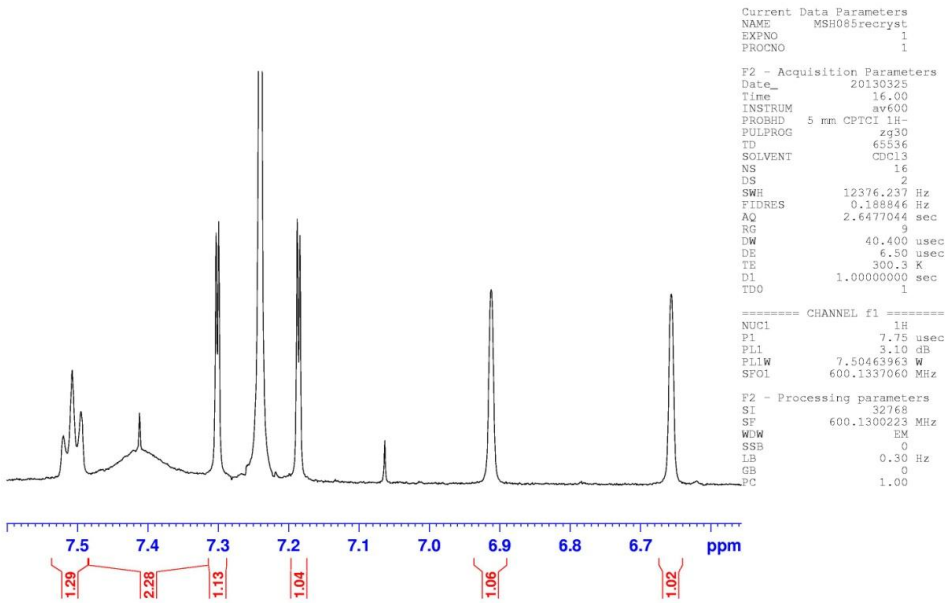

Figure 85: ^{1}H-NMR (600 MHz, $CDCl_3$) spectrum of **9**. Close-up of the aromatic region.

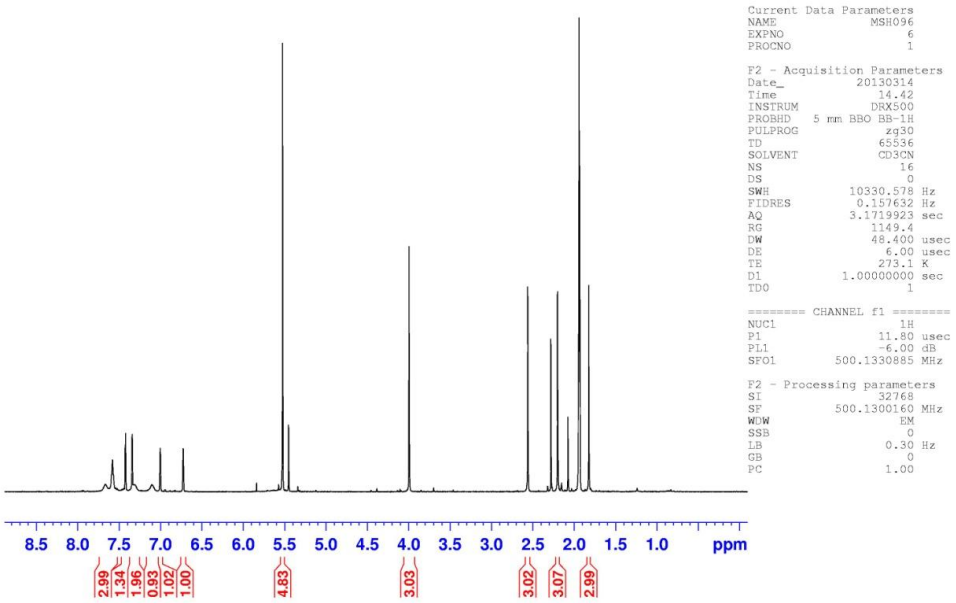

Figure 86: ^{1}H-NMR (500 MHz, MeCN-d_3, -21.0 ^{o}C) spectrum of **9**.

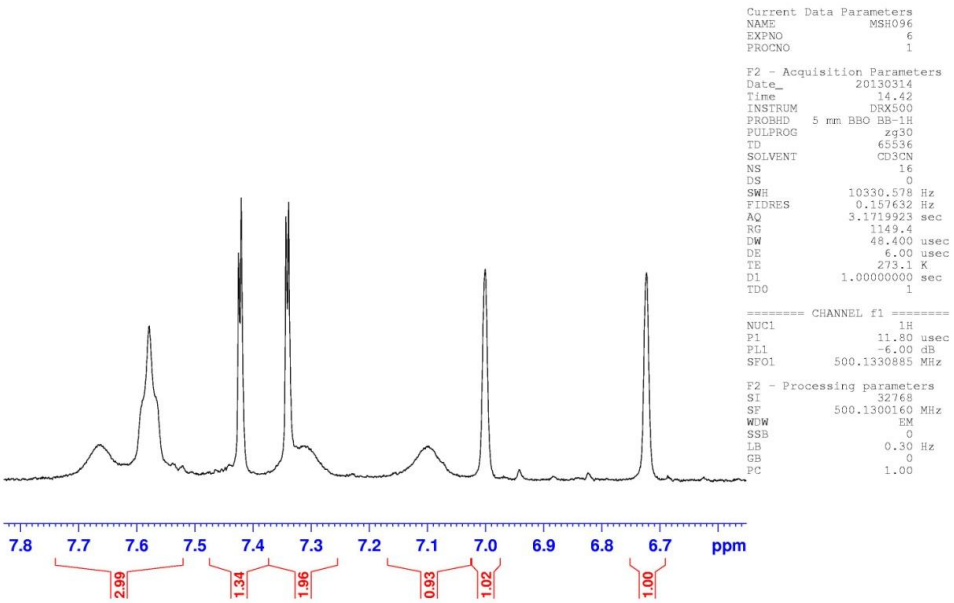

Figure 87: ^{1}H-NMR (500 MHz, MeCN-d_3, -21.0 ^{o}C) spectrum of **9**. Close-up of the aromatic region.

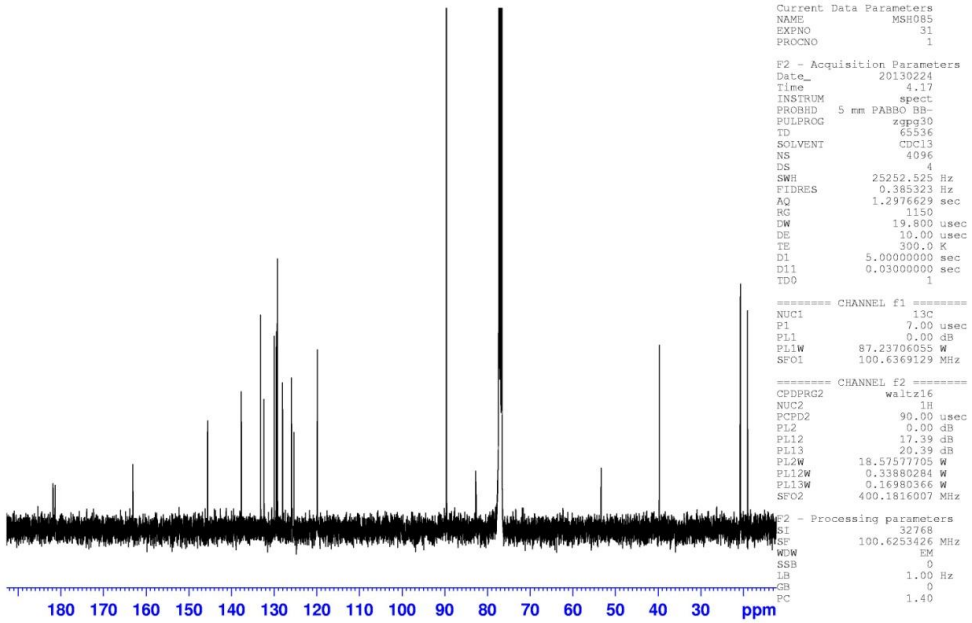

Figure 88: ^{13}C-NMR (100 MHz, $CDCl_3$, d1=5 s) spectrum of **9**. The peak at ca 55 ppm is due to CH_2Cl_2. The peak at ca 80 ppm is an unidentified impurity which has not been removed yet.

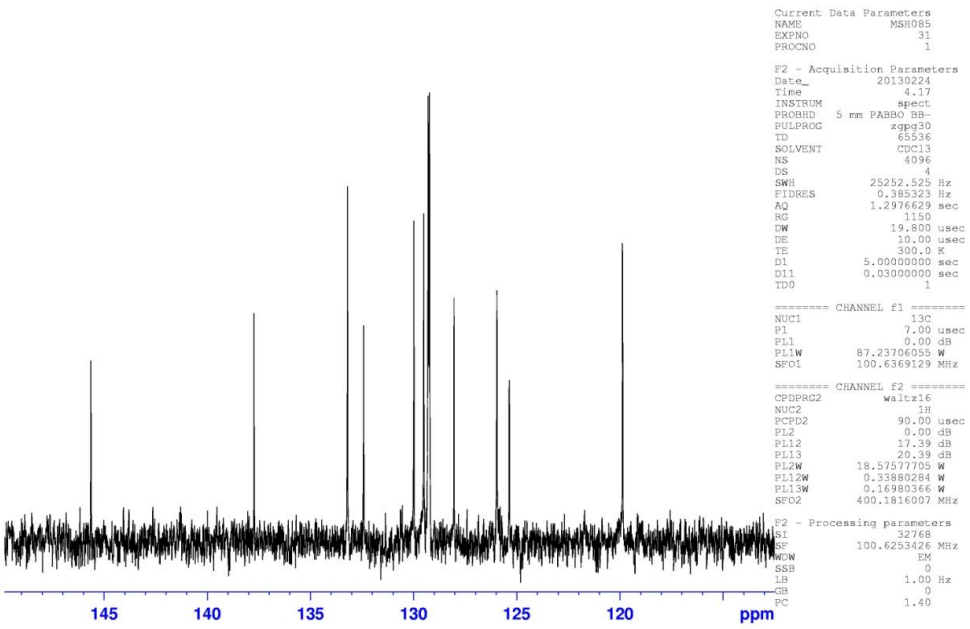

Figure 89: ^{13}C-NMR (100 MHz, $CDCl_3$, d1=5 s) spectrum of **9**. Close-up of the aromatic region.

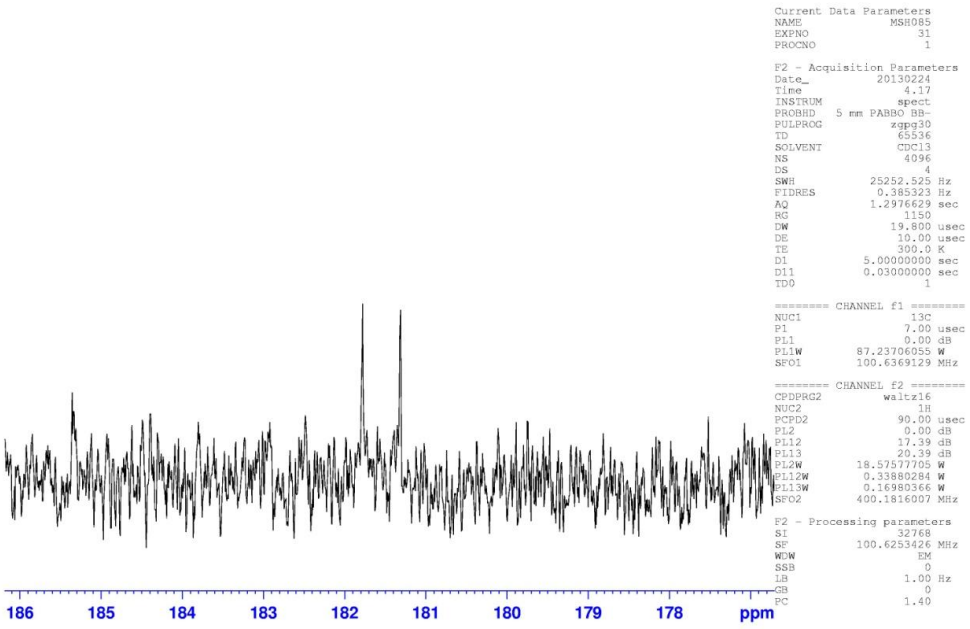

Figure 90: ^{13}C-NMR (100 MHz, $CDCl_3$, d1=5 s) spectrum of **9**. Close-up of the aromatic region.

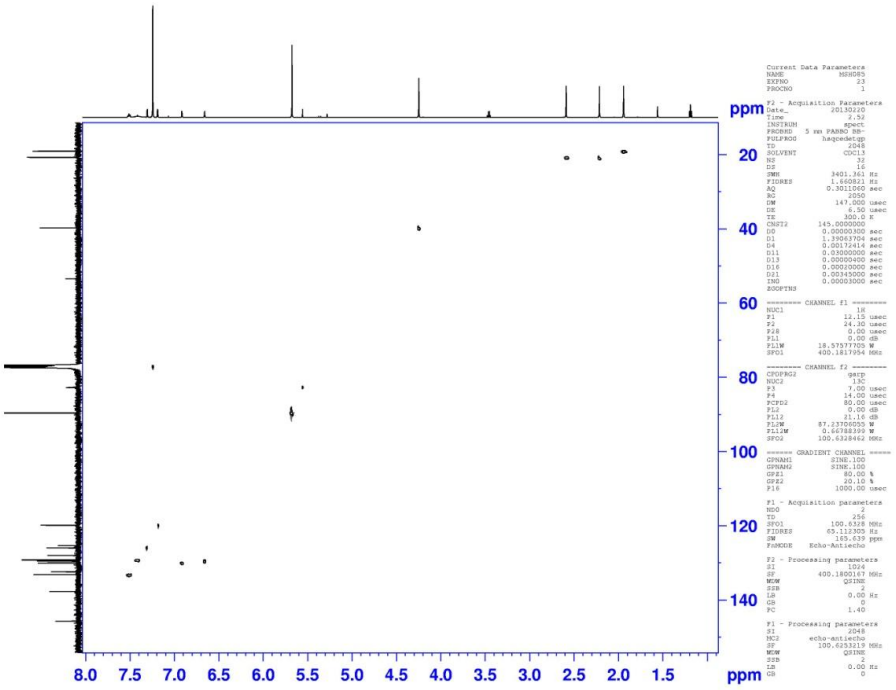

Figure 91: HSQC (400 MHz, $CDCl_3$) spectrum of **9**.

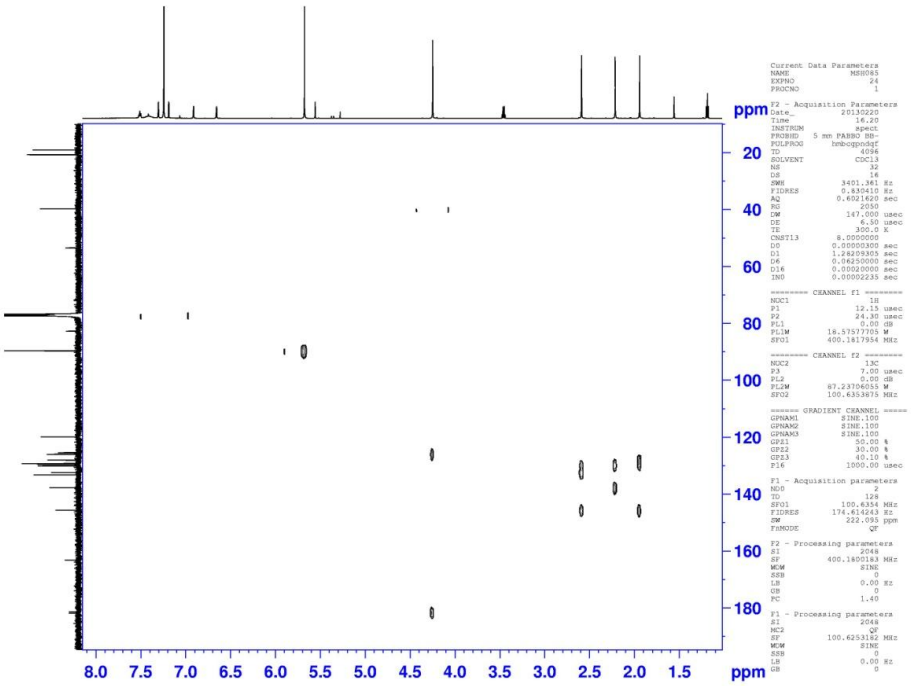

Figure 92: HMBC (400 MHz, $CDCl_3$, no decoupling) spectrum of **9**.

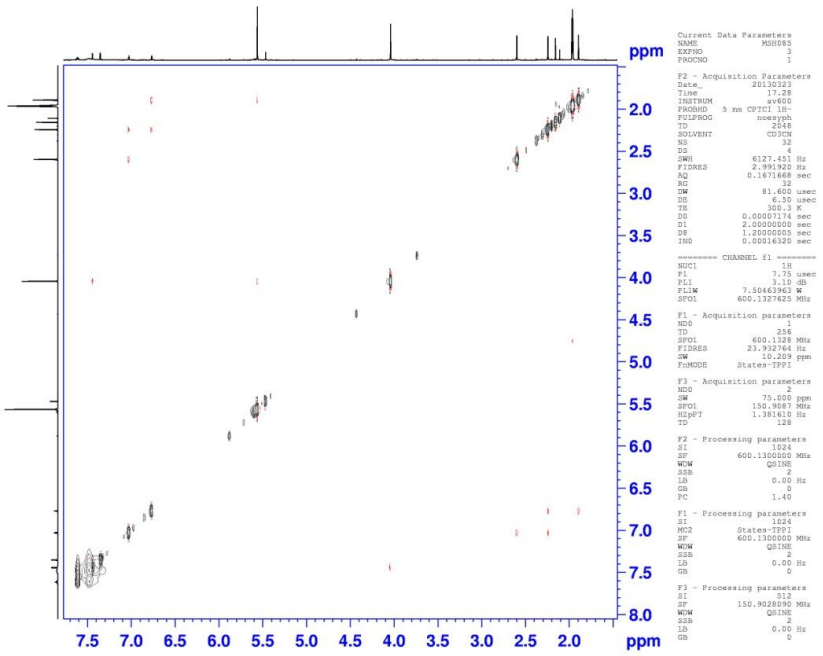

Figure 93: NOESY (600 MHz, MeCN-d_3, mixing time= 1.20 s) spectrum of **9**.

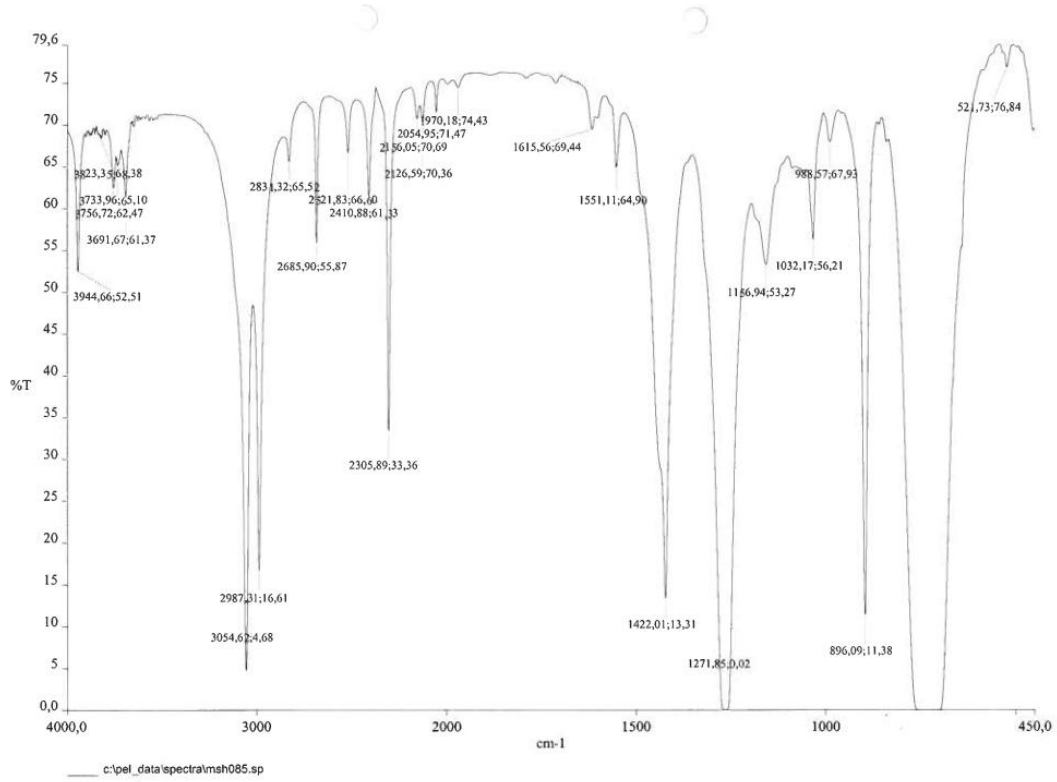

Figure 94: IR (CH_2Cl_2) spectrum of **9**.

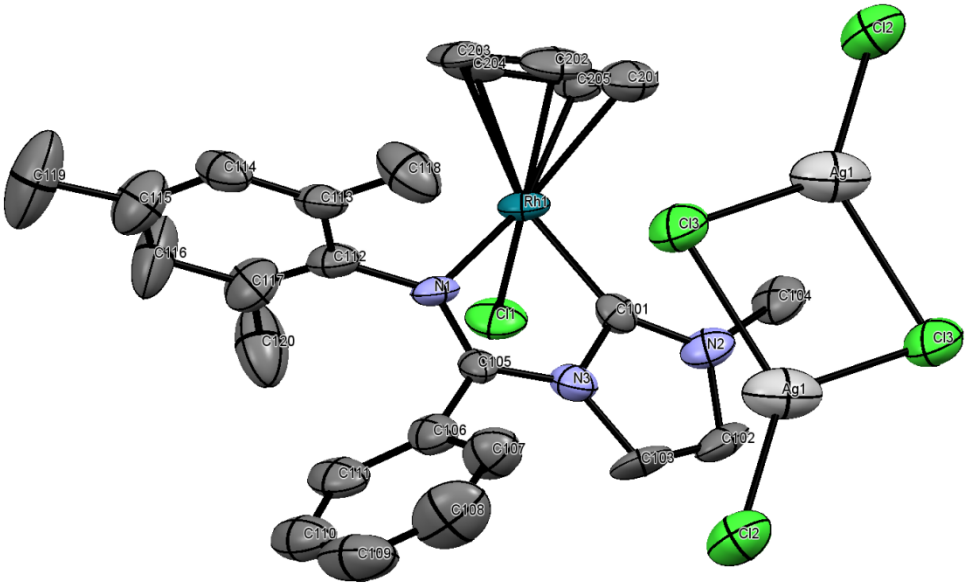

Figure 95: ORTEP-drawing of compound **9**. Hydrogens and CH_2Cl_2 are omitted for clarity. Ellipsoids at 50% probability.

Table 21: Selected bond lengths from the structure based on the X-ray analysis of compound **9**.

Bond	**Bond length [Å]**	**Bond**	**Bond length [Å]**
Rh(1)-C(101)	1.989(11)	C(105)-N(1)	1.273(13)
Rh(1)-N(1)	2.097(9)	C(101)-N(2)	1.335(14)
Rh(1)-Cl(1)	2.380(3)	C(101)-N(3)	1.375(13)
Rh(1)-C(201)	2.160(13)	C(201)-C(202)	1.391(19)
Rh(1)-C(202)	2.160(12)	C(202)-C(203)	1.462(19)
Rh(1)-C(203)	2.214(11)	C(203)-C(204)	1.389(16)
Rh(1)-C(204)	2.211(11)	C(204)-C(205)	1.410(17)
Rh(1)-C(205)	2.165(11)	C(205)-C(201)	1.411(17)
Rh(1)-Cp(avg.)	2.182		

Table 22: Selected bond angles from the structure based on the X-ray analysis of compound **9**.

Angle	**Degrees [^{o}]**
C(101)-Rh(1)-N(1)	76.2(4)
C(101)-Rh(1)-Cl(1)	83.5(3)
N(1)-Rh(1)-Cl(1)	92.9(2)
N(2)-C(101)-N(3)	106.9(9)
N(2)-C(101)-Rh(1)	137.3(8)
N(3)-C(101)-Rh(1)	114.8(8)

Table 23: Crystallographic data for compound **9**.

Crystal data	
Formula	$2(C_{25}H_{26}ClN_3Rh)\ (Ag_2Cl_4)\ (CH_2Cl_2)$
Formula weight	1456.50
Crystal size	0.30 x 0.10 x 0.05 mm
Colour, shape	Orange, needle
Crystal system	Triclinic
Space group	$P\overline{1}$
a	7.380(6) Å
b	13.31(1) Å
c	14.805(11) Å
α	88.642(10)^o
β	84.486(9)^o
γ	75.089(8)^o
V	1398.8(19)Å^3
Z	2
T	193 K
Radiation	Mo *K*α, λ=0.71073 Å
θ_{min}-θ_{max}	1.6-25.0^o
μ	1.29 mm^{-1}
D_x	1.729 Mg m^{-3}

Data Collection	
Instrument	Bruker Apex II CCD diffractometer
Measured reflections	6625
Independent reflections	4567
Reflections with $I>2\sigma(I)$	2552
R_{int}	0.057
h	-8→8
k	-15→15
l	-17→14
Refinement	
Refinement on F^2	
$R[F^2>2\sigma(F^2)]$	0.078
$wR(F^2)$	0.208
S	0.98
Reflections	4567
Parameters	338
Restraints	42
w	$1/[\sigma^2(F_o^2)+(0.1069P)^2]$ where $P=(F_o^2+2F_c^2)/3$
$(\Delta/\sigma)_{max}$	0.001
$\Delta\rho_{max}$	1.16 e Å^3
$\Delta\rho_{min}$	-1.73 e Å^{-3}
Hydrogen atoms treated by a mixture of independent and constrained refinement.	

Compound 10

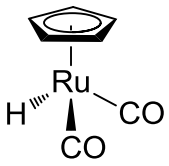

10

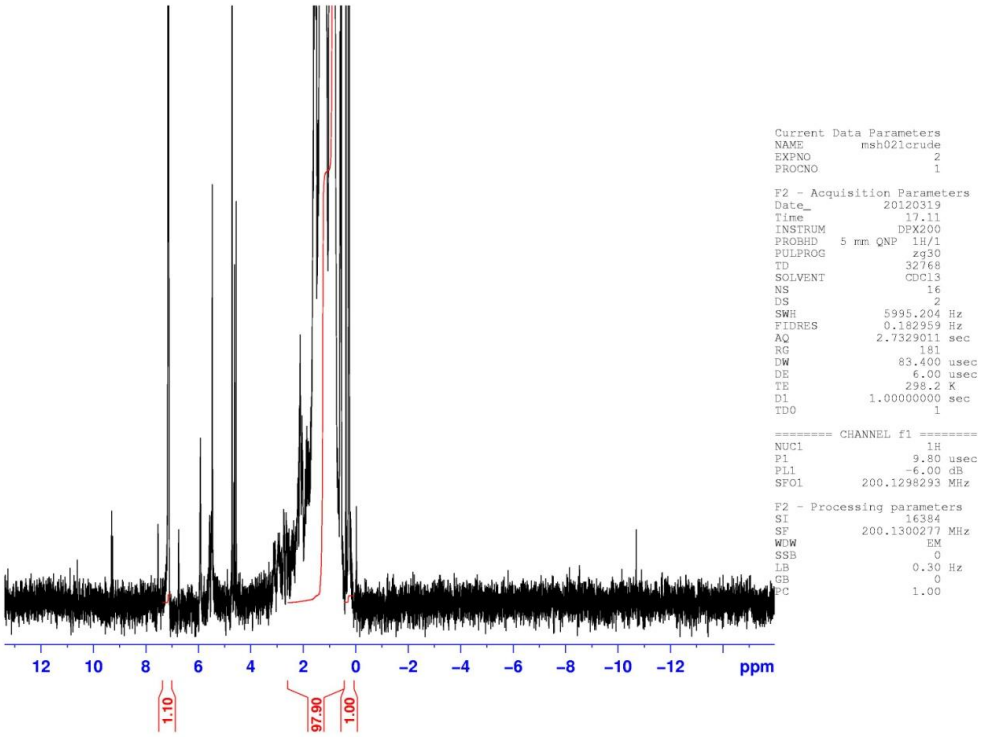

Figure 96: ^{1}H-NMR (200 MHz, C_6D_6) spectrum of the crude mixture of **10**.

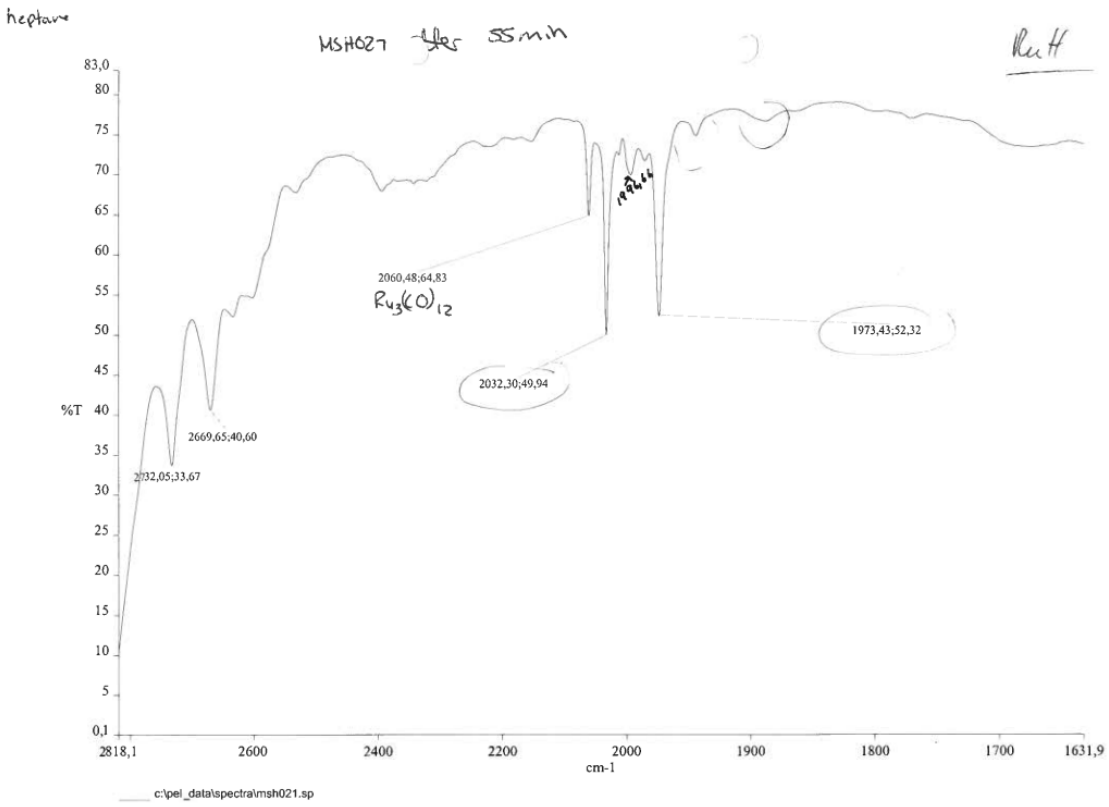

Figure 97: IR (heptane) spectrum of **10**.

Compound 11

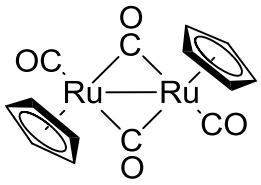

11

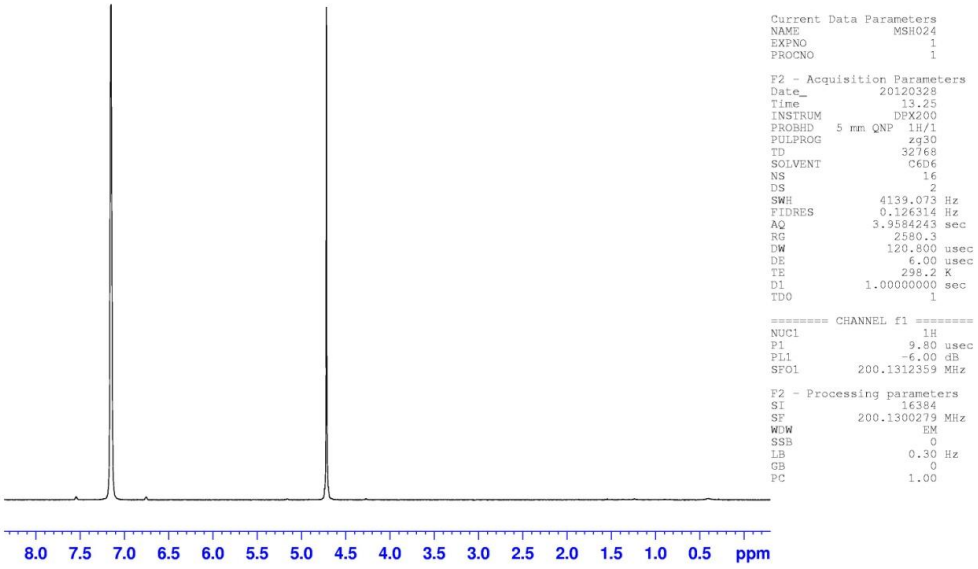

Figure 98: ^{1}H-NMR (200 MHz, C_6D_6) spectrum of **11**.

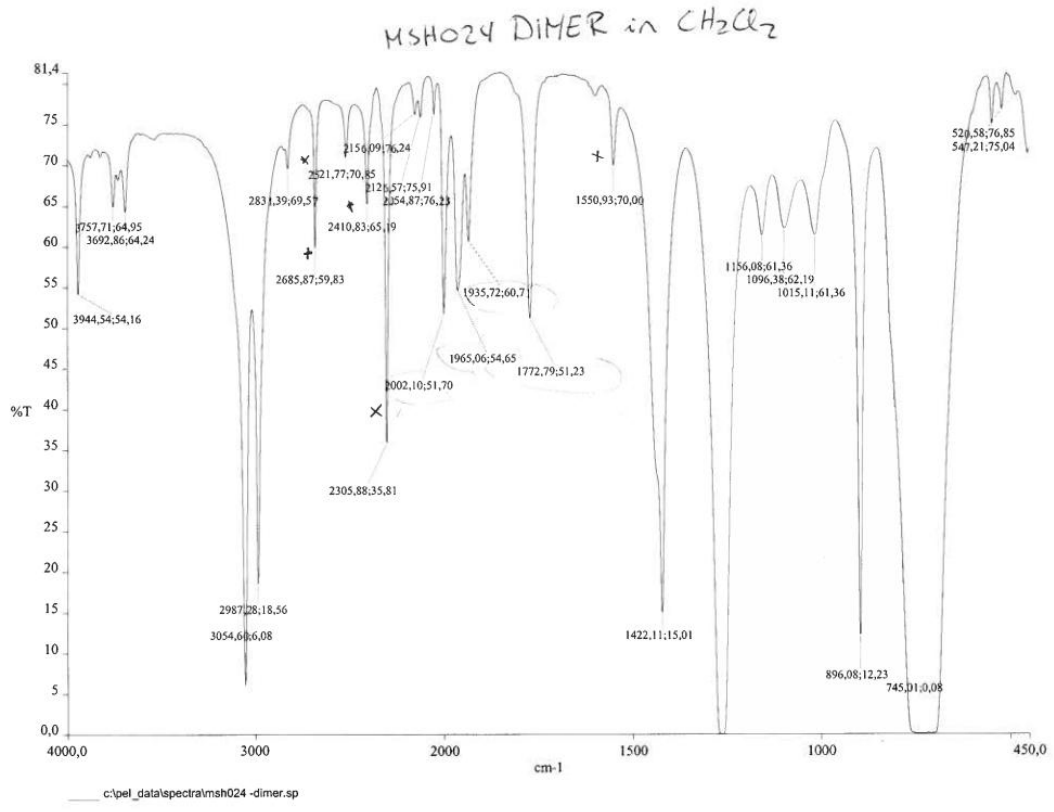

Figure 99: IR (CH_2Cl_2) spectrum of **11**.

Compound 12

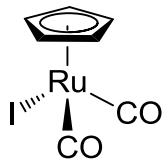

12

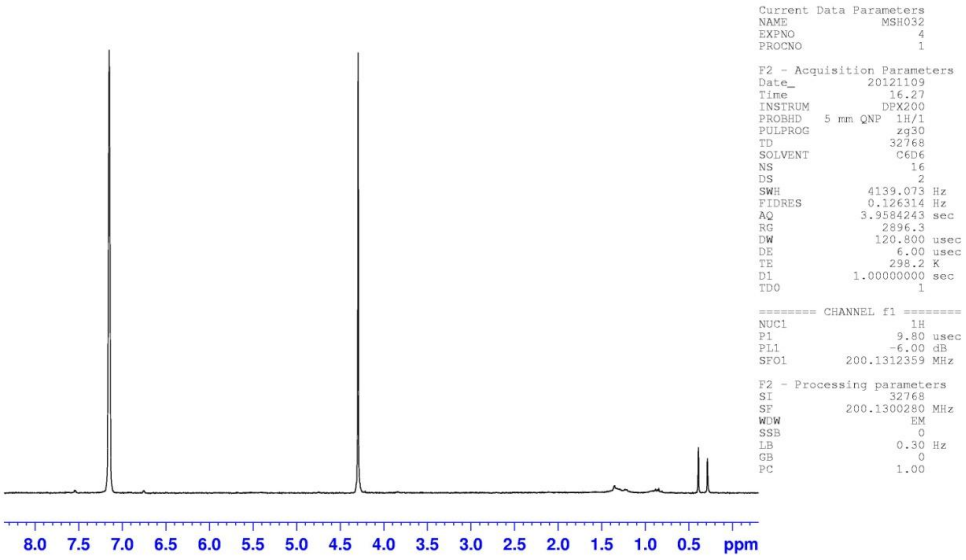

Figure 100: ^{1}H-NMR (200 MHz, C_6D_6) spectrum of **12**.

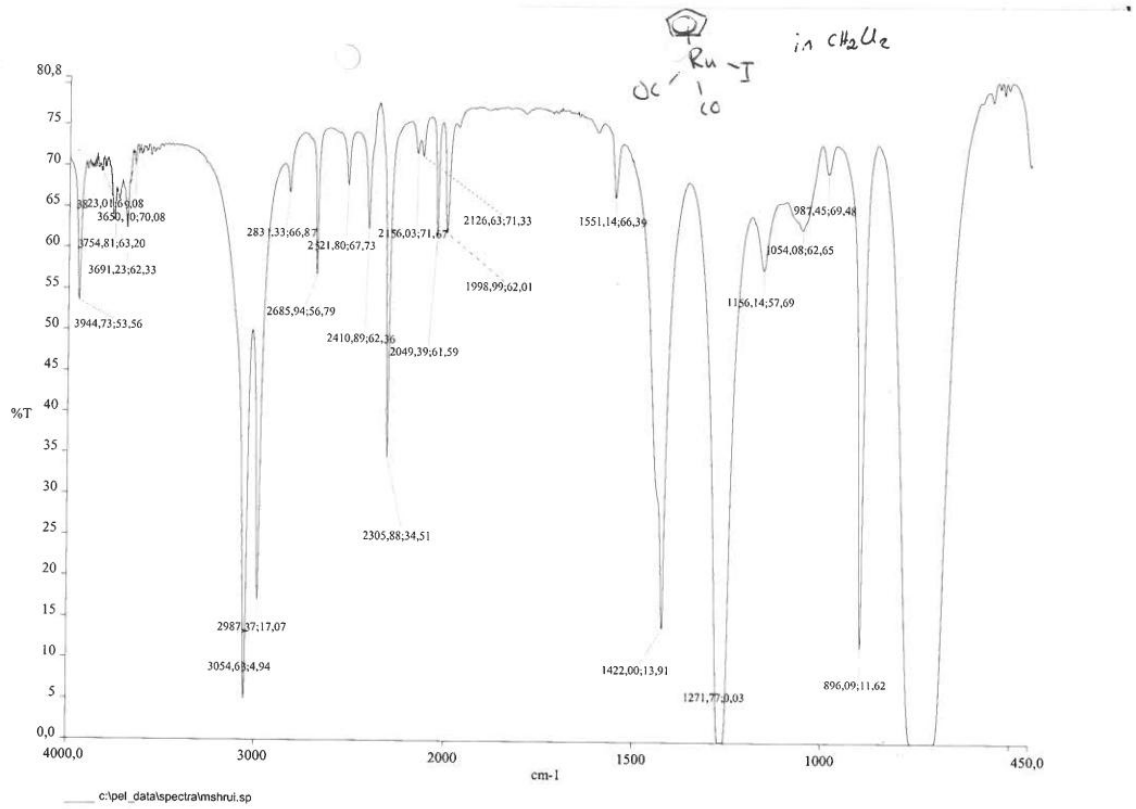

Figure 101: IR (CH_2Cl_2) spectrum of **12**.

Compound 13

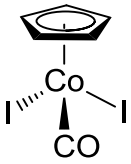

13

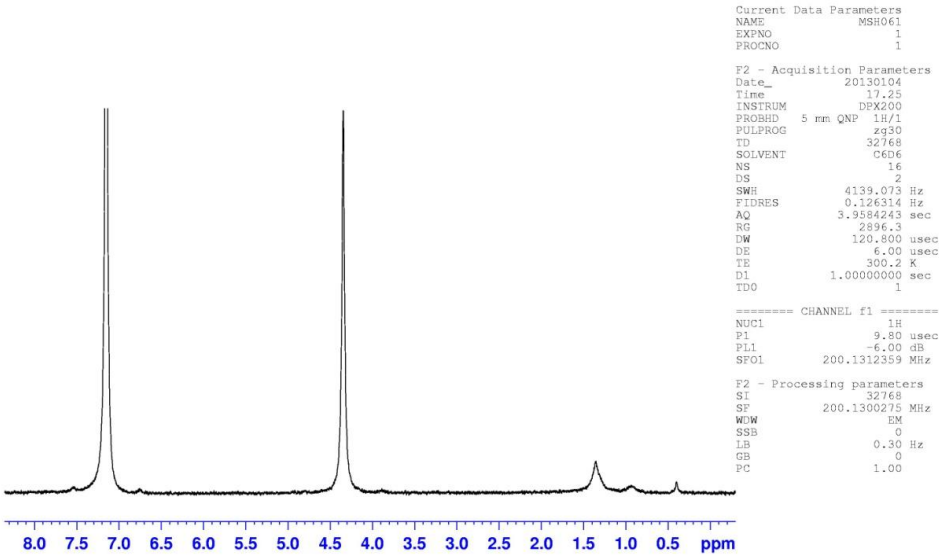

Figure 102: ^{1}H-NMR (200 MHZ, C_6D_6) spectrum of **13**.

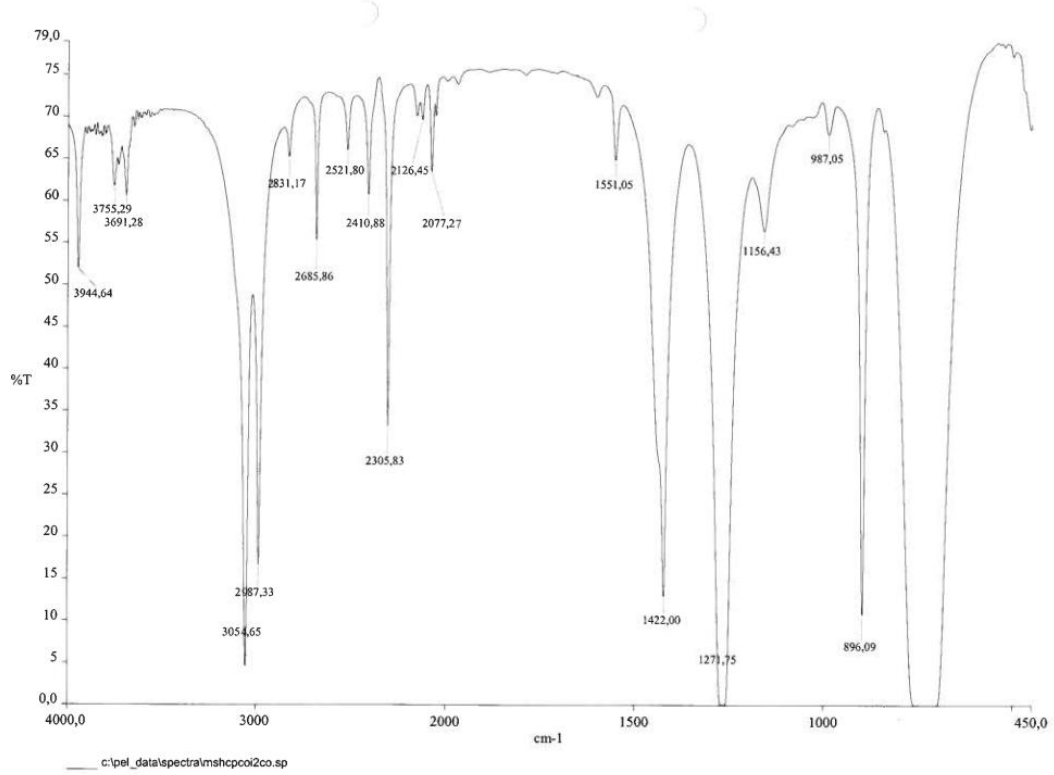

Figure 103: IR (CH_2Cl_2) spectrum of **13**.

Decomposition of imidazolium salt 3a

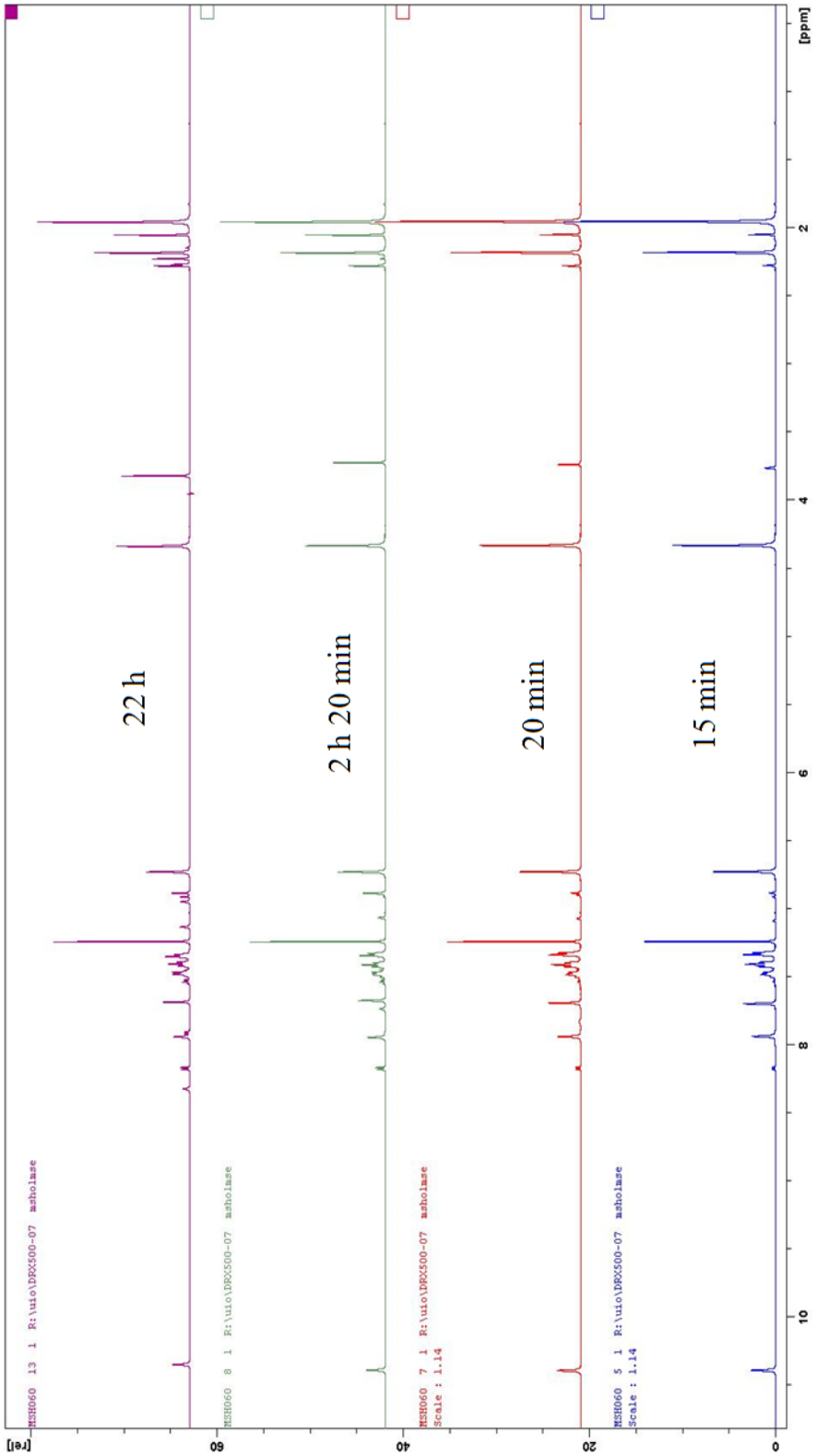

Figure 104: Decomposition of imidazolium salt **3a** observed by ^{1}H-NMR (500 MHz, $CDCl_3$)..

Variable temperature NMR of compound 8

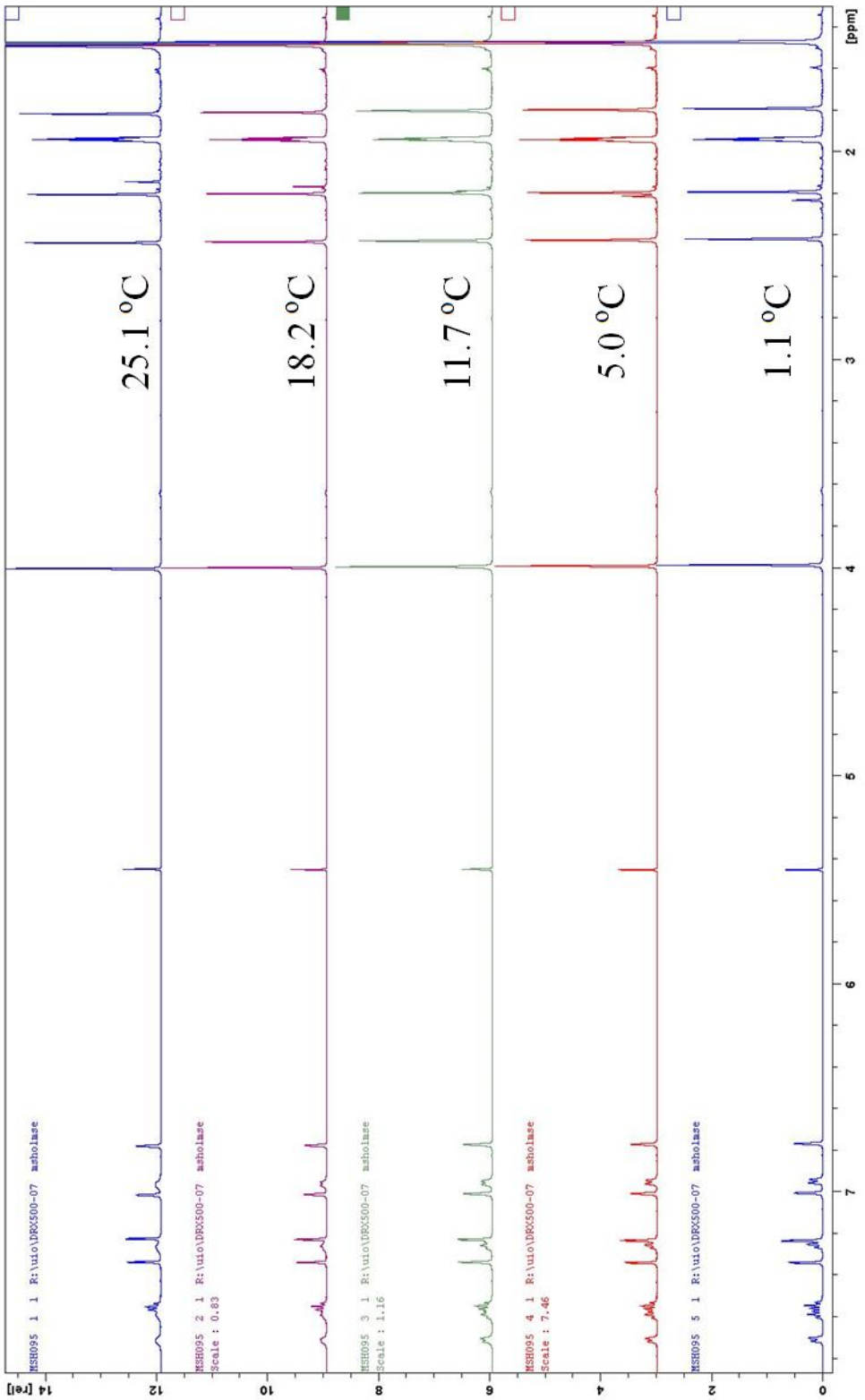

Figure 106: ^{1}H-NMR (500 MHz, MeCN-d_6) spectra of **8** with decreasing temperature.

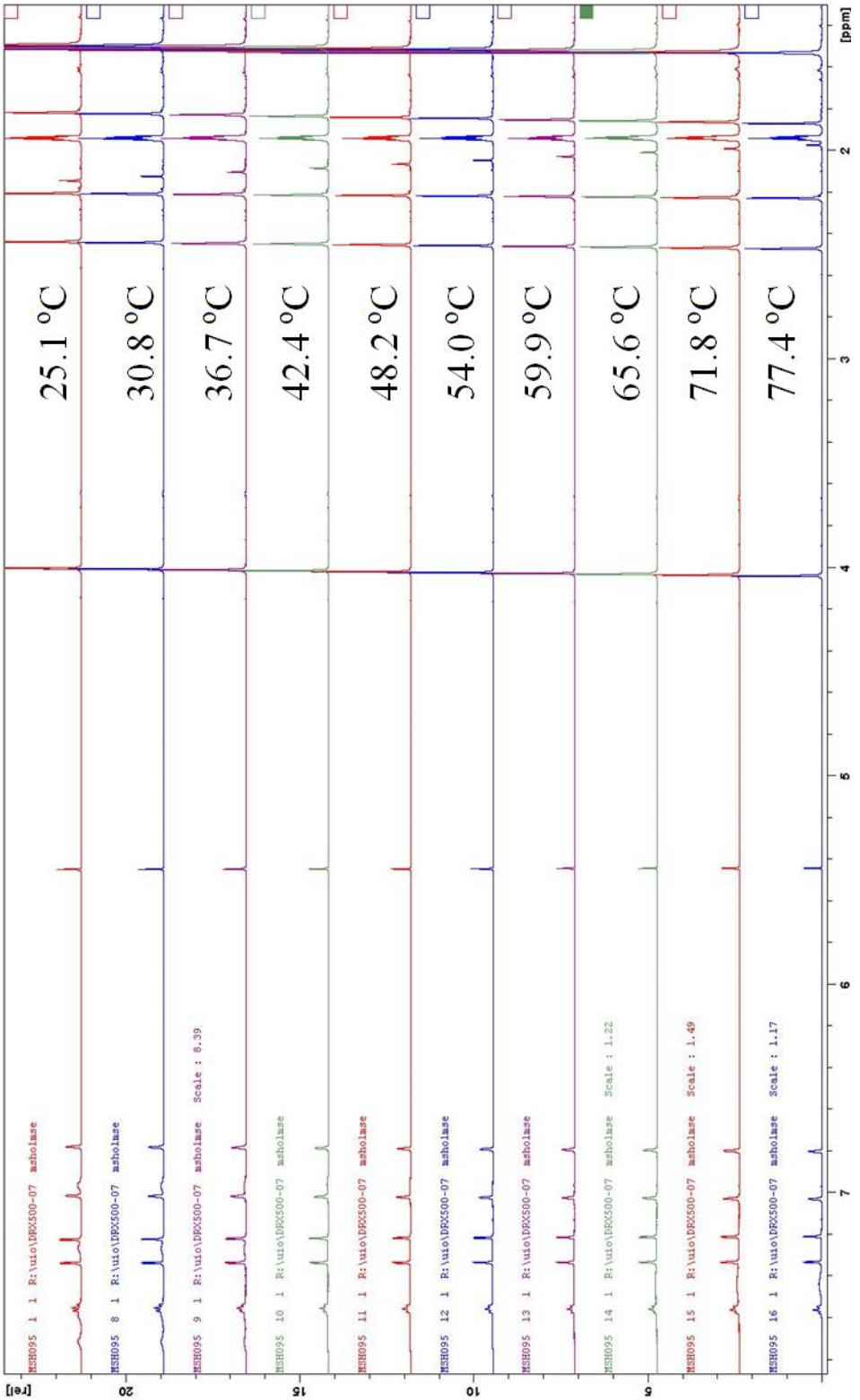

Figure 107: ^{1}H-NMR (500 MHz, MeCN-d_6) spectra of **8** with decreasing temperature

Variable temperature NMR of compound 9

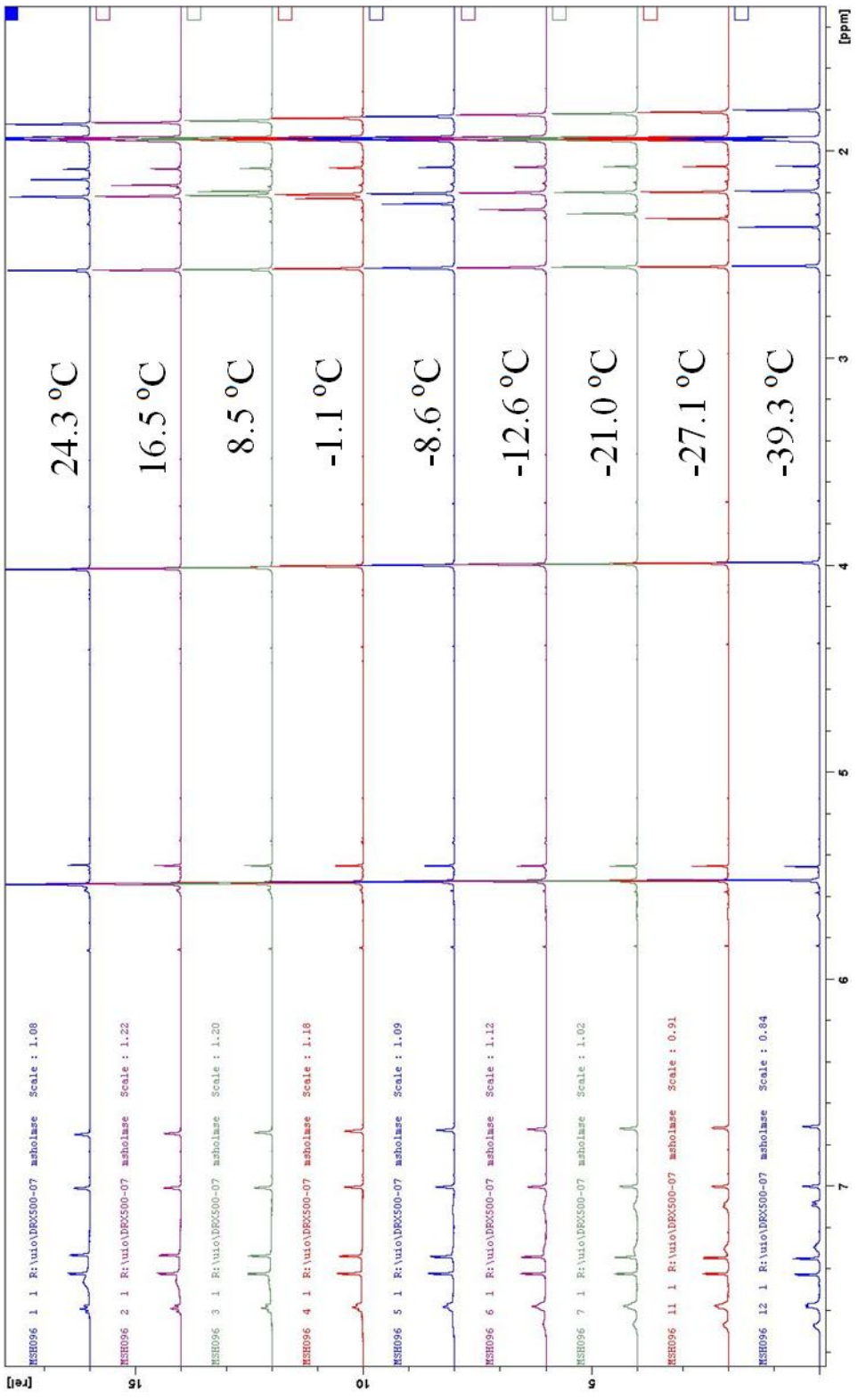

Figure 108: ^{1}H-NMR (500 MHz, MeNC-d_6) spectra of **9** with decreasing temperature.

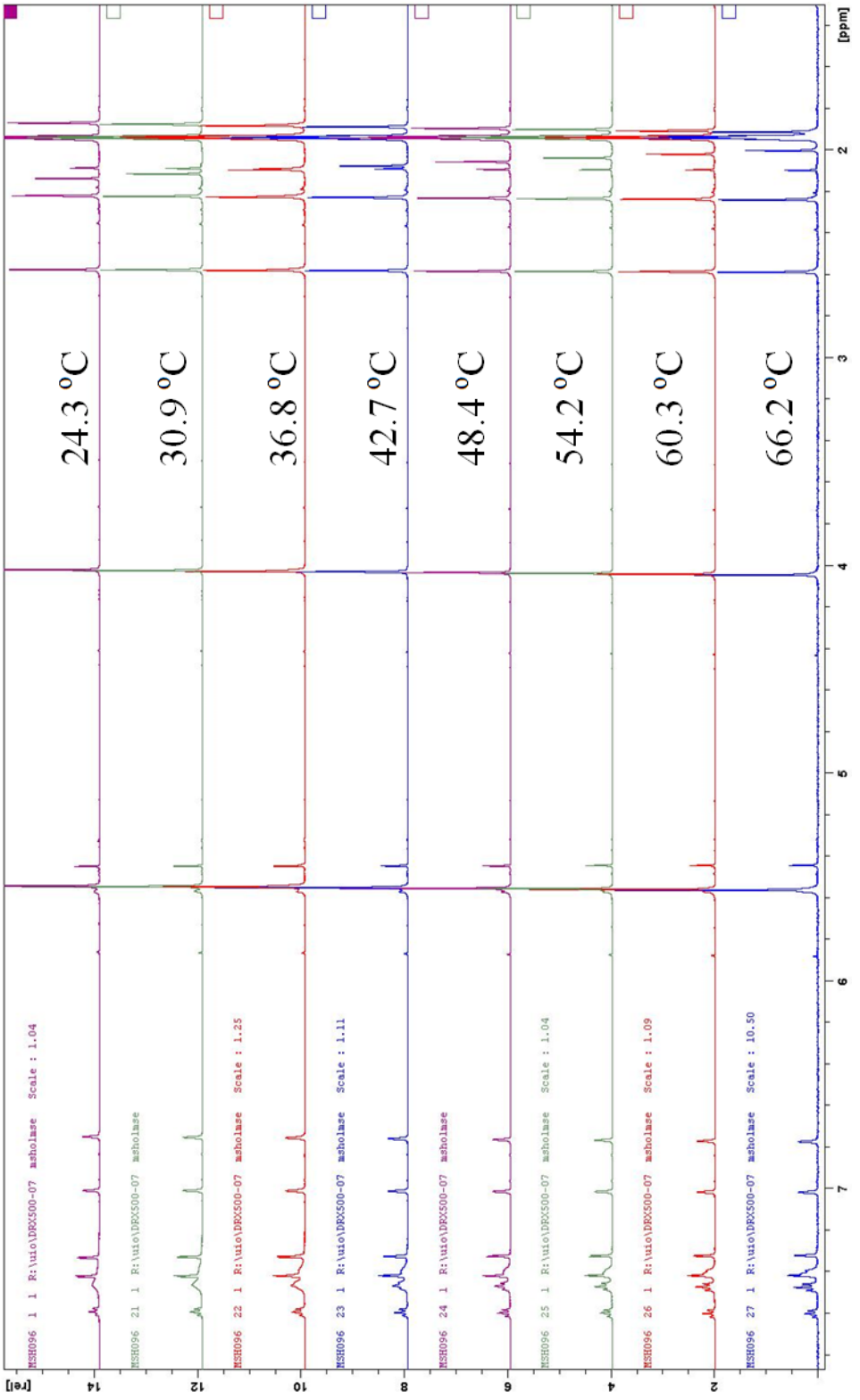

Figure 109: ^{1}H-NMR (500 MHz, MeCN-d_6) spectra of **9** with increasing temperature.

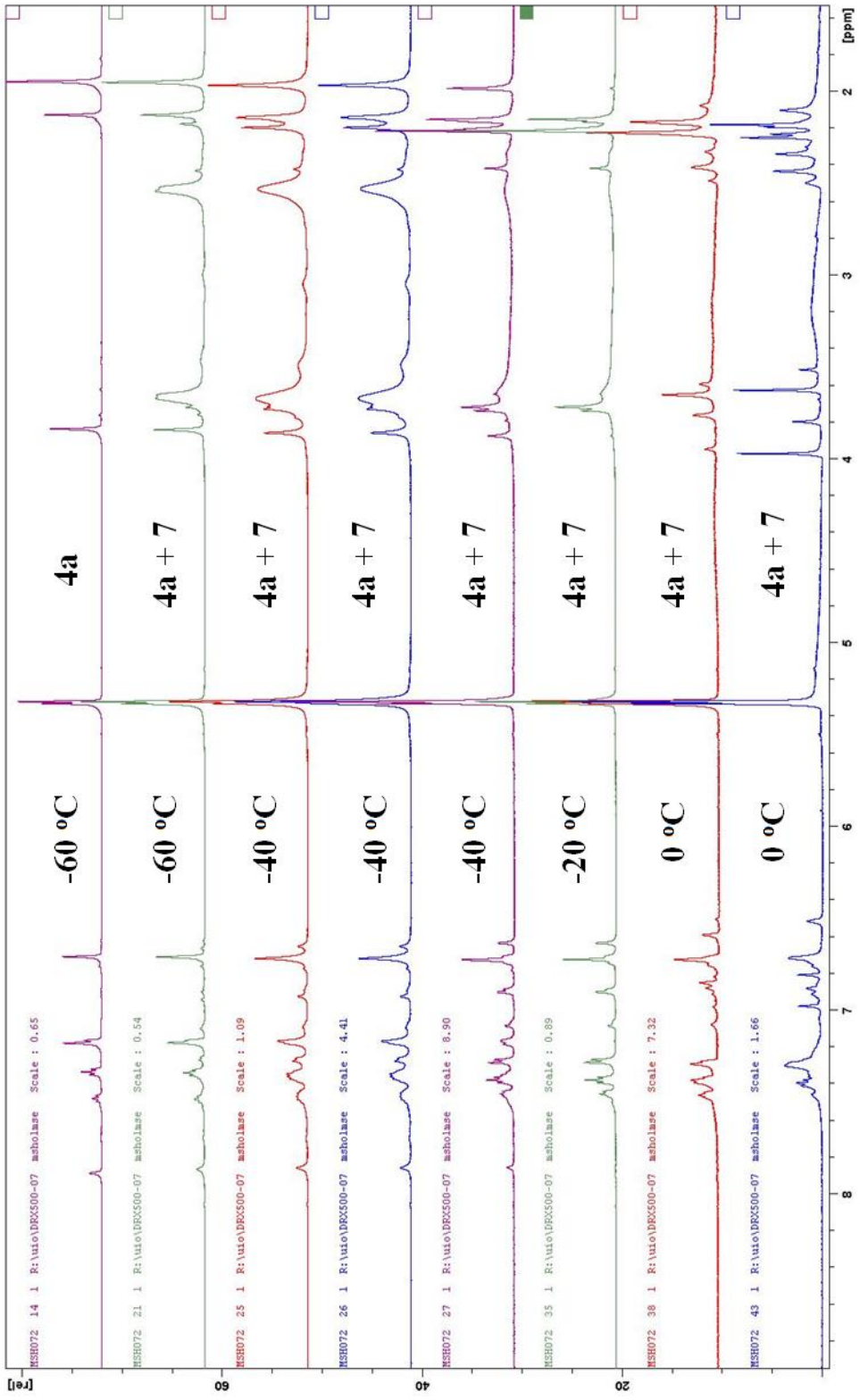

Figure 110: ^{1}H-NMR (500 MHZ, CD_2Cl_2) spectra of the reaction between **4a** and **7** at low temperatures.

Lineshape analysis of compound 8

Table 24: Data from the lineshape analysis of **8**.

Exp. Number	Temperature [°C]	Temperature [K]	Rate Constant [s^{-1}]	ln(k/T)	1/T
5	1.1	274.25	2	-4.92089	0.003646308
4	5	278.15	5	-4.01872	0.003595182
3	11.7	284.85	10	-3.34938	0.00351062
2	18.2	291.35	15	-2.96648	0.003432298
1	25.1	298.25	28	-2.36573	0.003352892
8	30.8	303.95	40	-2.02798	0.003290015
9	36.7	309.85	85	-1.29344	0.003227368
10	42.4	315.55	130	-0.88678	0.00316907
11	48.2	321.35	230	-0.33445	0.003111872
12	54	327.15	270	-0.192	0.003056702
13	59.9	333.05	320	-0.03997	0.003002552
14	65.6	338.75	500	0.389346	0.00295203
15	71.8	344.95	700	0.707681	0.002898971
16	77.4	350.55	1050	1.097042	0.00285266

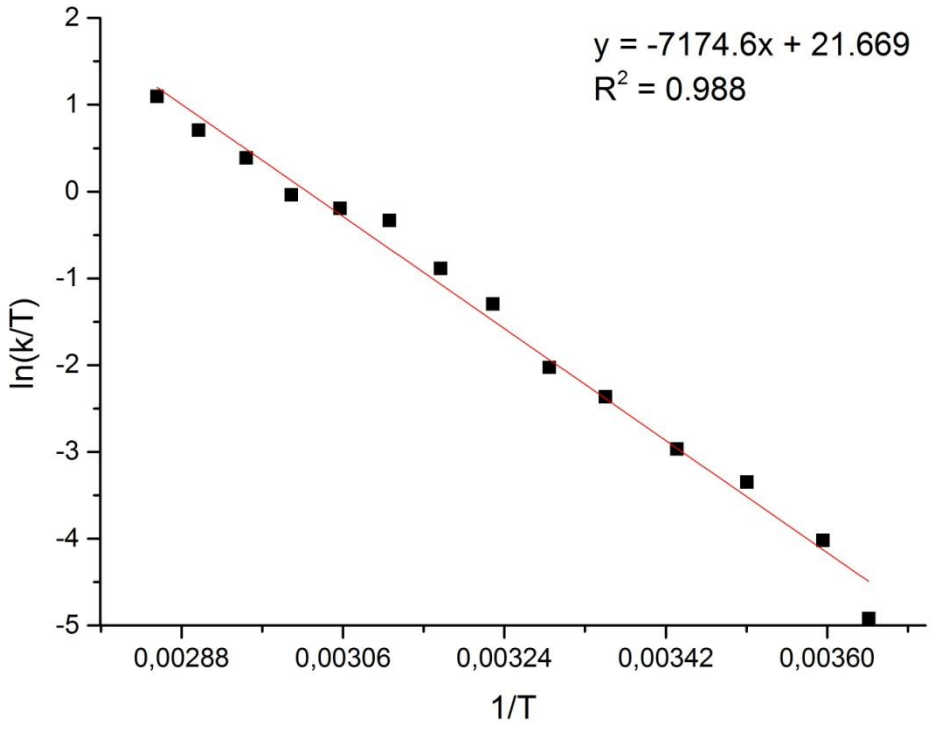

Figure 111: Eyring plot of the rotation process of the phenyl substituent in **8**. In this figure, comma is used instead of full stop to indicate the decimal points of the numbers on the axes

$$\ln\left(\frac{k}{T}\right) = \frac{-\Delta \mathrm{H}^{\#}}{\mathrm{R}} \cdot \frac{1}{\mathrm{T}} + \ln\left(\frac{k_B}{h}\right) + \frac{\Delta S^{\#}}{R}$$

Equation 1: The linear form of the Eyring equation.[15]

$$Slope = -7174.6 = -\frac{\Delta \mathrm{H}^{\#}}{R} \Rightarrow \Delta \mathrm{H}^{\#} = 7174.6 \cdot \mathrm{R}$$

$$Intercept = 21.669 = \ln\left(\frac{k_B}{h}\right) + \frac{\Delta \mathrm{S}^{\#}}{R} \Rightarrow \Delta \mathrm{S}^{\#} = (21.669 - \ln\left(\frac{k_\mathrm{B}}{h}\right)) \cdot \mathrm{R}$$

R is the gas constant

k_B is Boltzmann's constant

h is Planck's constant

Table 25: Enthalpy and entropy of rotation obtained from the visual lineshape analysis of **8** followed by an Eyring plot.

$\Delta H^{\#}$	59.7 ± 0.4 kJ mol^{-1}
$\Delta S^{\#}$	-17.4 ± 1.4 J $K^{-1}mol^{-1}$

References

[1] Netland, Krivokapic, Schröder, Boldt, Lundvall, Tilset, *J. Organomet. Chem.* **2008**, *693*, 3703-3710.

[2] Frøseth, Netland, Törnroos, Dhindsa, Tilset, *Dalton Trans.* **2005**, 1664-1674.

[3] Frøseth, Netland, Romming, Tilset, *J. Organomet. Chem.* **2005**, *690*, 6125-6132.

[4] Netland, Krivokapic, Tilset, *J. Coord. Chem.* **2010**, *63*, 2909-2927.

[5] Frøseth, Dhindsa, Røise, Tilset, *Dalton Trans.* **2003**, 4516-4524.

[6] Rosenberg, Langseth, Krivokapic, Gupta, Tilset, *New J. Chem.* **2011**, *35*, 2306-2313.

[7] Rosenberg, Vlašaná, Gupta, Wragg, Tilset, *J. Org. Chem.* **2011**, *76*, 2465-2470.

[8] Rosenberg, Krivokapic, Tilset, *Org. Lett.* **2009**, *11*, 547-550.

[9] Rosenberg, *PhD Thesis, Department of Chemistry, University of Oslo* **2011**.

[10] Netland, *PhD Thesis, Department of Chemistry, University of Oslo* **2013**.

[11] Langseth, *Master Thesis, Department of Chemistry, University of Oslo* **2010**.

[12] Hartwig, *Organotransition Metal Chemistry, From Bonding to Catalysis*, 1st. ed., University Science Books, **2010**.

[13] de Frémont, Marion, Nolan, *Coord. Chem. Rev.* **2009**, *253*, 862-892.

[14] Bourissou, Guerret, Gabbaï, Bertrand, *Chem. Rev.* **2000**, *100*, 39-92.

[15] Anslyn, Dougherty, *Modern Physical Organic Chemistry*, University Science Books, **2006**.

[16] Arduengo, Dias, Harlow, Kline, *J. Am. Chem. Soc.* **1992**, *114*, 5530-5534.

[17] Glorius, *Top. Organomet. Chem* **2007**, *21*, 1-20.

[18] Díez-González, Marion, Nolan, *Chem. Rev.* **2009**, *109*, 3612-3676.

[19] Jafarpour, Nolan, *Adv. Organomet. Chem.* **2000**, *46*, 181-222.

[20] Lin, Vasam, *Coord. Chem. Rev.* **2007**, *251*, 642-670.

[21] Garrison, Youngs, *Chem. Rev.* **2005**, *105*, 3978-4008.

[22] Clavier, Nolan, *Annu. Rep. Prog. Chem., Sect. B Org. Chem.* **2007**, *103*, 193-222.

[23] Arduengo, *Acc. Chem. Res.* **1999**, *32*, 913-921.

[24] Heinemann, Thiel, *Chem. Phys. Lett.* **1994**, *217*, 11-16.

[25] Arduengo, Harlow, Kline, *J. Am. Chem. Soc.* **1991**, *113*, 361-363.

[26] Huang, Schanz, Stevens, Nolan, *Organometallics* **1999**, *18*, 2370-2375.

[27] Wanzlick, Schoenherr, *Angew. Chem., Int. Ed. Engl.* **1968**, *7*, 141-142.

[28] Öfele, *J. Organomet. Chem.* **1968**, *12*, 42-43.

[29] Crabtree, *J. Organomet. Chem.* **2005**, *690*, 5451-5457.

[30] Peris, *Top. Organomet. Chem* **2007**, *21*, 83-116.

[31] Wang, Lin, *Organometallics* **1998**, *17*, 972-975.

[32] Fooladi, Dalhus, Tilset, *Dalton Trans.* **2004**, 3909-3917.

[33] Normand, Cavell, *Eur. J. Inorg. Chem.* **2008**, *2008*, 2781-2800.

[34] John, Ghosh, *Dalton Trans.* **2010**, *39*, 7183-7206.

[35] Steiner, Krajete, Kopacka, Ongania, Wurst, Preishuber-Pflügl, Bildstein, *Eur. J. Inorg. Chem.* **2004**, *2004*, 2827-2836.

[36] Colacino, Martinez, Lamaty, *Coord. Chem. Rev.* **2007**, *251*, 726-764.

[37] Huang, Stevens, Nolan, Petersen, *J. Am. Chem. Soc.* **1999**, *121*, 2674-2678.

[38] Hillier, Grasa, Viciu, Lee, Yang, Nolan, *J. Organomet. Chem.* **2002**, *653*, 69-82.

[39] Bauer, *Chem. Soc. Rev.* **2012**, *41*, 3153-3167.

[40] Malcolmson, Meek, Sattely, Schrock, Hoveyda, *Nature* **2008**, *456*, 933-937.

[41] Hapke, Tzschucke, *Angew. Chem., Int. Ed.* **2013**, *52*, 3317-3319.

[42] Cotton, Liehr, Wilkinson, *J. Inorg. Nucl. Chem.* **1955**, *1*, 175-186.

[43] King, *Inorg. Chem.* **1966**, *5*, 82-87.

[44] Budzelaar, *gNMR version 5.0*, IvorySoft, **1995-2006**.

[45] Clayden, Greeves, Warren, Wothers, *Organic Chemistry*, Oxford University Press, 1st ed., **2001**.

[46] Boeré, Klassen, Wolmershäuser, *J. Chem. Soc., Dalton Trans.* **1998**, 4147-4154.

[47] Ugi, Beck, Fetzer, *Chem. Ber.* **1962**, *95*, 126-135.

[48] Claridge, *High-Resolution NMR techniques in Organic Chemistry*, 2nd ed. Elsevier, **2009**.

[49] Harris, Becker, Menezes, Goodfellow, Granger, *Pure Appl. Chem.* **2001**, *73*, 1795-1818.

[50] Pavia, Lampman, Kriz, Vyvyan, *Introduction to Spectroscopy*, 4th ed., Brooks/Cole, Cengage Learning, **2001**.

[51] Bondi, *J. Phys. Chem* **1964**, *68*, 441-451.

[52] White, Yates, Maitlis, Heinekey, *Inorg. Synth.* **2007**, 228-234.

[53] Kang, Moseley, Maitlis, *J. Am. Chem. Soc.* **1969**, *91*, 5970-5977.

[54] Cramer, McCleverty, Bray, *Inorg. Synth.* **2007**, 14-18.

[55] McGrandle, Saunders, *J. Fluorine Chem.* **2005**, *126*, 449-453.

[56] Laeter, Böhlke, Bièvre, Hidaka, Peiser, Rosman, Taylor, *Pure Appl. Chem.* **2003**, *75*, 683-800.

[57] Danopoulos, Tulloch, Winston, Eastham, Hursthouse, *Dalton Trans.* **2003**, 1009-1015.

[58] Burling, Mahon, Reade, Whittlesey, *Organometallics* **2006**, *25*, 3761-3767.

[59] Spingler, Schnidrig, Todorova, Wild, *CrystEngComm* **2012**, *14*, 751-757.

[60] Humphries, Knox, *J. Chem. Soc., Dalton Trans.* **1975**, *16-17*, 1710-1714.

[61] Doherty, Knox, *Inorg. Synth.* **1989**, *25*, 179-187.

[62] Davison, McCleverty, Wilkinson, *J. Chem. Soc. (Res.)* **1963**, 1133-1138.

[63] Blackmore, Bruce, Stone, *J. Chem. Soc. A* **1971**, 2376-2382.

[64] Brown, Lyons, Manning, Rowley, *Inorg. Chim. Acta* **1969**, *3*, 346-350.

[65] Treichel, Shubkin, Barnett, Reichard, *Inorg. Chem.* **1966**, *5*, 1177-1181.

[66] Brown, Lyons, Manning, *Inorg. Chim. Acta* **1970**, *4*, 428-430.

[67] Heck, *Inorg. Chem.* **1965**, *4*, 855-857.

[68] This work was performed on the Abel Cluster, owned by the University of Oslo and the Norwegian metacenter for High Performance Computing (NOTUR), and operated by the Research Computing Services group at USIT, the University of Oslo IT-department. http://www.hpc.uio.no/.

[69] Frisch, Trucks, Schlegel, Scuseria, Robb, Cheeseman, Scalmani, Barone, Mennucci, Petersson, Nakatsuji, Caricato, Hratchian, Izmaylov, Bloino, Zheng, Sonnenberg, Hada, Ehara, Toyota, Fukuda, Hasegawa, Ishida, Nakajima, Honda, Kitao, Nakai, Vreven, Montgomery, Peralta, Ogliaro, Bearpark, Heyd, Brothers, Kudin, Staroverov, Keith, Kobayashi, Normand, Raghavachari, Rendell, Burant, Iyengar, Tomasi, Cossi, Rega, Millam, Klene, Knox, Cross, Bakken, Adamo, Jaramillo, Gomperts, Stratmann, Yazyev, Austin, Cammi, Pomelli, Ochterski, Martin, Morokuma, Zakrzewski, Voth, Salvador, Dannenberg, Dapprich, Daniels, Farkas, Foresman, Ortiz, Cioslowski, Fox, *Gaussian 09, Revision C01*, Gaussian, Inc., Wallingford CT, **2003**.

[70] Perdew, Burke, Ernzerhof, *Phys. Rev. Lett.* **1997**, *78*, 1396-1396.

[71] Perdew, Burke, Ernzerhof, *Phys. Rev. Lett.* **1996**, *77*, 3865-3868.

[72] Figgen, Rauhut, Dolg, Stoll, *Chem. Phys.* **2005**, *311*, 227-244.

[73] Hariharan, Pople, *Theor. Chim. Acta* **1973**, *28*, 213-222.

[74] Adamo, Barone, *J. Chem. Phys* **1999**, *110*, 6158-6170.

[75] Hehre, Ditchfield, Pople, *J. Chem. Phys* **1972**, *56*, 2257-2261.